# MODULATION OF THE IMMUNE RESPONSE FOLLOWING MYOCARDIAL INFARCTION UTILIZING BIOMATERIAL-BASED THERAPEUTIC DELIVERY STRATEGIES

A Dissertation

Presented to

The Academic Faculty

by

Inthirai Somasuntharam

In Partial Fulfillment

of the Requirements for the Degree

Doctor of Philosophy in the

Wallace H. Coulter Department of Biomedical Engineering

Georgia Institute of Technology

May 2015

# MODULATION OF THE IMMUNE RESPONSE FOLLOWING MYOCARDIAL INFARCTION UTILIZING BIOMATERIAL-BASED THERAPEUTIC DELIVERY STRATEGIES

Approved by:


Dr. Michael E Davis, Advisor
Department of Biomedical Engineering
*Georgia Institute of Technology & Emory University*

Dr. W. Robert Taylor
Department of Biomedical Engineering
*Georgia Institute of Technology & Emory University*

Dr. Andres Garcia
School of Mechanical Engineering
*Georgia Institute of Technology*

Dr. Mark Prausnitz
School of Chemical & Biomolecular Engineering
*Georgia Institute of Technology*

Dr. Tim Denning
Institute for Biomedical Sciences
*Georgia State University*


Date Approved: [March 30, 2015]

Gratefully dedicated to my family,

For the unwavering love, support and faith in me,

And for their numerous sacrifices

# ACKNOWLEDGEMENTS

First of all, I would like to thank my parents, Mangayarkarasi Somasuntharam and Sinnathamby Somasuntharam, for making me who I am today, and most importantly, getting me to where I am today. I will always remember the sacrifices you made for your children so they could have it all. You dreamed for me, and wanted me to have all the things you did not have and more. I love you both with all of my heart, and I am forever grateful for every single push you gave me and every little thing you did for me. I can only hope that I make you proud time to time in return. I will strive the rest of my life to make sure that I am worthy of the sacrifices and generosity you bestowed upon me.

I owe a lot of my successes in life to my brother, Thatparan, who has been a pillar of support I can lean on anytime. You have been selfless, and in our parents' absence when I first came to the US for college, you have been more of a parent and a friend to me than a brother. I will always remember the numerous sacrifices you made for our family and I would like to sincerely thank you for all that you have done, and continue to do for all of us. I would like to acknowledge my sister Aathirai for the unconditional love she gives me. I have always shared a special bond with you, and you took care of me for as long as I can remember growing up, including standing up for me at all times, and just being there when I needed help no matter how busy or tired you are. My brother-in-law Vivek, as a fellow PhD, you have understood many of my struggles throughout this process, and showed me your support at every opportunity. With that, I'd like to say that without my family, my PhD thesis would not have been possible, so my sincere heartfelt gratitude goes out to all of you.

I owe all of my sanity through this process of earning a PhDs to my significant other, Akhil Srinivasan. There is probably no other soul on earth that would put up with me and given me as many pep talks as you have given me through this whole process. You helped me to see the big picture, and to enjoy the process of a PhD, because as you wisely say, it is a journey of endurance, that is why you do a PhD, but it would have been a very lonely journey without you. Thank you for being here with me every step of the way, and taking care of me, and being my best friend in this world. I love you and am grateful to have found a soulmate in you.

I cannot thank my advisor Michael Davis enough. Mike, you have been supportive, approachable and always had faith in me even when at times I did not. You have given me the push I needed when I needed it, and let me explore my interests when I wanted to. My PhD would obviously not be possible without you, so my sincere thank you to you. My committee members have been an instrumental part of my thesis work, and their guidance and support has been incredible. Dr. Taylor, thank you for your contributions through divisional and my thesis meetings, for always setting aside time to talk to me despite your busy schedule. Your lab has been great help and a wealth of knowledge to tap into for many techniques instrumental for my work. Dr. Garcia, your lab has been incredible to work with, and I have been able to feel like I was a part of your lab through the last aim for my thesis. You are always a positive influence in committee meetings, constructive and incredibly supportive, thank you very much for that! I would like to acknowledge Apoorva and Jose from Dr. Garcia's lab for their part in helping me transfer PEG hydrogel work over to my lab. Dr. Prausnitz, as the drug delivery expert in my thesis committee, and through the class you taught, you have made me think about

drug delivery critically, and I want to sincerely thank you for all your guidance. I also draw inspiration from the translational focus in your work. Tim, as the immunology expert in my thesis, you have been instrumental in directing my thesis work, and I had worked with your lab, got antibodies from you, and learned multi-panel flow cytometry for which I'm very grateful.

Numerous people have made significant contribution to my thesis work, and to make my time at Georgia Tech fruitful, and although I won't be able to name all of them, I want to thank them all whole heartedly. My entering class of 2009, you have been a pleasure to know, as colleagues and friends. Patricia, thank you for getting us all to do fun stuff outside of lab and for cooking food and feeding us constantly! I have immensely enjoyed exploring the salsa scene at GT and Atlanta with you. Brian, you have been a dear friend, and made tireless attempts to get me to go running and I'll always look back to those memories fondly. Archana, you have been one of my best buddies in Atlanta, and who could ask for a better lab mate than you? The numerous late night chats in lab, and coming up with crazy experiments to do, it has been a fun ride with you around, and I will cherish our friendship forever. Warren, you have been a close friends and a great lab mate, and have seen you grow to be a great scientist. Thank you for the great companionship and the baked goods! Keon-young, you have been a special friend, and a fellow-monocyte lover, thank you for all that you have done for me and for being a great friend. Jessie, you have been a great friend to me throughout grad school, and got me to take breaks while in lab for walks on the lull water park that always made me feel better on days I was down. Nassir, your enthusiasm for science is inspiring, and thank you for all the chats about macrophages and help whenever I needed it with the IL-4 project.

Vivek, as our ex-neighbor, you are a life-long friend that we found at grad school, and you got us to have fun when we weren't slogging in lab. Rob Burke, my immediate manager at Merck where I interned during a summer while I was at graduate school, has been a significant part of graduate school experience and an incredible mentor. He played a major part in making my internship fruitful. We continued to work on a manuscript on work from that summer remotely even after I was through with the internship, which was published much to his credit in seeing it through with incredible commitment. He has been a mentor to me throughout the internship and even after with regard to guidance relating to my career progression and I owe him a great deal.

Every single labmate from the Davis lab has contributed to my thesis, and I would like to thank them all. A special thank you goes first to my undergrad Sheridan Carroll. You have made very significant contributions to my thesis, and I want to thank you with all my heart. You are a trooper, and I hope that you have learned a lot through the time we spent together. I have seen your immense scientific growth and wish you all the best things in your future endeavors. You are prepared to take on the world! Jay and Gokul for being great senior mentors, and Milton for all the surgeries and Echocardiography without which this thesis would not have been possible at all, and for your great company! Kristin for being an awesome pal and someone I can count on for support, and importantly for being on top of lab administration, and Mario for all the help you have done for my thesis, and for Srishti for helping me out whenever I needed it with eagerness and sincere dedication, Bernadette for all the craziness and exceptional kindness, and Raffay, just for being fun, and Karl, for teaching me a thing or two about life, and Udit and Amanda for help with protocols for staining. I would like to

acknowledge my collaborators Khalid Salaita and Kevin Yehl at Emory, thank you for your support and contribution for the side project that ultimately became part of both our thesis work. Dr. Niren Murthy and his lab, without our collaboration with your lab, my PhD wouldn't have been the same.

My best friends from my childhood, and through high school, have been the best of friends, and my life won't be the same without you. Despite oceans and several thousands of miles in between us, Kavi, Gasthi and Dilini, you have been part of my life, and a support network through and through, and my heartfelt gratitude to you. All my friends from undergrad are lifelong friends that I found, and I would like to especially thank Shaili and Priyanka, fellow PhDs, for all your support and especially for helping me get past difficult times when I'd get disillusioned with the process. As much as I have been lucky in my life to have some of the best friends one could ask for, I have lost a couple along the way, but I cherish their memories and the strength they displayed through trials and tribulations. Siva, I lost you to our country's terrible civil war even before I started graduate school, but your memories always follow me, and have been a strength through trying periods. Jennifer, I miss you dearly, and I learned some life lessons from you that I will never forget, and will always carry your memories with me.

Last, but not least, I would like to acknowledge the cardiology division at Emory, and name a few that have been instrumental in accomplishing this thesis work: Diana Weiss, Lu Hilenski, Giji Joseph, Alfiya Bikineyeva and Bernard Lassegue. I would also like to thank all the administrative staff at Tech including Shannon Sullivan and Sally Gerrish and Emory BME Leita Young. It's the things you do behind the scenes that keep this department running.

# TABLE OF CONTENTS

# LIST OF FIGURES

# LIST OF SYMBOLS AND ABBREVIATIONS

| | |
|---|---|
| AHA | American Heart Association |
| ANOVA | analysis of variance |
| Arg1 | arginase 1 |
| ATP | adenosine triphosphate |
| BMM | bone marrow-derived macrophages |
| CCR2 | C-C chemokine receptor type 2 (CCR2) |
| CECs | cardiac endothelial cells |
| Col I | collagenase I |
| CPC | cardiac progenitor cells |
| DHE | Dihydroethidium |
| DNAzyme | deoxyribozyme |
| Dz | TNF-α specific DNAzyme |
| ECM | extracellular matrix |
| ELISA | enzyme-linked immunosorbent assay |
| FDA | Food and Drug Administration |
| % FS | % fractional shortening |
| HPLC | high-performance liquid chromatography |
| i-Dz | catalytically inactive enzyme, but specific to TNF-α mRNA |
| IFN-γ | interferon gamma |
| IGF | insulin-like growth factor |
| IL | interleukin |
| iMAECs | induced Mouse Aortic Endothelial Cells |
| IR | ischemia-reperfusion |
| LAD | left anterior descending coronary artery |
| LPS | lipopolysaccharide |

| | |
|---|---|
| LV | left ventricle |
| Ly-6C | lymphocyte antigen 6C |
| M1 stimuli | IL-4 |
| M2 stimuli | IFN- γ + LPS |
| M1/M2 CM | Classically/alternatively activated macrophages conditioned media |
| MCP-1 | monocyte chemoattractant protein-1 |
| M-CSF | macrophage colony-stimulating factor |
| MI | myocardial infarction |
| MMP | metalloproteinase |
| MRC-1 | mannose receptor C 1 |
| NADPH | nicotinamide adenine dinucleotide phosphate |
| Nox | β-nicotinamide adenine dinucleotide phosphate oxidase |
| Nr4a1 | nuclear receptor subfamily 4, group a, member 1 |
| NS-Dz | non-specific DNAzyme, but retains catalytic activity |
| PBS | phosphate buffered saline |
| PEG | poly(ethylene glycol) |
| PK | empty polyketal microparticle |
| PK-siNox2 | siRNA targeting Nox2 loaded formulated into polyketal nanoparticles |
| PLGA | poly(lactic-co-glycolic acid) |
| PMN | polymorphonuclear leukocyte |
| PPCI | primary percutaneous coronary intervention |
| ROS | reactive oxygen species |
| SEM | scanning electron microscopy/standard error of mean |
| siRNA/RNAi | small silencing ribonucleic acid/ RNA interference |
| TNF-α | tumor necrosis factor alpha |
| VEGF | vascular endothelial growth factor |

# SUMMARY

In 2015, American Heart Association (AHA) reported that 1 in 9 deaths are attributed to heart failure (HF), the number one killer in the world. While advancements in interventional cardiology in conjunction with pharmacotherapies have significantly reduced the rate of mortality following MI, there has been a corresponding rise in HF in surviving patients, largely attributed to the limited regenerative capacity of the heart and the inadequate healing response. Myocardial ischemic injury triggers an exuberant local and systemic inflammation, and the extent and quality of the cardiac wound healing process is intricately tied to the delicate equilibrium of this inflammatory response. While cardiac regeneration is an important goal, it is imperative in the meantime to explore therapeutic strategies that target these inflammatory mediators of early cardiac repair. These interventions to influence and improve cardiac wound healing can represent a new therapeutic window to halt the progression of heart failure between the few hours that may be used to limit infarct size by reperfusion and an irreversible non-contractile cardiac scar. This dissertation examines three therapeutic delivery strategies aimed at modulating the immune response to enhance cardiac repair in rodent models MI: 1) Polyketal nanoparticles as siRNA delivery vehicles for antioxidant therapy; 2) Spherical nucleic acid particles for anti-inflammatory therapy and; 3) Bioactive PEG (polyethyleneglycol)-based hydrogel for immunomodulation.

Antioxidant therapy has shown promise in battling the excessive ROS production caused by infiltrating immune cells, although scarcity of specific and effective inhibitors to oxidant enzymes has been a major shortcoming. Here, we describe the biocompatible polyketal polymer formulated nanoparticles as a viable delivery system for siRNA-mediated gene silencing of a major oxidant enzyme Nox2-NADPH in the heart. The non-acidic degradation products of polyketals make them a prime candidate for treating inflammatory diseases, and especially for nucleic acid delivery to such disease states, as most successful delivery vehicles for nucleic acids are cationic lipid/polymers that elicit

an immune response. We demonstrated intracellular localization of these particles in macrophages, the ability to knockdown Nox2-NADPH and scavenge extracellular superoxide levels *in vitro*. At a low dose of 5μg siRNA/kg, the delivery of these particles restored acute cardiac function following MI injury in mice.

TNF-α is a critical regulator of the inflammatory response following MI. Catalytic DNA (DNAzyme) targeted against TNF-α mRNA was functionalized to gold particles. These spherical nanostructures exhibited no cytotoxicity, and superior uptake and knockdown efficiency in primary macrophages compared to widely used cationic lipid particles. *In vivo* studies demonstrate significant anti-inflammatory effects conferred by the knockdown of TNF-α by DNAzyme particles and significant improvement in acute cardiac function.

Increasing evidence suggests that macrophages exhibit remarkable plasticity, allowing them to adopt distinct activation states with specific functional roles according to changing cues. We employed a PEG-based hydrogel to deliver the polarizing cytokine IL-4 to the myocardium to influence cardiac repair via modulating the pro-inflammatory macrophages at the site of infarct towards a reparative macrophage phenotype. We validated this approach *in vitro* to demonstrate beneficial effects of alternately activated macrophages on endothelial tube formation and cardiac progenitor cell migration. We evaluated the functional effects of this approach in a rat model of MI and observed acute functional improvement compared to bolus delivery of IL-4, although future studies optimizing the delivery approach are needed to effect favorable chronic repair.

The work presented here applies novel nucleic acid delivery strategies for cardiac gene silencing and has contributed to new knowledge with regard to modulating the immune response following MI.

# CHAPTER 1 INTRODUCTION

## 1.1 Motivation

Heart failure (HF) is the leading cause of death in the developed world, and myocardial infarction (MI) is the dominant cause [1]. A million new and recurring MI events occur every year accounting for $300 billion in direct and indirect costs yearly, with an expectation for this cost to triple in the next decade [2]. Optimized reperfusion strategies employ sophisticated designs of stents to restore blood to the injured myocardium. In conjunction with neurohormonal and thrombolytic pharamcological agents, advancements in the management of acute MI has reduced the mortality due to MI [3-5]. Even with improvements in clinical interventions however, 25% of patients surviving MI develop HF, which poses an enormous burden for the healthcare systems worldwide [4, 6, 7]. Ultimately, the only cure for HF is transplantation, and given the shortage of donor organs and the continuous battles with organ rejections, there is a clear need to identify approaches that can halt the progression of HF.

Most research approaches focus on renewal of cardiomyocytes from existing cardiomyocytes or stem cells with the hope of garnering the heart's limited regenerative capacity [8-10]. While some stem cell clinical trials have shown promise, cell survival and retention have been huge hurdles [11, 12]. These efforts are supplemented by efforts in gene therapy and exploration of growth factors or microRNAs as therapeutics, although none have been clinically translated thus far [8, 11-15], largely due to the limitations in the delivery technologies to the heart. Therefore identification and development of suitable delivery vehicles to the heart can drastically improve the efficacy of these existing promising therapies.

The progression to HF originates from the heart's failed attempt to compensate for the ischemic injury. The dynamic network of complex molecular and structural processes initiated following the loss of viable myocardium often lead to adverse cardiac

remodeling, eventually culminating in cardiac dysfunction. Central to these processes are the inflammatory response to the MI injury, and interventions to modulate these responses favorably can represent a new therapeutic window between the few hours that may be used to limit infarct size by reperfusion and an irreversible non-contractile cardiac scar.

## 1.2 Specific Aims

Recent studies have shed light on key roles of macrophages in MI injury [16-18]. In the early phase following injury, classically activated macrophages (M1) dominate the infarct and clear dead cells and debris from the wound. Production of reactive oxygen species (ROS) and upregulation of pro-inflammatory cytokines are key events involved in this phase. In later stages of wound healing, alternatively activated macrophages (M2) dominate and propagate tissue repair. While the initial pro-inflammatory response is necessary, prolonging of these signals is detrimental to wound healing and could contribute to adverse cardiac remodeling [17]. Therefore, optimal healing response after MI requires a well-balanced biphasic macrophage response and the overall inflammatory response. In this thesis work, we explore several inflammatory mediators/regulators as therapeutic targets with the goal of controlling the overall inflammatory response.

Nox2- NADPH oxidase is a major source of reactive oxygen species (ROS) that are integral part of the inflammatory events in the myocardium [19-21], and we aim to inhibit this enzyme at the genetic level as an anti-oxidant therapeutic strategy that can suppress the excessive ROS levels in the heart following MI. TNF-$\alpha$ is a key inflammatory mediator implicated in several pathophysiological processes in the progression of HF [22-24], and we seek to transiently suppress this cytokine to suppress the exuberant inflammatory response post-MI. Increasing evidence suggests that macrophages exhibit remarkable plasticity, allowing them to adopt distinct activation states with specific functional roles according to changing environmental signals [17, 25,

26] In a comprehensive approach to influencing cardiac repair, we aim to modulate the macrophages to transition from an inflammatory state (M1) to that of a reparative activation state (M2). To do this, we took advantage of the well-known fact that cytokine Interleukin-4 (IL-4) polarizes monocytes into alternatively activated macrophages, and explore the delivery of IL-4 to the myocardium.

Translation of such approaches, however, is limited by the key challenge facing the field of regenerative cardiology: technologies that enable delivery of therapeutics to the heart in a spatially and temporally controlled manner [12, 27]. In order for attempts to repair or regenerate the heart to be effective, temporal and spatial control of therapeutics become essential given the complex nature of the inflammatory and healing processes that ensue MI. Delivering a particular drug at the wrong time or location can either turn out to be futile or even worse, deleterious given the pleiotropic functions of many of the mediators of cardiac repair. Therefore, drug delivery vehicles appropriately tailored to deliver therapeutics to an inflammatory myocardial injury environment can afford spatiotemporal control over the drug concentration in the myocardium and can enhance therapeutic efficacy.

We focus on three different materials for drug delivery to the heart in this thesis work. Some of these materials have already been evaluated in the heart in the context of MI, and have been well tolerated. Polyketals are a class of polymeric drug delivery vehicles that contain acid-degradable ketal linkages and produce neutral degradation products, and have this advantage over many polymeric delivery vehicles in wide use today such as polyesters or polyimides. This biocompatibility is especially advantageous for nucleic acid delivery, and in stark contrast to the most widely used cationic lipid nanoparticles. Polyketals also offer a unique advantage of pH sensitivity for delivery of nucleic acids for gene silencing purposes. Endocytosis/phagocytosis is the most common mechanisms of drug/drug delivery vehicle uptake by cells, and polyketals degrade within the acidic endosomes to release the cargo in a timely manner to effect gene silencing. We

also explore spherical DNA structures to confer catalytic gene silencing activity in the heart [28]. These unique nanostructures created by modifying gold particles with catalytic DNA (DNAzyme) capable of site-specifically cleaving target mRNA offer the advantages of biocompatibility as well efficient cellular uptake not limited to phagocytic immune cells [29-31]. Finally, we evaluated a non-immunogenic, non-fouling PEG-based hydrogel that incorporates a protease cleavable linker to confer enzymatically triggered release [32, 33]. This is a useful property in the inflammatory myocardial environment to release therapeutics in an on-demand fashion as macrophage-secreted proteases are abundantly present in the myocardium following MI. Hydrogels are also ideal delivery vehicles for proteins as they afford a 3-dimensional, hydrophilic environment that better preserve protein structures.

The main objective of this project was to evaluate therapeutic drug delivery systems that can modulate the immune response earlier in the process of myocardial inflammation. Long-term goal for this work is to open up a therapeutic window to enhance other molecular and stem-cell based therapeutics to regenerate the heart following MI. [12]. **Our central hypothesis is that biomaterial-based therapeutic delivery strategies can modulate the initial immune response following myocardial infarction to create a pro-healing environment and improve cardiac function.** This hypothesis was evaluated by the following three specific aims:

**Specific Aim 1: Evaluation of polyketal nanoparticle mediated siRNA delivery for silencing Nox2-NADPH oxidase following MI** [1]

*We hypothesize that polyketal nanoparticles can deliver siRNA to the heart to silence a major oxidant enzyme Nox2-NADPH in the heart to improve cardiac function*. Nox2-NADPH is primarily expressed in macrophages and upregulated following MI. Therefore, macrophages were used as an *in vitro* model for the evaluation of polyketal mediated Nox2-siRNA delivery. Nox2-NADPH gene expression in the infarct and acute cardiac function (day 3 post-injection) in response to delivery of these particles to the myocardium of a mouse model of permanent arterial occlusion MI were evaluated.

**Specific Aim 2: Evaluation of catalytic DNAzyme-gold nanoparticles for silencing pro-inflammatory cytokine TNF-α following MI**

*We hypothesize that delivery of catalytic DNAzyme modified gold particles can knockdown pro-inflammatory cytokine TNF-α expression in the myocardium to create an anti-inflammatory environment and improve cardiac function*. DNAzyme particles were evaluated for biocompatibility and gene silencing effects *in vitro* in primary macrophages. These particles were directly injected into the myocardium in a rat model of permanent arterial occlusion MI, and particle biodistribution was evaluated *ex vivo*. At day 3 post-injection *in vivo*, cardiac function and inflammatory gene and plasma expression markers were evaluated.

---

[1] Somasuntharam, I., Boopathy, A. V., Khan, R. S., Martinez, M. D., Brown, M. E., Murthy, N., & Davis, M. E. (2013). Delivery of Nox2-NADPH oxidase siRNA with polyketal nanoparticles for improving cardiac function following myocardial infarction. *Biomaterials*, *34*(31), 7790–7798.

**Specific Aim 3: Modulation of pro-inflammatory macrophages towards a reparative phenotype following MI via hydrogel-mediated IL-4 cytokine therapy.**

*We hypothesize that modulating pro-inflammatory (M1) macrophages towards a reparative (M2) functional phenotype during the initial inflammatory phase following MI can help direct an improved reparative process.* In this aim, we take advantage of the fact that cytokine interleukin-4 (IL-4) polarizes monocytes into alternatively activated macrophages [34]. An injectable protease-cleavable polyethylene glycol (PEG) based hydrogel delivery system was evaluated for the delivery of IL-4 to the myocardium following acute MI. The overall strategy was validated *in vitro* and upon intramyocardial injection into a rat model of MI, acute (day 3) inflammatory marker expression was evaluated and the healing response was assessed via acute (day 7) and chronic (day 21) cardiac functional and immunohistological measures of capillary density and fibrosis (day 21).

# CHAPTER 2 BACKGROUND

## 2.1 Myocardial infarction and progression of cardiac dysfunction

Ischemic heart disease is the major origin for heart failure (HF), the leading cause of death in the developed world today [2]. Myocardial infarction (MI), most commonly known as a "heart attack" is the initial occurrence, and it starts with a thrombotic occlusion of a coronary artery cutting off the oxygen supply to the myocardium in a segmental manner. Ischemic myocardial injury results in decreased oxygen tension with loss of oxidative phosphorylation and subsequent decreased generation of high energy phosphates (ATP), which leads to failure of the sodium pump, loss of potassium, influx of sodium and water, and cellular swelling. The major mode of metabolism in the myocardium shifts from aerobic oxidative phosphorylation in mitochondria to anaerobic glycolysis through glycogen breakdown, thus leading to ATP depletion and accumulation of byproducts like lactic acid within seconds of ischemia. This leads to loss of contractility, and within minutes, reversible ultrastructural cardiomyocyte changes appear, including cellular and mitochondrial swelling and glycogen depletion. After 20-40 min of sustained ischemia, irreversible cardiomyocyte injury and necrosis take place, associated morphologically with mitochondrial and lysosomal swelling and loss of the integrity of the cytoplasmic membrane. [6, 35, 36]. Myocardial necrosis leads to a systemic activation of the humoral immune system increasing the regional cellular inflammatory response during an ischaemic event [6, 36, 37].

Current clinical standards for MI rely largely on the crucial early reperfusion by way of primary percutaneous coronary intervention (PPCI) in order to limit the initial extent of hypoxic myocardial damage [7, 38]. While this has proven benefits in reducing infarct size and improving clinical outcomes as illustrated in Figure 1, paradoxically, re-introduction of coronary flow triggers vascular inflammation and production of reactive oxygen species (ROS) that can further damage the myocardium, a phenomenon known as

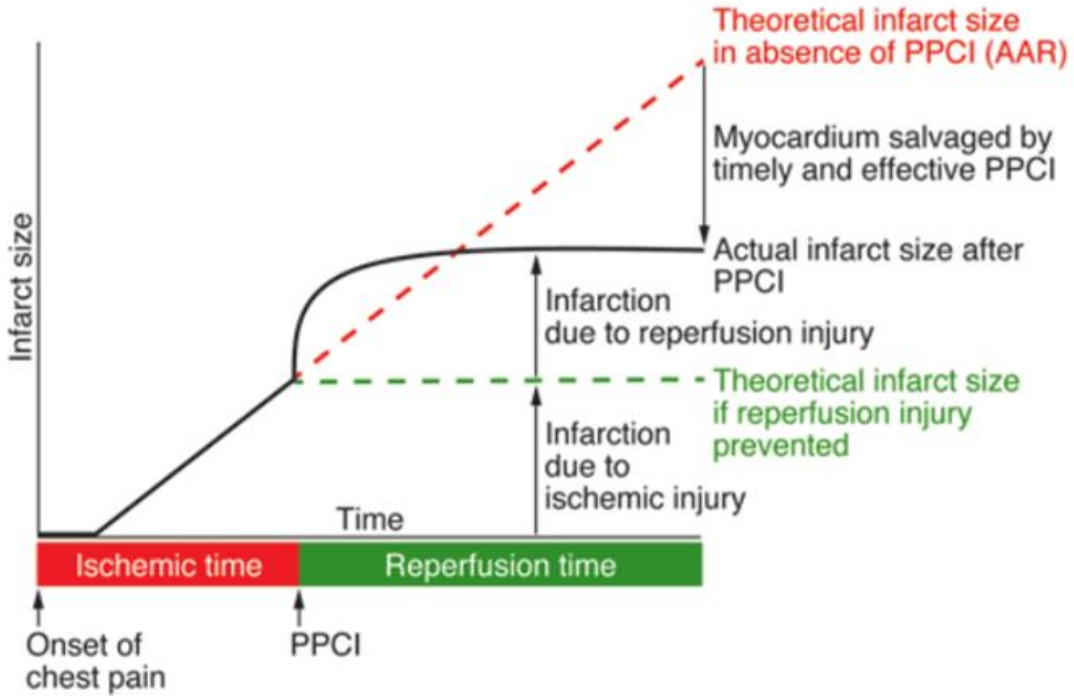


**Figure 1. Contribution of myocardial injury and reperfusion injury to infarct size.** Figure from Hausenloy et al 2013.

reperfusion injury [6, 7, 39-41], to which there is still no effective therapeutics and minimizes the best potential outcomes from PPCI Figure 1 [42].

The loss of viable myocardium affects the ventricular pump performance in direct proportion to the magnitude of lost tissue, initiating a dynamic network of genetic, molecular and structural processes that compensate for the ischemic injury [4, 43, 44]. The complex myocardial healing process is depicted in three distinct phases using a simplified schematic in Figure 2. The first acute inflammatory phase is where the inflammatory response is initiated to absorb necrotic tissue and clear the wound, and takes place within the 1–7 days following ischemia reperfusion injury. In the second proliferative/wound healing phase, myofibroblasts are recruited to the heart and they proliferate to increase the myocardial tensile strength and promote blood vessel proliferation thereby improving tissue perfusion and cell survival, and this phase lasts

about 1–3 weeks. In the final maturation/chronic scar phase, fibroblasts are formed and micro-vessel regression takes place generating the final collagen-rich scar tissue (~1 month). However, myocardial infarct size is dynamic even after the loss of viable myocardium has terminated. In large infarcts, or if reperfusion is established too late, infarct expansion is often observed, and this process is mainly attributed to the extent and quality of the inflammatory response following MI that occurs during the wound healing response before scar tissue formation. Infarct expansion is closely related to adverse ventricular remodeling, a process that induces pathological epigenetic, molecular, cellular, structural and functional changes in both the infarcted and the remote viable myocardium. Ventricular remodeling is a powerful prognostic factor after acute MI and eventually leads to left ventricular dilatation and cardiac dysfunction [45, 46]. These multitudes of factors contribute to the prevalence of HF in patients that survive acute MI, which poses an enormous burden for the healthcare systems worldwide [4, 6, 7].

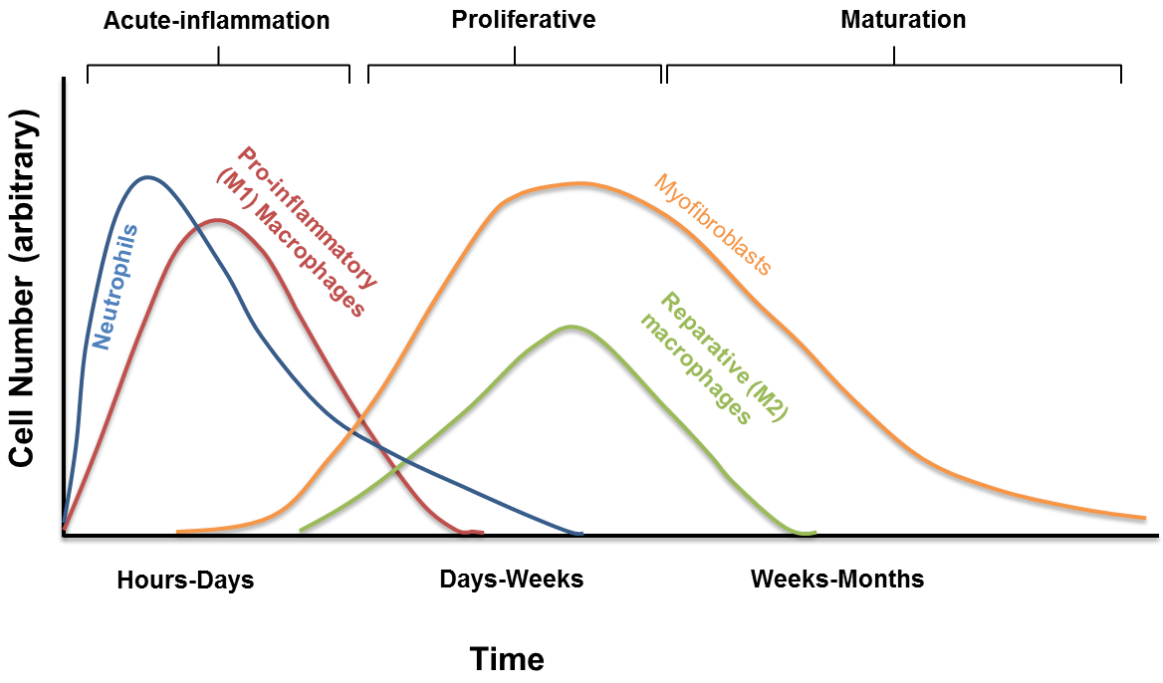


**Figure 2. Phases of myocardial wound healing.** Adapted from Frangogiannis et al (2006) and [17] Nahrendorf et al (2010) [43]

## 2.2 Role of inflammation in the progression of heart failure

Interestingly, many of the underlying pathological mechanisms associated with ischemic injury and the ensuing healing process are tightly intertwined with the inflammatory response, signifying it as a logical therapeutic intervention for the prevention of HF. Systemically circulating cytokines originating from the heart, vessel wall or macrophages stimulate the liver to produce several inflammatory markers such as C-reactive protein (CRP) clinically used to quantify systemic inflammatory reaction, and has been shown to directly correlate to early and late post-MI morbidity and mortality. Therefore not surprisingly, many of the therapeutics with demonstrated efficacy for the clinical management of MI have anti-inflammatory properties distinct from their primary mechanism of action [6, 41]. For example, Angiotensin Converting Enzymes (ACE) inhibitors and Angiotensin receptor II blockers that target the renin-angiotensin neurohormonal system to dilate blood vessels and improve blood flow also diminish oxygen radical production and cytokine levels. Furthermore, both thrombolytic agents ("antiplatelet" therapies) aspirin and clopidogrel possess anti-inflammatory effects, and anti-inflammatory properties of cholesterol lowering statins are now well established. The hypothesis generated from these observations is that modulation of the inflammatory response following MI is at least partly responsible for the long-term clinical benefits ascribed to these medications. However, despite encouraging results from direct immunomodulation therapies in pre-clinical animal models, human trials have thus far not shown a convincing clinical impact [6, 41].

While there is solid evidence that inflammation plays a central pathological role in the progression of coronary atherosclerotic disease, acute MI, and HF, the therapeutic strategies targeting the immune response likely need revision [47]. Judicious design in terms of not only the specific target, but also the temporal window of application, appropriate dosage and delivery systems, and additionally, careful patient selection are crucial factors to consider. Immune response following MI is incredibly complex in that

many components of the immune system are in play, and some considered double-edged swords that induce both beneficial and deleterious effects. The subsequent sections will in detail review the inflammatory response post-MI and outline some targets that may be master regulators capable of favorable manipulation to restore inflammatory balance and ameliorate remodeling after MI.

### 2.2.1 Humoral mediators of inflammation

Myocardial necrosis results in the release of intracellular contents of cells that initiate an intense inflammatory response by activating the body's non-specific innate immunity. Toll-like receptor (TLR)-mediated pathways, complement, chemokine and cytokine activation, and reactive oxygen species generation play a significant role in triggering the post-infarction humoral inflammatory response which regulates locomotion and trafficking of leukocytes [36, 48]. The chemokines constitute a family of small highly basic proteins with molecular weights in the range of 8-14 kDa. They are divided into two main families, according to the position of the first two cysteines, which are separated by one amino acid (CXC chemokines), or are adjacent (CC chemokines) [35]. Chemokines play significant roles in the recruitment of neutrophils and monocytes to the site of infarct and will be detailed further in the section 1.3 describing monocyte/macrophage roles in cardiac repair. Numerous studies show that myocardial necrosis and the subsequent release of subcellular membrane constituents that are abundant in the mitochondria activates the early acting components of the complement cascade (C1, C4, C2 and C3). As indicated in the section describing the cellular mediators of inflammation (section 1.2.2), complement activation also plays an important role in mediating neutrophil and monocyte recruitment in the injured myocardium. [37, 49]. In this section, we focus on the role of reactive oxygen species and cytokines in mediating the inflammatory response post-MI.

2.2.1.1 Reactive oxygen species, oxidative stress and cardiac remodeling

Reactive oxygen species (ROS) such as superoxide ($O_2^{\cdot -}$), Nitric oxide ($NO^{\cdot}$), hydroxyl ($^{\cdot}OH^{-}$), hydrogen peroxide ($H_2O_2$) and free radical forming oxidants such as peroxinitrite ($ONOO^{-}$) are highly reactive molecules characterized by the presence of unpaired electrons. They serve as signaling molecules under normal concentrations and play a role in several cellular processes [20, 50]. For instance, NO is essential for regulating the tension in blood vessels. However, high levels of ROS and/or low levels of antioxidants (superoxide dismutase (SOD)), catalase or easily oxidized organic molecules like Vitamin E and C) can interfere with this natural redox balance within the cells, and lead to a state of oxidative stress where biological molecules are increasingly susceptible to oxidative damage. ROS have gained importance in the recent years due to their roles in the pathophysiology of numerous cardiovascular diseases [21, 40], and especially due to the oxygen paradox alluded to earlier with regard to PPCI procedures causing reperfusion-injury [39, 40].

Furthermore, ROS have been shown to modulate several of the processes underlying ischemic injury induced cardiac remodeling such as pro-inflammatory cytokine release, cardiomyocyte apoptosis, the activation and expression of matrix metalloproteinases (MMPs), interstitial fibrosis, cell proliferation and hypertrophy [40, 50-52]. Pre-clinical studies have shown that overexpression or delivery of antioxidants to scavenge ROS has reduced myocardial injury and improved function in the setting of ischemia and reperfusion [53-56].

*2.2.1.1.1 Role of NADPH oxidases in cardiac remodeling*

Potential sources of ROS in the heart include intracellular sources such as mitochondria and uncoupled nitric oxide synthase, as well as membrane bound proteins like the Nicotinamide adenine denucleotide phosphate (NADPH) oxidase and xanthine oxidase [21, 50]. Among these, NADPH oxidases are major sources of $O_2^{\cdot -}$ in the heart.

Originally identified in phagocytes of the innate immune system, NADPH oxidases play a critical role in host defense by releasing a burst of $O_2^{\cdot -}$ from molecular oxygen using NADPH as an electron donor. The prototypic NADPH oxidase is a multi-subunit enzyme complex consisting of a membrane-bound cytochrome $b_{558}$ composed of $p22^{phox}$ and the catalytic subunit $gp91^{phox}$, and four cytosolic regulatory subunits (p47phox, p67phox, p40phox and the small G protein Rac1 or 2) that associate with the membrane bound subunits in the activated enzyme. A family of $gp91^{phox}$ homologues termed Noxs (Nox1-5) form the basis of distinct NADPH oxidases. In the cardiovascular system, Nox2 and Nox4 are expressed in cardiomyocytes, fibroblasts and endothelial cells, while vascular smooth muscle cells express Nox1 and Nox4 [51, 57]. After MI, Nox2-NADPH oxidase expression is significantly increased in the infarcted myocardium, primarily in neutrophils, macrophages and myocytes in both animal models and human patients [19, 20, 51, 58]. Suppression of Nox2 has shown beneficial effects in the setting of permanent occlusion MI in mice and therefore represents a potential target for modulation [51, 59, 60].

2.2.1.2 Cytokine cascade

Induction and release of the pro-inflammatory cytokines TNF-α, IL-1β and IL-6 is consistently found in experimental models of myocardial infarction [61, 62]. Although the heart's macrophages are a rich source of several inflammatory cytokines, other cell types and several humoral components can also effect cytokine production in experimental models of I/R or MI. Complement activation, mechanical stress, free radical generation and NF-κB activation are all such factors capable of stimulating cytokine mRNA synthesis in the immune cells populating the infarct as well as cardiomyocytes and endothelial cells in the face of injury, resulting in marked local and systemic cytokine upregulation [36, 37, 61, 63].

TNF-α release occurs early in the infarcted myocardium implicated in many of the pathophysiological processes associated with ischemia/reperfusion injury [22, 23, 64-77]. It has been shown to stimulate the production of other pro-inflammatory cytokines such as IL-6 and IL-1β by infiltrating cells, promote chemokine and adhesion molecule expression on vessel wall, contribute to reactive oxygen and nitrogen radical mediated as well as other cytokine mediated endothelial as well as contractile dysfunction and overall, strongly implicated in the regulation of the inflammatory response post-MI as suggested by several studies [24, 78-81]. However, the role of TNF-α in MI is complex. Its pleiotropic effects have been well demonstrated where it has been shown to be cardioprotective by inhibiting cardiomyocyte apoptosis [68, 70, 73, 82, 83] suggesting that complete negation TNF-α in the context of MI is not beneficial. The mixed results regarding clinical outcomes in human clinical trials that attempted to neutralize TNF-α in chronic HF patients (discussed in detail in Chapter 4) further highlight the need to identify an ideal temporal window, dosage and judicious design of therapeutic strategy for interventions that target TNF-α in the context of MI.

Knowledge of the singular roles of other pro-inflammatory cytokines, such as IL-6 and IL-1β is more limited compared to the wealth of knowledge available for TNF-α, and partially it is because these cytokine effects are mediated by TNF-α. IL-6 synthesis is rapidly induced in mononuclear cells and cardiomyocytes of the ischemic myocardium and may mediate ligand-specific adhesion of neutrophils to cardiac myocytes by modulating cell adhesion molecule ICAM-1 expression [36]. IL-6 may also affect the phenotypic characteristics and gene expression of many cell types involved in infarct healing [61]. Furthermore, in a recent study, IL-1β was found to play a key role in triggering splenic monocyte production after MI, the site from which monocytes are deployed to the infarct [16, 84].

### 2.2.2 Cellular mediators of inflammation

Myocardial inflammation is characterized by accumulation of circulating leukocytes, which, once stimulated by the vascular endothelium, migrate through the vessel wall into the ischemic myocardial region [35, 41]. Adhesion of leukocytes to the damaged vascular endothelium results in a massive migration of other inflammatory leukocytes such as neutrophils, monocytes as well as mast cells into the ischemic myocardium. Complement activation has an important role in the neutrophil chemotaxis in the infarcted myocardium demonstrating the complex interplay between the humoral and cell-mediated immune response that follows ischemia [37]. It is suggested that endothelial adhesion of leukocytes and the trans-vascular migration process may be enhanced by spontaneous or PPCI-induced coronary plaque rupture [41]. Neutrophils increase the infarct size by promoting tissue inflammation, and by their direct entrapment in the capillary micro-vessels, both leading to reduced myocardial local perfusion [41, 48].

As the number of neutrophils declines, monocytes arrive at the infarct, and differentiate into active macrophages, representing the predominant phagocytic cells in the infarct [17, 43]. Figure 3 depicts the spatial and temporal aspects of monocyte/macrophage kinetics following MI, and it shows that monocytes spend only an average of 20 hours at the infarct and within 24 hours, the majority of cells are replenished by a new generation of cells. This signifies the involvement of monocytes/macrophages as key factors in the development and progression of cardiovascular diseases. The function of macrophages is not limited to removal of dead cells and debris. Macrophages are capable of producing a wide range of growth factors and cytokines that stimulate fibroblast and endothelial cell proliferation and appear to be key regulators of the healing response. The next section will be devoted entirely to discussing the recent knowledge gathered with regard to macrophage biology in the context of MI as well as in the multi-faceted nature of these intriguing cell types.

Mast cells are also implicated in the post-MI inflammatory response, and are stimulated by the complement 5a (C5a)-adenosine-reactive oxygen complex. These are multifunctional resident cells, capable of secreting a wide range of inflammatory mediators including TNF-α, thus initiating a cytokine cascade. These cells are strongly implicated in the fibrotic processes, due to their secretion of pro-fibrotic factors and accumulation of these cells in areas of collagen deposition [37].

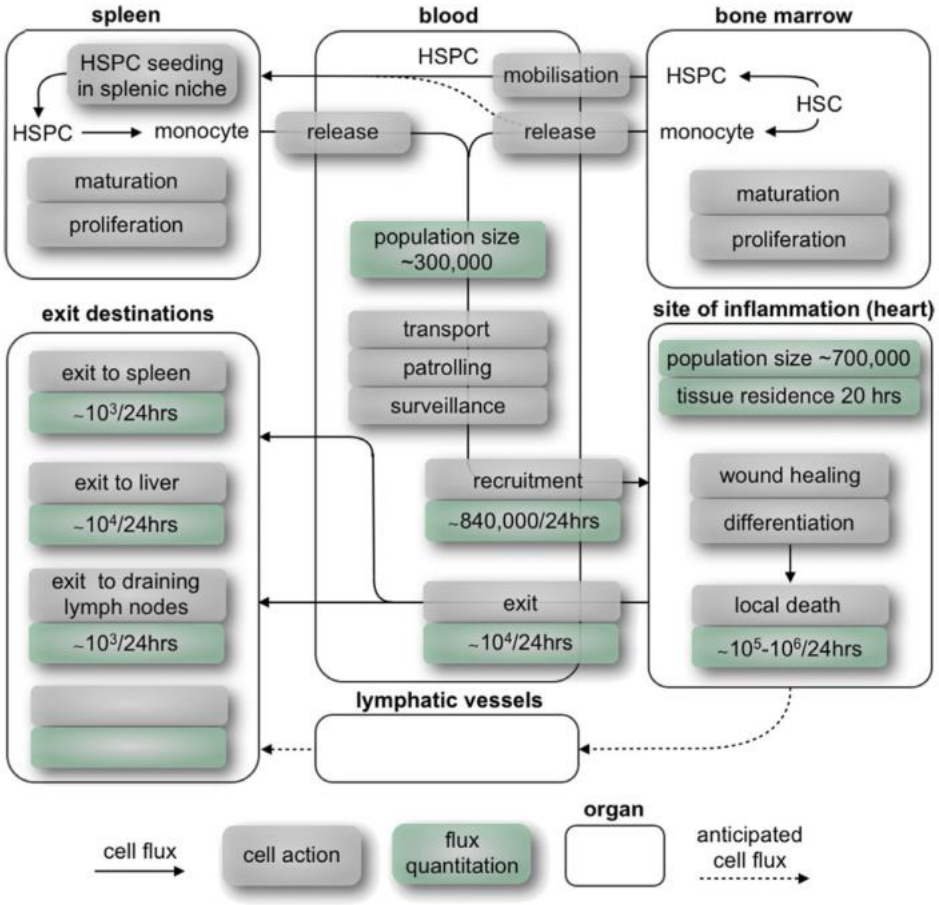


**Figure 3. Systemic monocyte kinetics in the inflammatory heart following MI [16]**

### 2.3 Macrophages as key regulators of cardiac repair

Macrophages and their circulating progenitors (monocytes) are key immune cells that respond to injury regardless of the type and location of injury. Ischemic injury and consequent loss of viable myocardium is followed by cardiac remodeling which includes

progressive changes in the molecular and structural components of the myocardium. Macrophages are a central protagonist in all these diverse processes [17, 48, 85]. However, the potential of these cells as a therapeutic target has only come to light following a series of recent findings on the macrophage heterogeneity, disposition, and in the context of injury, their source of deployment and kinetics of recruitment to the site of injury.

### 2.3.1 Heterogeneity of macrophage population

The recent color wheel classification of macrophage activation type presents three classes based on their activation type; The "classically" activated (M1 or pro-inflammatory) macrophages are induced by IFN-γ and/or bacterial endotoxin lipopolysaccharide (LPS) and characterized by the increased expression of nitric oxide synthase (NOS) and pro-inflammatory cytokines. The "alternatively" activated (M2 or reparative) macrophages are induced by IL-4 and/or IL-13 and characterized by the increased expression of Arginase 1 (Arg1) and mannose receptor 1 (Mrc1). The "regulatory" macrophages are activated by LPS in combination with immune complexes, IL-10 or apoptotic cells [26]. All these macrophages play specific functional roles; while classically activated macrophages display microbicidal activity, regulatory macrophages exhibit immune suppressive functions and alternatively activated macrophages play a role in tissue repair by producing anti-inflammatory cytokines, which mediate angiogenesis as well as ECM deposition [26, 34, 86]. However, macrophages exhibit remarkable plasticity, allowing them to adapt to changing environmental signals and adopt distinct activation states with specific functional roles, and even adopt hybrid phenotypes [17, 26].

### 2.3.2 Biphasic macrophage roles in inflammation and resolution

After MI, monocytes extravasate into the injured tissue and can give rise to inflammatory macrophages that accumulate at the target sites of injury. Interestingly, the

inflammatory response triggered by MI consists of two primary phases. During the first phase (~4 days), activation of cytokine and chemokine cascades lead to recruitment of the primary responders (neutrophils and pro-inflammatory Ly-6C$^{high}$ that differentiate into M1 like macrophages) to the infarct zone within a day of ischemic injury as shown by Figure 3. These cells carryout phagocytosis and wound debridement to clear dead cells and matrix debris. Pro-inflammatory cytokine/chemokine cascades and excessive production of ROS are key characteristics of this phase [17, 85, 87]. These biological functions are regulated by secretion of cytokines and growth factors: Ly-6Chigh monocytes express IL-1β, TNF-α, myeloperoxidase, matrix metalloproteinases. During the second phase (~5-7 days), resolution of inflammation takes place and the dominant population of monocytes/macrophages now represent a reparative phenotype (M2 or alternatively activated macrophages) which carries out matrix deposition, angiogenesis and remodeling [16, 17, 88].

It is well established that during the first phase of this inflammation, monocyte chemotactic protein 1 (MCP-1) release initiated by the humoral immune system effects following MI recruits C-C chemokine receptor type 2 (CCR2) expressing pro-inflammatory Ly-6C$^{high}$ monocytes to the myocardium [84, 88]. It was initially thought that a different population of monocytes (Ly-6C$^{low}$ monocytes) that can give rise to a reparative M2 like macrophages are recruited in a sequential manner partially brought on by Fractalkine ($CX_3CL1$) release during the secondary healing phase. However, the field is now increasingly of the view that pro-inflammatory macrophages or Ly-6C$^{high}$ monocytes are capable of changing or differentiating into a M2 like phenotype in response to changing signals around the injury or as a recent discovery suggests, via a molecular nuclear hormonal switch, Nr4a1 [89, 90]. These recent findings give support to the idea of channeling the macrophage response towards a favorable cardiac repair mode by providing appropriate cues to the healing myocardium. It has become increasingly clear that although the temporal singularity macrophages exhibit may be necessary for a

very early time window following MI, inflammation often exhibits self-propagating behavior that likely delays the inflammation resolution phase of cardiac wound healing (Figure 4). Therefore mitigating the pro-inflammatory response and/or promoting inflammation resolution are emerging as important targets in treating MI injury.

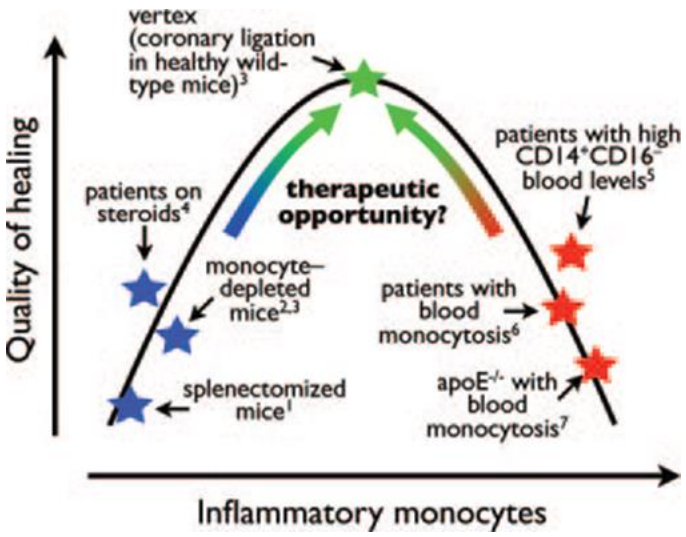


**Figure 4. Hypothetical relationship of monocyte numbers in the infarct and the healing outcome based on literature** (Figure from Nahrendorf et al 2010) **[17]**

### 2.4 Cardiac drug delivery systems

Many of the pharmacological therapies used in the clinical management of MI are systemically delivered and require multiple doses. The most modern drug delivery for the heart is achieved by drug eluting stents, but it is limited in the nature of therapeutics, expensive and placement is not ideal to localize/target the therapeutics to the myocardium, but rather to target vascular inflammation [91]. Local controlled delivery to the myocardium could be achieved via intramyocardial or transendocardial routes by exploiting advancements in catheter technology for minimally invasive delivery, reduced cost, shorter hospital times and potential for spatial and temporal control of administrations [92].

The underlying principal of controlled release systems is that a depot of drug is implanted in the body, and through multitude of factors including diffusion, degradation, or more sophisticated stimuli-sensitive release mechanisms, the drug is slowly administered to the affected area [93]. The ultimate goal of controlled delivery is that therapeutic concentrations of the drug can be sustained over a longer period of time with fewer administrations. This is especially crucial for biotechnology based therapeutics such as proteins and nucleic acids than the traditional small molecule drugs, as many of these biological molecules have short half-life in circulation or can have pleiotropic/toxic effects at high concentrations.

However, cardiac-specific drug delivery vehicles are scarce, and controlled delivery is reported as one of the major challenges that face regenerative cardiology today [12]. One of the main challenges is that the heart is an extensively vascular organ subjected to constant blood flow, and therefore even localized delivery is challenging as therapeutics are quickly washed into the bloodstream, diluting the effective local concentration. Biomaterials that can provide sustained release formulations therefore present an attractive solution to this problem. Biodegradable polymers are most commonly explored for controlled drug delivery, and the most widely used are polyesters such as PLGA. Although not used for drug delivery directly to the myocardium, PLGA has been used as stent coating and in cardiac tissue engineering applications[94]. However, the hydrolysis and degradation products of microspheres based on these polymers are acidic, and they can lead to denaturation of pH sensitive proteins and cause an inflammatory response [95], thus making them less a less desirable material in the context of the inflammatory heart diseases. In this section, we discuss few of the most promising biomaterials for controlled delivery formulations of proteins and nucleic acids to the heart.

### 2.4.1 Protein delivery

Besides the ability for controlled and sustained release over prolonged periods of time, successful implementation of biomaterials for delivery of proteins to the myocardium depends on a variety of important factors including preservation of bioactivity, biocompatibility/lack of immunogenicity, controlled degradation with non-toxic metabolites and ease of functionalization for incorporation/encapsulation of proteins. Furthermore, the material must be robust, and endure the fatigue cycling of the heart throughout the course of the delivery. If a biomaterial patch were to be used, mechanical properties that match that of the myocardium would be ideal as they can also provide mechanical support to the infarcted heart, influencing cardiac remodeling favorably [96]. Despite the numerous studies evaluating synthetic and natural materials for such properties, many of them have not yet been resolved for a single system. Traditional hydrophobic polymeric drug delivery vehicles have shortcomings when it pertains to protein delivery, as traditional organic solvents used in microencapsulation of small-molecule drugs could potentially denature proteins.

#### 2.4.1.1 Hydrogels as protein delivery platform for the myocardium

Hydrogels are cross-linked networks of hydrophilic polymers. They are porous, capable of retaining large amounts of water yet remain insoluble and maintain their 3D structure. The theoretical loading efficiency could be almost 100% (limited only by the solubility of the protein being encapsulated) inside a 1% weight percentage hydrogel since 99% in this case constitutes of water. These properties make them ideal reservoirs of protein therapeutics as they help preserve protein structural integrity and stability within the porous network. Injectability into the myocardium is a design criterion if these materials are to be delivered as injectable hydrogel. To ensure injectability, however, the material must facilitate loading into a catheter, fast gelation kinetics at the site but avoid premature gelation and catheter blocking. Advances in biomaterial design and fabrication

processes have led to tunable synthetic hydrogels engineered with physical or biochemical stimuli responsive gelation and/or degradation properties. These stimuli could include temperature, pH, enzymatic, redox, UV light and laser [97]. In order to achieve controlled protein delivery of proteins using hydrogel materials, the mesh size in the fibrous 3-D matrix has to match the particular size and composition of the protein molecule being delivered [98, 99], and it is this area that warrants further studies to optimize delivery systems to achieve desired release profiles for various proteins. The most established strategy is increasing the weight percentages of the macromer to form stiffer gels with smaller mesh size, but striking a balance of increased stiffness with injectability is challenging. Other approaches, discussed in detail in section 6.3 include physically tethering the therapeutics to the hydrogel to slow down the release. Further, while designing biomaterials for therapeutic protein delivery, it is critical to ensure that they are released in biologically active forms. This process of protein denaturation could occur at various stages of the process including the process of encapsulation, protein's residence in the gel solution, or the release process.

An immense number of hydrogels have been developed and studied for a number of biomedical applications such as tissue engineering, contact lenses, drug delivery and coating for stents and catheters [100]. Naturally derived hydrogel scaffolds include extracellular matrix (ECM) proteins such as collagen, gelatin, matrigel, chitosan, hyaluronic acid or decellularized ECM and bioinspired self-assembling peptides. These materials are often supplemented with synthetic hydrophilic hydrogels, such as poly(ethylene glycol) (PEG) in order to improve mechanical properties or incorporate other functionalities [101]. Among these, self-assembling peptides are perhaps the most studied for protein/cellular delivery applications following MI [102-104]. Self-assembling peptides have numerous inherent advantages amenable to protein delivery. Specifically advantageous for delivery to the heart is their lack of immunogenicity, biocompatibility and the ability to form stable nanofiber hydrogels that are injectable,

which allows catheter-based approaches in the context of MI. Peptides for self-assembly can be easily produced from naturally occurring building blocks with extreme sequence flexibility. This incredible advantage of programmability allows for rational design and modification of a scaffold network for properties desired in various applications.

Among the synthetic hydrogels, polyethyleneglycol (PEG) has been the gold standard biomaterial extensively studied due to their inertness, biocompatibility, and the synthetic ease with which chemical modifications could be made change material properties [97, 105]. However, only few studies have explored PEG hydrogels in the application of post-MI [33, 106, 107]. Our group has previously studied a 4-arm PEG macromere end-functionalized with maleimide groups reactive with cysteines groups. Peptides with cysteines groups can be functionalized with ease on to this hydrogel as cross-linkers or cell-adhesion peptides motifs (RGD, a motif that binds to integrins) or even a therapeutic peptide/proteins with free cysteines. This hydrogel demonstrated excellent *in situ* gel formation upon injection into the myocardium, as the Michael-type addition reaction occurs rapidly to crosslink the gel at $37^0$C. This thesis work further evaluates this material for immunomodulatory cytokine IL-4 delivery to the myocardium.

### 2.4.2 Nucleic acid delivery

The applications of nucleic acid delivery in the context of heart disease are numerous [8, 108-111]. Gene delivery and delivery of gene regulating nucleic acids such as siRNA/antisense/miRNA/mRNA or the catalytic Deoxyriobozyme (DNAzyme) [28, 112, 113] as well as the recent advent of genome editing sgRNA of the CRISPR/Cas9 system are of great interest as a therapeutic modality to the heart because of their potency in manipulating gene expression. However, successful translation of this class of therapeutics to the clinic is severely limited by the challenges in designing efficient and specific delivery systems to drive cellular uptake of these highly negatively charged molecules [114, 115], and further, sequestration by lysosomes make delivery into the

cytosol difficult [115, 116]. Transfection of phagocytic immune cells such as macrophages is especially challenging due to the presence of potent degradative enzymes that disrupt nucleic acid integrity [117]. Apart from viral delivery for genes, the most successful delivery vehicles for nucleic acids to date are cationic lipid nanoparticles or cationic polymers that facilitate condensing of nucleic acids via electrostatic interactions[116, 118]. However, cellular cytotoxicity induced by the positive charges of these vehicles make them less suited for therapeutic applications in the inflammatory myocardium following MI [118, 119]. Current methods being inadequate, successful applications of RNAi technology will require more research into appropriate carriers and efficient packaging of siRNA to improve local and systemic delivery in vivo.

2.4.2.1 Polyketal nanoparticles as nucleic acid delivery vehicles

Polyketals (PKs) are a new class of delivery vehicles formulated from a novel class of polymers which contain pH sensitive, hydrolyzable ketal linkages in their backbone. Unlike the predominantly polyester based delivery vehicles (PLGA) currently in use, PKs do not generate acidic degradation products as they degrade into neutral, biocompatible components acetone and diols, and are ideal for applications in an inflammatory disease context without evoking further immune response [120]. The polymerization strategy is such that it is possible to form polymers between any diol and 2,2-dimethoxypropane affording great flexibility for generating biomaterials with properties such as variable hydrolysis and pH sensitivities suitable for a variety of applications [120-125]. The properties of PKs can be easily modified to alter particle size, shape and porosity. Among these, the polyketal copolymer PK3 formed by reacting the diols cyclohexanedimethanol and 1,5-pentanediol with 2,2-diethoxypropane
makes an excellent delivery vehicle for siRNA due to its faster hydrolysis at the acidic pH of the endosome (hydrolysis half-life of 1.8 days at pH 4.5 and 39 days at pH 7.4), thus allowing for escape from the phago/endosomes into the cytoplasm for gene

silencing. [123]. Oligonucleotides are first charge-neutralized by ion-pairing with a cationic lipid molecule prior to nanoparticle formulation, and previous work from our laboratory demonstrates that after phagocytosis, these particles hydrolyze and cause an osmotic imbalance in the phagosome, leading to release of siRNA into the cytoplasm in a timely manner [123]. Additionally, PK3 is a hard material that is water insoluble and can maintain their integrity in vivo due to the high energy cost of being exposed to water, providing serum stability [122, 123].

#### 2.4.2.2 Spherical nucleic acids

Spherical nucleic acids (SNA) are polyvalent nucleic acid−nanoparticle conjugates employed for gene silencing. These spherical nanostructures were first described by Mirkin's group with gold cores and densely functionalized with highly oriented nucleic acid shell and subsequently adapted for various commercial applications and other nucleic acid delivery applications [31, 126-128]. These particles exhibit unique abilities to efficiently transfect cell membranes without the need for co-carriers. Furthermore, they exhibit cooperative hybridization to complementary nucleic acids for efficient gene silencing (for instance, siRNA functionalized gold particle hybridizing to target mRNA for gene silencing). These properties are akin to similar nanostructures widely employed in nature such as the assembly of enzymes at the lipid membrane to enhance substrate channeling or alter catalytic activity.

# CHAPTER 3 Polyketal nanoparticle mediated siRNA delivery as an anti-oxidant therapy following myocardial infarction

## 3.1 Introduction

Ischemic injury and consequent loss of viable myocardium is followed by adverse cardiac remodeling which includes progressive changes in the molecular and structural components of the myocardium [129] that eventually lead to cardiac dysfunction. An early step in this process is the inflammatory reaction that begins with the influx of neutrophils and macrophages in the infarcted area of the myocardium followed by invasion of myofibroblasts that deposit non-contractile scar tissue [4]. Production of excessive amounts of reactive oxygen species (ROS) is a key event involved in this pathogenesis [40, 52, 130, 131]. At high levels of ROS, cells undergo oxidative stress leading to many of the injury associated changes: proinflammatory cytokine release, cardiomyocyte apoptosis, interstitial fibrosis, fibroblast proliferation and myocyte hypertrophy [51, 57]. Although surgical reperfusion, angioplasty and thrombolysis have been traditionally used to restore blood flow to the ischemic myocardium, re-introduction of coronary flow triggers further production of ROS, a phenomenon known as reperfusion injury, causing further damage to the myocardium [39, 40]. Scavenging ROS have received great attention due to their contributions to reperfusion injury as evidenced by animal studies where overexpression or delivery of antioxidants has reduced myocardial injury in the setting of ischemia and reperfusion [53-56].

Among all the potential sources of ROS in the heart, NADPH oxidase, with Nox2 as the catalytic subunit, has been identified as a major source for cardiac superoxide levels ($O_2^-$) and has been shown to be upregulated locally in neutrophils, macrophages and myocytes following MI in both animal models in human patients [19-21, 51, 57-59]. Complete knockout of Nox2 prevents cardiomyocyte apoptosis and adverse remodeling

following experimental MI in mice, and improves cardiac function [51]. Moreover, Nox2-NADPH oxidase is implicated in a direct functional role in the pathogenesis of Angiotensin-II induced cardiac hypertrophy [59]. In another study, $Nox2^{-/-}$ mice were shown to exhibit attenuated interstitial fibrosis following aortic constriction, suggesting a possible role for Nox2-NADPH on cardiac remodeling post-MI [60]. These studies highlight the therapeutic potential of targeting Nox2-NADPH in the remodeling heart in order to prevent heart failure in MI patients. Despite these results, clinical studies are lacking due to the unavailability of a Nox2-specific inhibitor. This is critical as other members of the Nox family, specifically Nox4, offer protection against cardiac remodeling and hypertrophy [132, 133]. With specific inhibitors to NADPH oxidase lacking, silencing Nox2-NADPH oxidase gene expression in macrophages, the primary responders to ischemic injury, is an exciting potential therapeutic target to improve cardiac function and prevent progression heart failure following MI.

RNA-mediated silencing (siRNA) of gene expression holds great promise as therapeutics owing to high specificity and potency. However, delivery barriers for siRNA therapeutics have slowed down the successful translation of RNAi therapeutics into the clinic [114, 115]. Renal clearance and serum RNAses considerably reduce the half-life of naked siRNA in the blood stream [115]. Additionally, siRNA is highly membrane impermeable, and even upon endocytosis, endosomal escape into the cytosol for binding to the RNAi machinery is another challenging barrier to overcome [115, 116]. Further, endosomal/phagosomal compartments of macrophages contain nucleases that disrupt nucleic acid integrity to a larger extent, and therefore successful transfection of macrophages is especially challenging [117]. Chemical modifications that increase the stability of siRNA have had limited success due to often compromised RNA silencing activity and the expensive nature of these modifications [116]. Evolved delivery methods include complexing of siRNA to cationic lipids or polymers [116, 118]. However, inherent toxicity and the positively charged surface characteristics that elicit immune

responses deem such vehicles undesirable for in vivo disease applications [118, 119], especially for an inflammatory disease such as post-MI cardiac dysfunction.

Here, we demonstrate use of acid-degradable polymers, polyketals [120, 123, 125], as delivery vehicles for Nox2 specific siRNA to the post-MI environment. Polyketals have controllable release kinetics and neutral degradation products and therefore cause minimal inflammatory responses [124]. The polyketal PK3 was chosen for this application due to its fast hydrolysis rate [120, 122, 123]. An endosomal disruptive molecule, chloroquine, was co-encapsulated with siRNA in order to enhance the endosomal escape of delivered siRNA [123]. Nox2 siRNA was delivered to macrophages and Nox2 expression and activity were evaluated, as well as whether this could be used as a delivery vehicle in vivo following MI.

## 3.2 Materials and Methods

### 3.2.1 Synthesis of polyketal PK3

PK3 was synthesized as described in Sungmun Lee et al [123]. Briefly, the diols, cyclohexanedimethanol and 1,5-pentanediol were dissolved in distilled benzene and heated to $100^0$C. Recrystallized p-toluenesulfonic acid (PTSA) was dissolved (~1 mg) in ethyl acetate and added to the benzene solution to catalyze the reaction. The polymerization reaction was initiated by the addition of equimolar 2,2-diethoxypropane (DEP). Additional 2,2-dimethoxy propane (DMP) and benzene were subsequently added to the reaction to compensate for loss of volume in the form of Ethanol/methanol and the solvent benzene that had distilled off. After 48 h, the reaction was stopped with triethylamine and isolated by precipitation in cold hexanes. The solid polymer was then filtered off, rinsed in hexanes and vacuum dried prior to storage at $-20^0$C. Polymer molecular weight/Polydispersity was determined by gel permeation chromatography.

### 3.2.2 Preparation and characterization of siRNA loaded PK3 particles

Double stranded Nox2-siRNA (mouse) (sense strand: 5'AGAGUUUGGAAGAGCAUAAUUUAGA3') and a universal negative control siRNA (siNeg) were custom made (IDT) to contain a fluorescent FITC label. Fluorescent (FI)-siNox2 or FI-siNeg was ion-paired to the cationic lipid N-[1-(2,3-Dioleoyloxy)propyl]-N,N,Ntrimethylammonium methylsulfate (DOTAP) as shown in Figure 5. Briefly, 1 mg siRNA in water and 2.2 mg of DOTAP dissolved in dichloromethane (DCM) were brought to one phase by addition of 1.05 mL of methanol. Following 15 min incubation, an additional 0.5 mL of water and DCM were added and the mixture was vortexed, and centrifuged at 750 rpm for 5 min. The siRNA:DOTAP complex in the bottom organic layer was encapsulated in PK3 via an oil/water single emulsion procedure, using DCM as the oil phase and polyvinyl alcohol (PVA) as the surfactant stabilizer [120]. Empty particles containing DOTAP not ion-paired to siRNA were also prepared to control for any effect on cells from DOTAP. Next, 1 mL of DCM containing ion paired FI-siRNA was added to 40 mg of PK3 with 1 mg of chloroquine free base. This solution was homogenized into 8 mL of 5% (w/v) PVA solution at the highest setting in the Power Gen 500 (Fisher Scientific) for 30 seconds, and sonicated at an intermediate speed (Sonic dismembrator model 100, Fisher Scientific) with 10 pulses of 1 sec duration. The emulsion was then dispersed in a 20mL 0.5% PVA solution and stirred for a period of 4-5 hours to allow the DCM to evaporate. The resulting particles were isolated by centrifugation (15000 rpm, 20min), washed three times, freeze-dried and stored in $-20^0$C until further use. Particle size and shape were determined by scanning electron microscopy (Zeiss SEM Ultra60).

### 3.2.3 Quantitation of siRNA loading efficiency of PK3 particles

FI-siNox2 particles, FI-siNeg siRNA particles and empty PK particles were prepared as described above. In order to determine loading efficiency of siRNA within PK3, 2-3mg of particles were dispersed in a 1N HCl solution and incubated for 1 hr to allow for complete hydrolysis. Afterwards, the solution was neutralized with 1N NaOH solution, and the fluorescence of the total FI-siRNA released from the particles was measured (ex/em=494/510nm) using a fluorescent plate reader (Biotek Synergy 2). A fluorescent standard curve previously constructed using the FI-siRNA was compared against the obtained fluorescent intensity blank subtracted from any background fluorescence from empty PK particles in order to calculate the loading efficiency of prepared particles.

### 3.2.4 Particle uptake by macrophages

RAW 264.7 macrophages obtained from American Type Culture Collection (ATCC number: TIB-71) were maintained at $37^0$C under a humidified atmosphere of 5% $CO_2$ in Dulbecco's Modified Eagle's Medium (DMEM) containing 10% (v/v) fetal bovine serum (FBS), supplemented with penicillin (100U/mL) and streptomycin (100mg/mL) and 2mM L-Glutamine. For flow cytometry, macrophages ($1x10^6$ cells) were incubated with PK-FI-siNox2 (1µg siRNA) for 24 hours. Cells were then washed three times with ice cold phosphate buffered saline (PBS) and scraped into tubes for flow cytometry. Untreated control cell population was used to gate population of interest and the fluorescent population was measured by flow cytometer (FACSCalibur, Becton Dickinson) using a laser for fluorescein ($l_{ex}/l_{em}$ = 494/510 nm) and analyzed using FlowJo (TreeStar, Inc).

In order to confirm the intracellular distribution of siRNA delivered by PK3 particles, we used laser scanning confocal microscopy (Zeiss LSM 510 META). RAW264.7 macrophages treated with PK-FI-siNox2 particles for 6 hours (1µg siRNA).

Cells were then washed in PBS three times and stained with DAPI for nuclei and rhodamine-phalloidin for actin filaments.

### 3.2.5 *In vitro* delivery of Nox2-siRNA particles

For gene expression studies, RAW264.7 macrophages were plated in 6-well plates at a density of $1x10^6$ cells/well in 10% FBS DMEM media and left to adhere overnight. The following day, cells were treated with PK-siNox2, PK-siNeg, or empty PK3 particles at a concentration of particles equivalent to 1 µg siRNA/well or equivalent amount of empty particles. Following 24 hours of treatment, the cells were harvested and RNA extracted using Trizol (Invitrogen) for gene expression analysis. For assessment of functional activity of Nox2-NADPH in macrophages following treatment, RAW macrophages were plated at a density of $2x10^5$ cells/well in 24-well plates and treated with 1µg siRNA/well or equivalent amount of empty particles as above for 72 hours following which cells were subjected to analysis of $O_2^-$ production.

### 3.2.6 Gene expression

Total RNA from cells was isolated using Trizol (Invitrogen) according to the manufacturer's protocol. Complementary DNA (cDNA) was synthesized using SuperScript III kit (Invitrogen). Quantitative real-time PCR (qRT-PCR) was performed using Power SYBR Green (Invitrogen) master mix with Applied Biosystems StepOne Plus real time PCR system and the following primer pairs were used: Nox2, 5' GTT GGG GCT GAA TGT CTT CCT CTT T 3' (forward primer) and 5' CCA CAT ACA GGC CCC CTT CAG 3' (reverse primer); 18s rRNA, TTCCTTACCTGGTTGATCCTGCCA (forward primer) and AGCGAGCGACCAAAGGAACCATAA (reverse primer). Nox2 gene expression levels were normalized relative to the endogenous housekeeping gene 18s rRNA and expressed as a fold change compared to expression levels in untreated cells.

### 3.2.7 Detection of extracellular superoxide *in vitro*

To determine Nox2 activity, extracellular production of $O_2^-$ following stimulation with phorbol-12-myristate 13-acetate (PMA) was measured. To determine levels of $O_2^-$ following treatments in vitro, quantitative dihydroethidium (DHE) measurements were taken. DHE reacts with $O_2^-$ to form a cell impermeable, characteristic fluorescent product, 2-hydroxyethidium (ex=360nm, em=567nm) that can be measured quantitatively using HPLC [134-138] and/or a fluorescent plate reader. Following 72 hours of particle treatment in 24-well plates, media was aspirated from the wells containing RAW macrophages and washed carefully with fresh cold Krebs-Hepes buffer (KHB) at a pH of 7.35. Then KHB was added to all wells and 10 µM PMA (Sigma) added to the appropriate wells. Following incubation with PMA for 10 min at $37^0$C, 20 µM DHE (Sigma) was added to both PMA stimulated and unstimulated wells under dark conditions and incubated for 20 minutes while obtaining kinetic readings using a fluorescent plate reader (Biotek Synergy 2), after which 100 µl of the extracellular buffer from each well was taken in 300 µl of methanol for quantitative DHE-HPLC (reverse phase-HPLC over an acetonitrile gradient, (ex=360nm and em=570 nm) analysis [137].

### 3.2.8 Myocardial infarction and particle injection

A randomized and blinded study was conducted using adult male C57BL/6 mice 8 weeks of age weighing 25g. Mice were assigned to treatment groups (n=7-10) using a random number generator and the animal surgeon was only given letter codes to identify groups. While one group was subjected to sham surgery, the other four groups received myocardial infarction. Animals were subjected to myocardial infarction surgeries as described [121, 124]. Briefly, the animals were anesthetized (1-3% isoflurane) and following tracheal intubation, the heart was exposed by separation of the ribs. Myocardial infarction was performed by ligation of the left anterior descending coronary artery. For groups receiving particle injections, immediately after coronary artery ligation, 50 µL of

one of the following was injected into the cyanotic ischemic zone (3 locations) through a 30-gauge needle while the heart was beating: empty PK3 particles, PK-siNeg particles or PK-siNox2 particles. The dose of siRNA injected was 5μg/kg or the corresponding amount of empty PK3 particles. Following injection, the chests were closed and animals were allowed to recover on a heating pad until functional assessments were made at 3 days following MI surgery using echocardiography. These studies conformed with the Guide for the Care and Use of Laboratory Animals published by the US National Institutes of Health (NIH Publication No. 85-23, revised 1996) and all animal studies were approved by Emory University Institutional Animal Care and Use Committee.

### 3.2.9 *In vivo* gene expression

Animals were then sacrificed and left ventricle tissue was harvested and subjected to Trizol extraction for RNA isolation. Following reverse transcription of obtained left ventricle tissue RNA, the cDNA was subjected to qPCR for the gene expression analysis of Nox2 and the house keeping gene 18s rRNA. The copy numbers of Nox2 mRNA present in the tissue per million copies of 18s rRNA was determined using the quantitative standard curve method and results were normalized to copy number ratios from sham animals in order to minimize batch-to-batch variability in tissue processing.

### 3.2.10 Echocardiography

Anesthetized rats were subjected to echocardiography at 3 days following MI surgery. Short axis values of left ventricular end systolic (ES) and end diastolic (ED) dimension were obtained using a Vevo 770 small animal ultrasound system (Visualsonics). An average of 3 consecutive cardiac cycles was used for each measurement and was performed three times in an investigator-blinded manner. Fractional shortening was calculated as (end-diastolic diameter – end-systolic diameter)/end-diastolic diameter and expressed as a percentage.

### 3.2.11 Statistics

All statistical analyses were performed using Graphpad Prism 5 software. Quantitative results were presented as means ± SEM. Statistical comparisons were performed by one way analysis of variance (ANOVA) followed by the appropriate post-test as described in the figure legends. P values of less than 0.05 were considered significant.

## 3.3 Results

### 3.3.1 Characterization of PK-siRNA particles

The encapsulation efficiency of siRNA within the PK3 particles was evaluated following ion-pairing with DOTAP as well as the final single oil/water emulsion step. Efficiency of ion-pairing was > 98% as measured by the fluorescence reading of the remaining FI-siRNA in the aqueous phase following extraction of DOTAP:siRNA into the organic phase. After particles were generated, hydrolysis confirmed 10 µg of siRNA per 1 mg of particle, or roughly 40% encapsulation efficiency. Further, particles were analyzed by SEM and the particle diameter measurements were made and averaged using ImageJ. As the representative image and histogram in Figure 5 demonstrate, particles ranged from 200-1200 nm with an average size of 500 ± 175 nm.

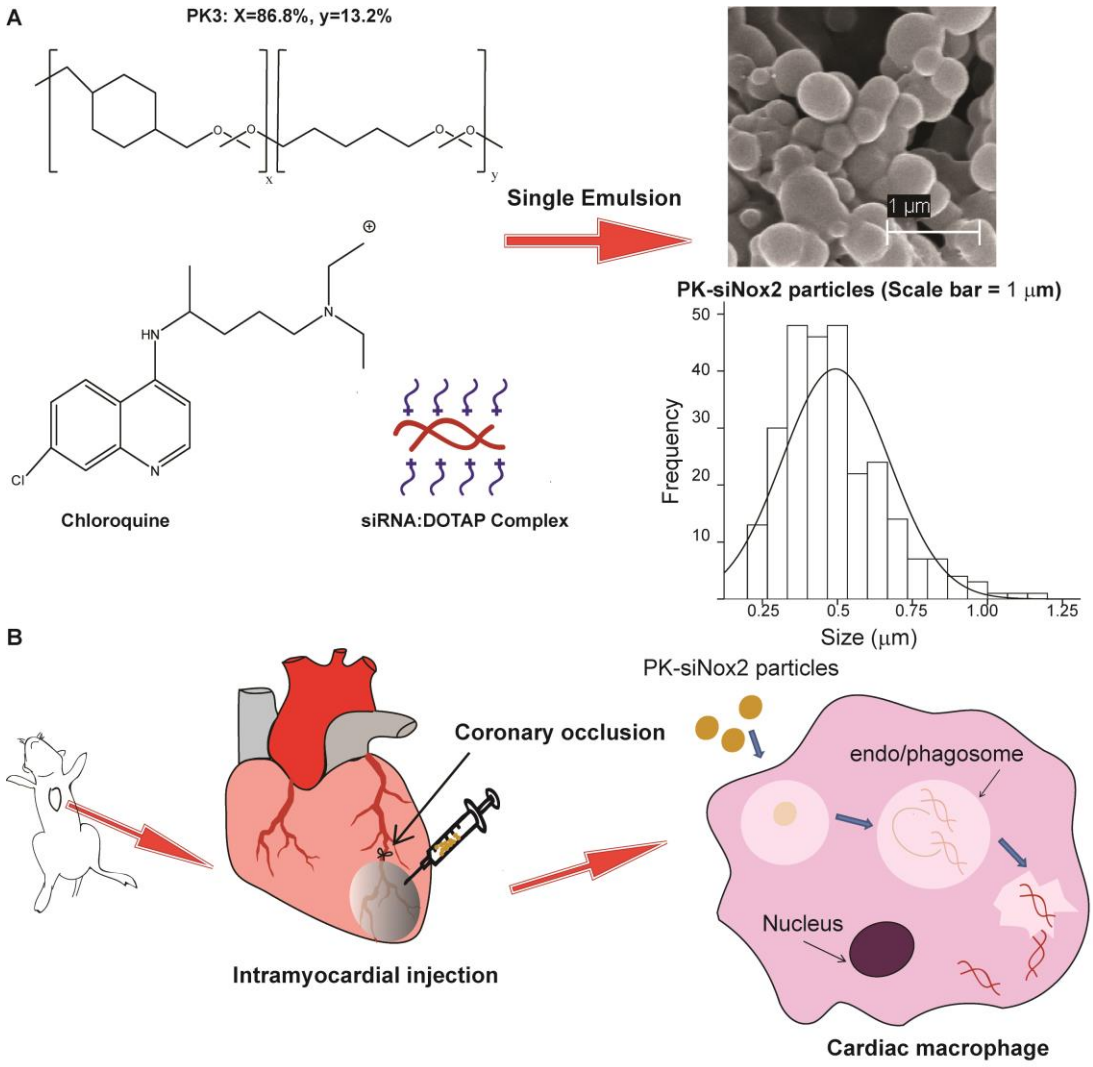


**Figure 5. Schematic of PK-siNox2 particle formulation and delivery.**
(A) Ion-paired siRNA:DOTAP and endosomal disruptive agent chloroquine are encapsulated into the PK3s via a single emulsion/solvent evaporation procedure generating submicron particles (500 ± 175 nm). (B) The PK3s encapsulating siRNA are intramuscularly injected into mice hearts following permanent coronary occlusion (MI) surgery. The particles are taken up my macrophages in vivo with high efficiency due to their ability to protect siRNA from serum proteins and stimulate phagocytosis and/or endocytosis. Once taken up, they degrade in the acidic environment within these compartments due to the acid-sensitive ketal linkages in PK3 (also aided by chloroquine) and escape the phagosome/endosome via a colloid osmotic mechanism to release siRNA into the cytoplasm.

### 3.3.2 Particle uptake by macrophages

Internilization of PK-siNox2 particles by macrophages was determined by flow cytometry. Macrophages treated with FI-siNox2 loaded PK3 particles (at 1 µg siRNA/well) for 24 hours demonstrated >80% uptake as shown in the representative histogram in Figure 6A. Further, confocal microscopy confirmed that the particles were not just sticking to the cell surface, but were internalized and localized within the cellular cytoplasm as shown in the representative 2D image and z-stack image (Figures 6B&C).

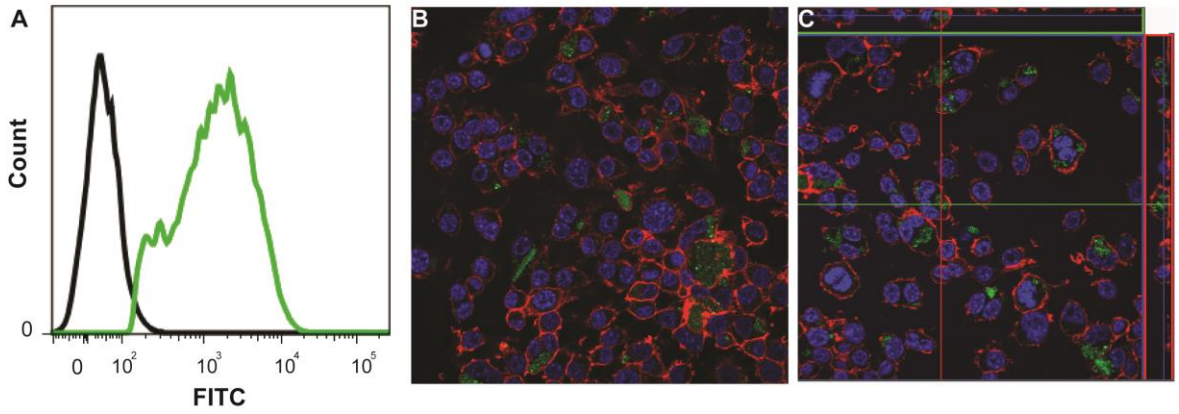


**Figure 6. *In vitro* particle uptake by macrophages.** RAW macrophages were treated with FITC labeled siRNA loaded PK3 particles. (A) Following 24 hours of treatment, flow cytometry was used to determine the percentage of FITC positive cells (Green) that are indicative of percent uptake of PK-FI-siNox2 particles compared to the control cell population (Black). Following 6 hours of treatment, cells were imaged using confocal microscopy to visualize cytoplasmic localization of siRNA. A representative 2D image (B) and Z-stack image (C) confirm internalized siRNA within macrophages. FI-siNox2 (green). Nucleus (Blue, DAPI), Actin filaments (Red, Rhodamine phalloidin).

### 3.3.3 *In vitro* gene knockdown

To determine whether Nox2-siRNA particles knockdown Nox2 mRNA expression in vitro, we investigated the efficacy of Nox2-siRNA particles in the mouse macrophage cell line RAW 264.7. Following 24 hours of treatment, total RNA was isolated from cells and Nox2 mRNA expression levels were analyzed via qRT-PCR. Results were normalized to Nox2 expression levels in untreated macrophages. Figure 7 demonstrates that PK-siNox2 particles knocked down Nox2 mRNA expression by 41.3 ± 10.0%

compared to the Nox2 expression levels in the untreated macrophage group ($p<0.05$), empty PK3 ($p<0.01$) and PK-siNeg ($p<0.05$) treatment groups. The empty PK3 particle and PK-siNeg particle treatment groups did not show any significant difference from the untreated cells.

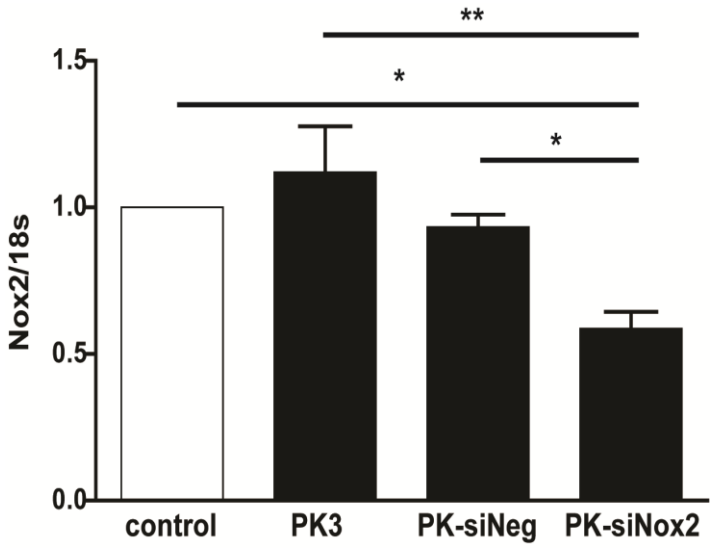


**Figure 7. *In vitro* Nox2 mRNA expression.** Grouped data (mean ± SEM; n=3 per group) from 1 day following treatment of RAW macrophages. There was a significant decrease in Nox2 mRNA expression only in the PK-siNox2 treatment group compared to the untreated, empty PK3 and PK-siNeg particle treated groups. Gene expression was evaluated by qRT-PCR using a $\Delta\Delta C_T$ method, and the results were normalized to 18S expression and reported as fold changes in mRNA expression (*$p<0.05$, **$p<0.01$; One-way ANOVA followed by Newman-Keuls Multiple Comparison post-test).

### 3.3.4 *In vitro* functional knockdown

To determine whether gene knockdown by Nox2-siRNA particles resulted in functional changes, we treated RAW macrophages for 72 hours with similar particle formulations as in the gene expression studies and then stimulated with PMA to induce $O_2^-$ production. The fluorescent DHE dye was then added in to the cells to determine kinetic activity of Nox2-mediated $O_2^-$ production over a 20 minute period of time. The fluorescent intensity was expressed as fold changes in $O_2^-$ production as normalized to basal $O_2^-$ levels. As shown in figure 8A, the traces from all treatment groups except PK-siNox2 treatment exhibited similar levels of fold increase in $O_2^-$ production while PK-

siNox2 treatment showed little fluorescence over the entire 20 minute reading. These results were further confirmed by quantitative DHE-HPLC that PK-siNox2 treated macrophages demonstrated a significant reduction in Nox2 activity ($p<0.05$) compared to empty PK3 particle treatment (Figure 8B).

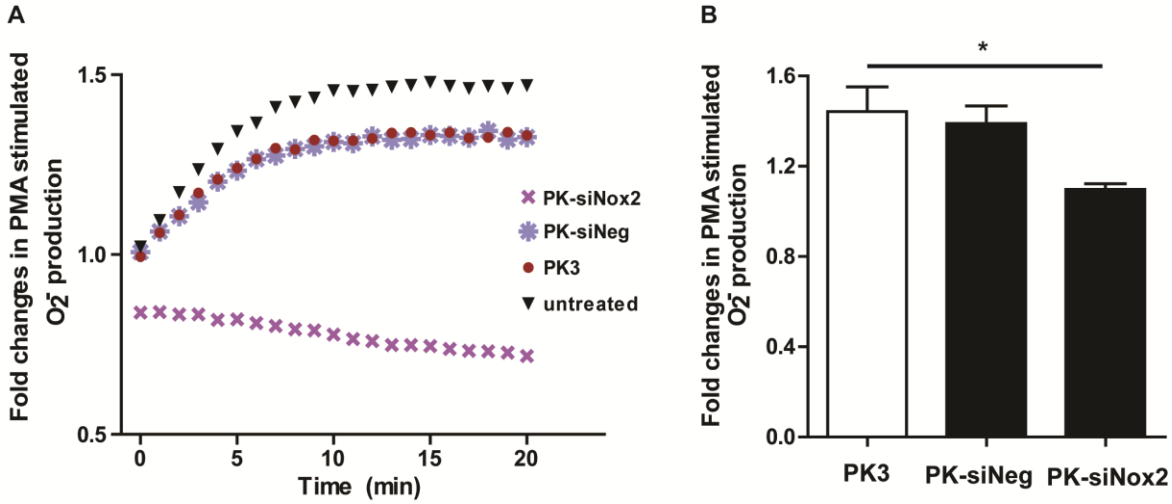


**Figure 8. *In vitro* Nox2-NADPH activity.** Grouped data (mean ± SEM; n=4 per group) from 3 days. (A) Kinetic measurement of PMA-stimulated $O_2^-$ production from macrophages using DHE fluorescence. (B) There was a significant decrease in the production of $O_2^-$ in PK-siNox2 treated macrophages compared to the empty PK3 treatment group as quantitatively measured by DHE-HPLC method (*$p<0.05$ vs. empty PK3; one-way ANOVA

### 3.3.5 PK-siNox2 delivery *in vivo*

To determine the *in vivo* efficiency of siRNA delivery using polyketal particles, adult male C57BL/6 mice were randomized into 5 treatment groups. While one group was subjected to sham surgery, the other four groups received MI surgeries followed by either no injections (MI) or injections of either empty PK3 particles (MI + Empty PK3), negative control siRNA encapsulating PK3 particles (MI + PK-siNeg) or siNox2 containing PK3 particles (MI + PK-siNox2) ($n\geq8$ for each group, $N=47$ total). At 3-days following injury, the expression of Nox2 at the mRNA level increased significantly ($P<0.01$) in MI group by 2.50±0.30 fold compared to sham mice. The treatment groups receiving Empty PK3 or PK-siNeg particle injections following MI showed no

differences in Nox2 mRNA expression compared to the group receiving MI alone. In contrast, mice receiving PK-siNox2 particles following MI demonstrated a significantly lower levels of Nox2 mRNA expression than the MI group ($P$<0.05) (Figure 9). In order to determine the specificity of siRNA delivery towards the Nox2 isoform, Nox4 mRNA expression levels were also analyzed. There was a trend towards an increase in Nox4 mRNA expression in all animals that received MI although it was not statistically significant. There was no observed knockdown of Nox4 mRNA expression in any treatment groups (Figure A2).

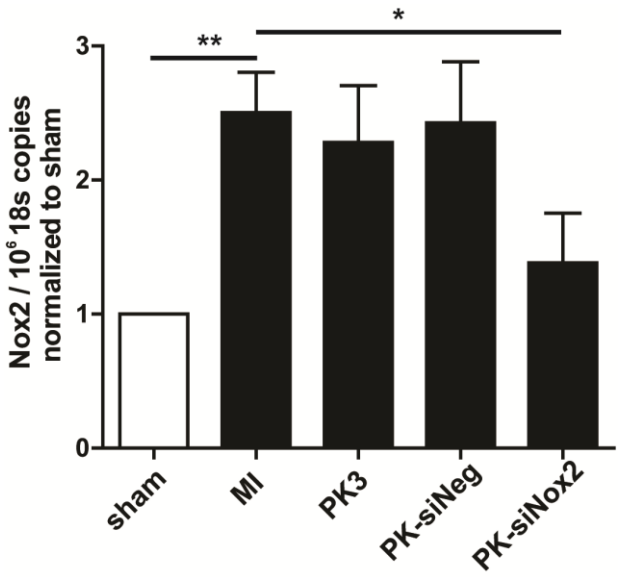


**Figure 9. *In vivo* Nox2 mRNA expression.** Grouped data (mean ± SEM; n≥8 per group) from 3 days. There was a significant increase in Nox2 mRNA expression in animals that received an MI compared to sham. Among treatment groups, there was a significant decrease in mRNA expression only in the PK-siNox2 treated mice compared with untreated MI group. Gene expression was evaluated by qRT-PCR using the quantitative standard curve method, and the results were normalized to 18S levels and reported as fold changes in copy number of mRNA levels compared to sham animals (*p<0.05; **p<0.01 vs. MI; one-way ANOVA followed by Dunnett's Multiple Comparison post-test).

### 3.3.6 Cardiac function following myocardial infarction

To determine the effect of sustained PK-siNox2 delivery on cardiac function following acute MI, echocardiography data was collected three days after MI surgery as described in methods. As shown in Figure 10, MI significantly reduced cardiac function (p<0.05) as measured in absolute change in fractional shortening 3 days post-injury

compared to sham animals. While there was no effect of empty PK3 or PK-siNeg particles, PK-siNox2 particles significantly ($p<0.05$) improved function, restoring it to sham levels.

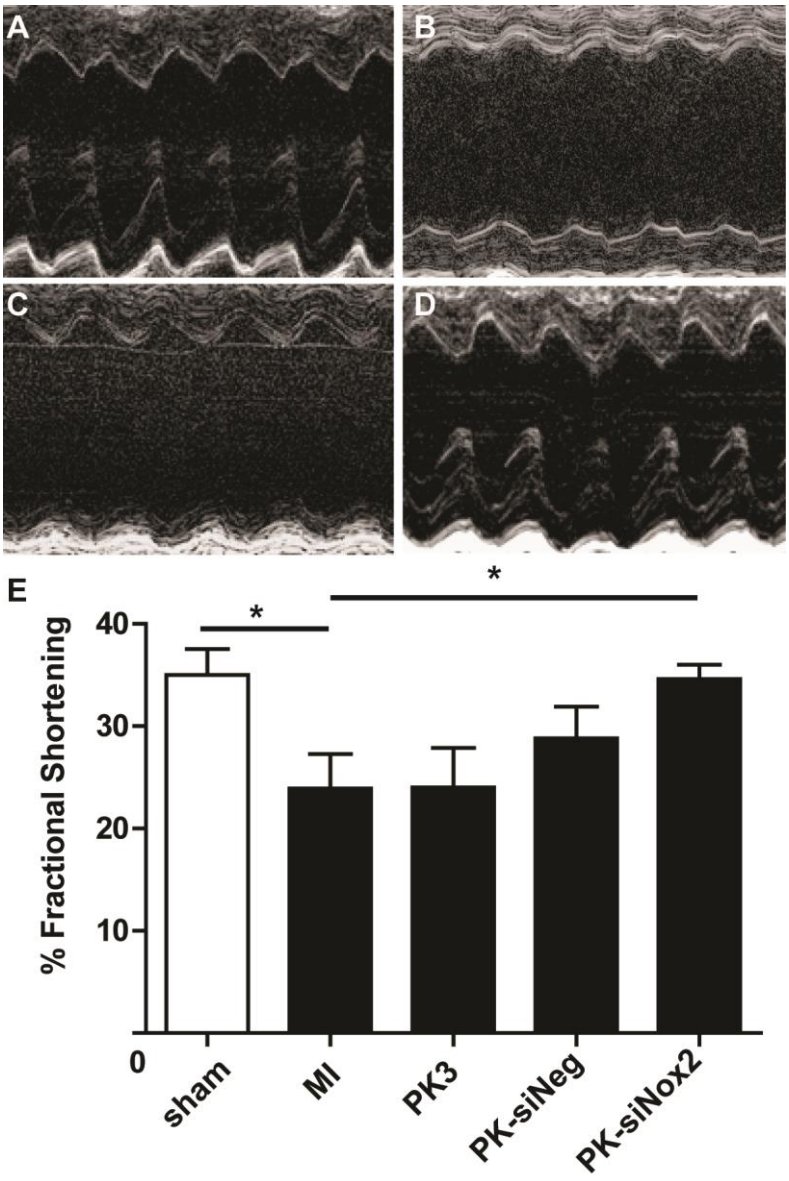


**Figure 10. Echocardiographic measurement of function.**
Grouped data (mean ± SEM; n≥4 per group) from 3 days. There was a significant decrease in function animals that received an MI compared to sham. Among treatment groups, there was a significant increase in function only in the PK-siNox2 treated mice compared with untreated MI group (*$p<0.05$; vs. MI; one-way ANOVA followed by Dunnett's Multiple Comparison post-test).

## 3.4 Discussion

Considerable evidence supports a role for oxidative stress due to excessive ROS such as $O_2^-$ in the progression of HF [40, 50, 52]. Chronic antioxidant treatment following MI in animal models improves myocyte survival, attenuates ventricular remodeling, and leads to partial preservation of left ventricular function [53, 55]. While chronic antioxidant therapy may be feasible, the damage to the myocardium is local and oxidant signaling may be critical for homeostasis in many tissues. Therefore a localized and sustained antioxidant treatment that could be achieved by RNAi silencing during the critical earlier inflammatory stage following MI could be beneficial for the treatment of acute MI.

NADPH oxidases are major sources of $O_2^-$ in the heart. [21, 50]. Originally identified in phagocytes of the innate immune system, they play a critical role in host defense by releasing a burst of $O_2^-$ from molecular oxygen using NADPH as an electron donor. The prototypic NADPH oxidase of the phagocytes is a multisubunit enzyme complex consisting of a membrane-bound cytochrome $b_{558}$ composed of $p22^{phox}$ and the catalytic subunit $gp91^{phox}$ (Nox2), and in association with four cytosolic regulatory subunits following activation. Over the past decade, there has been much interest in the cardiovascular NADPH oxidases [51, 57]. A family of $gp91^{phox}$ homologues termed Nox (Nox1-5) form the basis of distinct NADPH oxidases. Nox2 is expressed in macrophages, cardiomyocytes, fibroblasts and endothelial cells and significantly upregulated in the myocardium following MI [51, 57]. Despite the fact that there are 5 distinct Nox family members, there are no specific inhibitors for any subtype. These proteins all have different functions in many cell types and there is strong evidence suggesting that broad inhibition of NADPH oxidase activity can exacerbate ischemic injury [133]. Therefore great care is needed to ensure specific targeting in relevant cells.

In this report, we successfully encapsulated Nox2-specific siRNA into the acid sensitive polyketal PK3 particle for silencing of the Nox2 gene in cardiac macrophages

and inactivation of NADPH oxidase. Polyketals (PKs) are a class of polymers with tunable pH sensitivity afforded by the hydrolyzable ketal linkages in their backbone. They are highly suitable for applications in an inflammatory disease setting compared to other predominantly polyester based delivery vehicles such as PLGA currently in wide use that generate acidic degradation products. PKs degrade into neutral, FDA approved components, acetone and diols. [120-125]. This property of biocompatibility presents a unique advantage for siRNA delivery to the inflammatory heart following MI as compared to cationic lipid particles that cam exert cytotoxicity, potentially further damaging the mycoardium. The polyketal PK3 chosen for this study exhibits faster hydrolysis rates (half-life of 1.8 days at pH 4.5 and 39 days at pH 7.4) as reported in a previous study from our laboratory where PK3 was used to deliver TNF-α siRNA to liver macrophages *in vivo* [123]. This property makes PK3 an excellent delivery vehicle for siRNA as it can be degraded quickly at the acidic pH of the endosome, allowing for early endosomal escape prior to degradation in the late endosomal compartments. Published studies from our laboratory demonstrate that polyketal nanoparticles are retained in the myocardium following injection and are stable at neutral pH levels [121, 124]. When engaged by macrophages, present in high quantities during MI, particles are taken up and trafficked into phagosomes/endosomes where they degrade due to the acidic environment. Although the mechanism of release of siRNA is not clearly known, it is speculated that after phagocytosis/endosomes, these particles hydrolyze and potentially cause an osmotic imbalance within these compartments, leading to release of siRNA into the cytoplasm in a timely manner.

As the schematic in Figure 5A illustrates, siRNA was loaded into PK3 particles in two steps. Firstly, the siRNA is ion paired to the cationic lipid DOTAP and the siRNA:DOTAP complex is extracted into the organic layer with greater than 95% efficiency. Chloroquine was then added to the complex and subsequently subjected to an oil-in-water single emulsion/solvent evaporation procedure to generate particles ranging

from 200-1200 nm and averaging 500 nm. Addition of another pH sensitive molecule such as chloroquine to these pH sensitive polymeric vehicles enhances their ability to be hydrolyzed at low pH of the endosomes/phagosomes while maintaining their integrity at the physiological pH of 7.4. Further, the weak base chloroquine gets protonated in the acidic environment of endo/phagosomal compartments, triggering swelling and destabilization of their membranes to facilitate release of siRNA into the cytoplasm [139]. Since chloroquine can inhibit acidification and maturation of endosomes, it can also protect siRNA from degradation. Additionally, complexing siRNA with a cationic lipid such as DOTAP can enhance siRNA transfection ability by increasing siRNA stability and aiding in endosomal escape [140-142]. Further, in a previous study from our laboratory, complexing with DOTAP was shown to render nanoparticles with a positive charge which enhances phagocytosis by macrophages [125]. While we did not see toxicity with DOTAP in this or prior studies, alternative cationic molecules such as spermidine could be used in the future. Additionally, by altering the homogenization speeds and/or the sonication speeds during single emulsion procedure, we were able to obtain varying size distributions (Figure A1). The mechanism of particle internalization by macrophages is dependent on particle size, and accordingly, the size range chosen for our experiments facilitates uptake by both endocytosis as well as phagocytosis [143-145]. The siRNA loading efficiency of PK3 particles was calculated to be around 40%, which amounts to about 10μg siRNA/mg of particles. This loading efficiency allowed us to conduct *in vitro* and *in vivo* studies at less than 0.1mg/mL and 1mg/mL particle concentrations respectively.

As depicted in Figure 5B, for *in vivo* studies, these particles were delivered into the heart via intramyocardial injection into the infarct zone of mice immediately following MI surgery. Two key requirements for the successful delivery of siRNA are cellular uptake and endosomal escape [114, 115]. We demonstrate the efficient cellular uptake of these particles *in vitro* by macrophages using flow cytometry following

treatment of RAW 264.1 macrophages with fluorescently labeled siRNA loaded PK-FI-siNox2 particles (Figure 6A). This high transfection efficiency (>80%) in especially hard-to-transfect-macrophages demonstrates the ability of these particles to be efficiently taken up. Further, using confocal microscopy, we observe non-punctate, diffuse fluorescence inside cells (Figure 6B-C) indicating that the siRNA is not trapped in endosomes, but localized in the cytoplasm.

We then investigated whether PK3 particles could deliver functional siRNA into macrophages and inhibit Nox2 gene expression and function *in vitro*. Compared to untreated cells, PK-siNox2 particles demorated significant reduction in Nox2 mRNA expression while PK-siNeg and empty PK3 particles showed no effect (Figure 7). In order to confirm the corresponding impairment in function due to the knockdown of Nox2 mRNA expression, we stimulated macrophages with PMA following particle treatment. PMA is known to stimulate Nox2-specific extracellular $O_2^-$ production in macrophages [146-148]. While other Nox isoforms are expressed, recent studies demonstrate that Nox4 mainly produces hydrogen peroxide and is likely an intracellular source [149].Thus, measuring the extracellular superoxide production in macrophages upon PMA stimulation can serve as an appropriate assay for Nox2 activity [134, 136]. The kinetic traces as well as the quantitiave results from the DHE-HPLC method (Figure 8A-B) demonstrate the ability of PK-siNox2 particle tretament to significantly reduce the PMA induced $O_2^-$ production by macrophages compared to empty PK3 particle treatment.

Encouraged by our *in vitro* functional results, we then investigated the ability of PK-siNox2 particles to knockdown Nox2 mRNA expression *in vivo*. At an acute 3-day time point following experimental MI, delivery of PK-siNox2 significantly reduced the Nox2 mRNA levels in LV tissue compared to MI only, as well as empty and negative control siRNA loaded PK3 particle injections (Figure 9). In most siRNA delivery studies, targeting cells such as macrophages is known to be difficult and requires high doses upwards of 2mg/kg doses at multiple time points [125, 150] while our study

demonstrated gene silencing at a low dose of 5μg/kg animal. We also sought to confirm the specificity of siRNA mediated knockdown of Nox2 by determining the mRNA expression of the structurally related Nox4 isoform in these tissue samples and demonstrated that the Nox4 mRNA levels are unchanged due to PK-siNox2 treatment (Figure A2). Corresponding to the Nox2 mRNA expression knockdown, an improvement in cardiac function was observed in this treatment group compared to MI alone with no effect from controls treatments (Figure 10). These results corroborate with published studies where upregulation of Nox2-NADPH expression and derived ROS was shown to play significant role in the pathophysiology of human congestive heart failure (CHF) [19] and genetic deletion of Nox2 in transgenic mice demonstrated significantly improved cardiac function and remodeling response [51].

Increased ROS in the heart can impact cardiac remodeling and function via several mechanisms. Most ROS are key signaling molecules and are critical in maintaining cellular homeostasis. Aberrant activation of redox-sensitive signaling pathways following ischemic injury can alter gene expression and has been implicated in cardiac hypertrophy, fibrosis and remodeling leading to cardiac dysfunction [151-153]. However, this study did not investigate the mechanistic aspect for the beneficial restoration in cardiac function observed in Nox2-siRNA treated MI animals. Additionally, the chronic effects of Nox2-siRNA delivery such as its effect on fibrosis as well as long-term functional improvement will need to be studied to determine whether higher dosage or repeated injections or targeting of other cardiac cell types that also upregulate Nox2-NADPH oxidases are necessary to sustain benefits of knocking down Nox2 at the initial inflammatory stage following MI. While limitations exist, our results uphold Nox2-NADPH as an important target in the treatment of acute-MI, and further, establish polyketals as biocompatible siRNA delivery vehicles to the myocardium.

# CHAPTER 4 Catalytic DNA modified gold particles as anti-inflammatory therapeutics to the infarcted heart

## 4.1 Introduction

During the early stages of the cardiac repair process, loss of viable myocardium triggers a dynamic network of molecular and structural processes designed to compensate for lost function as well as repair the wound [4, 154, 155]. An early step crucial for this healing process is the inflammatory reaction that begins with the influx of neutrophils and macrophages that absorb the necrotic tissue [18, 36, 37, 84, 88, 90, 155, 156]. However, the delicate equilibrium of the myocardial inflammation is critical for an optimal healing response. Unbridled inflammation fueled by continuous up-regulation of pro-inflammatory cytokines can exacerbate tissue damage, thus contributing to adverse cardiac remodeling and non-contractile scar formation that ultimately culminates in heart failure [35, 41, 44, 80, 81, 157]. Specifically, the pro-inflammatory cytokine TNF–α is shown to be crucially involved in this pathogenesis and progression of myocardial injury. The pathological mechanism for TNF–α mediated myocardial dysfunction is thought to occur through a combination of factors that includes induction of reactive oxygen and nitrogen species, initiation of pro-inflammatory cytokine cascades and down-regulation of contractile proteins [22, 23, 64-75]. However, several reports have also indicated that TNF–α involvement in the early repair process as a double-edged sword in that physiological levels of TNF–α can be cardioprotective [68, 70, 82, 83]. Therefore, selection of an optimal therapeutic window as well as duration of action are critical in targeting TNF–α as an anti-inflammatory therapy in order to suppress the elevated inflammatory response immediately following MI.

Despite the numerous pre-clinical studies highlighting the therapeutic potential of targeting TNF–α in the remodeling heart, human trials employing TNF–α antagonists have failed to prove clinical benefit in chronic heart failure patients [158, 159]. Failure

analyses of these studies showed that these protein based therapeutics could act as agonists and stabilizers of TNF–α and even induce cytotoxicity in cells, which renders them highly unsuitable as therapeutic candidates in the context of heart failure [159, 160]. Gene silencing therapeutics derived from nucleic acid oligomers (ssDNA or siRNA) are excellent candidates since they are potent, yet transient in regulating TNF–α expression. We investigated catalytic DNA, a novel modality of gene silencing molecules, to inhibit TNF–α mRNA. These DNA enzymes (DNAzymes) are composed of a 15 base catalytic core and flanked by two recognition arms that can selectively degrade target mRNA independent of RNAi, thus avoiding the need to hijack the host cell's machinery for catalysis [161]. Compared to siRNA mediated gene silencing, they offer the added advantages of enhanced stability (DNA versus RNA), cost-effecive synthesis and lack of immune response caused by double stranded RNA [162, 163]. However, delivery of therapeutic nucleic acids is an immense challenge due to the difficulties in getting highly negatively charged oligomers across a cell membrane and protecting them from nuclease-mediated degradation [161, 164]. The most mature delivery approach involves complexing oligonucleotides to cationic lipids or polymers. Although very efficient, the positive charges often elicit an immune response which renders such vehicles unsuitable for applications post-MI, a disease setting characterized by inflammation [118, 119, 165]. A powerful, yet emerging approach for transfection entails spatially organizing therapeutic oligonucleotides into a compact spherical nanostructure.[166] Such structures enable very efficient transfection through a scavenger receptor mediated mechanism without eliciting an inflammatory response.[167] In fact, transfection is so efficient that spherical nucleic acids have been shown to readily enter a mouse's epithelial layer to regulate EGFR expression and even cross the blood brain barrier to treat glioblastoma.[168, 169]

In previous work, when functionalized in similar spherical nucleic acid structures, DNAzymes exhibited enhanced catalytic gene silencing activity *in vitro* [170]. Here we describe, to the our knowledge, the first *in vivo* use of DNAzyme-gold nanoparticle conjugates as potent gene regulation agents following MI. Specifically, we show these particles can regulate TNF–α both *in vitro* in primary macrophages and *in vivo* in a rat model of MI without eliciting an immune response, and even favoring an anti-inflammatory response.

## 4.2 Materials and Methods

### *4.2.1* Gold-DNAzyme nanoparticle synthesis

Citrate-stabilized gold nanoparticles (AuNP; 14±3 nm) were prepared using published procedures.[171] A 500 mL solution of 1 mM hydrogen tetrachloroaurate(III) trihydrate solution was brought to a vigorous boil, and once boiling, 50 mL of a 38.8 mM sodium citrate tribasic dihydrate solution was added and allowed to reflux for 15 min. The reaction mixture was filtered using a 0.45 μm acetate filter, producing monodisperse AuNPs. The resonance wavelength of the gold nanoparticles was determined using UVvis spectrometry, and particle size was determined using transmission electron microscopy (TEM).

### *4.2.2* Preparation of DNAzyme-functionalized gold nanoparticles

Disulfide-modified oligonucleotides at either the 3’ end were purchased from Integrated DNA Technologies (IDT). The disulfide was reduced to a free thiol by incubating 50 nmols of lyophilized oligonucleotide with 1.0 mL of disulfide cleavage buffer (0.1 M dithiothreitol (DTT), 170 mM phosphate buffer at pH 8.0) for 3 hours at room temperature. The reduced oligonucleotides were purified using a NAP-25 column (GE Healthcare, Piscataway, NJ) with Nanopure water as the eluent. Subsequently, 40 nmol of DNA was added to 10 mL of 14 nm gold nanoparticles (10 nM), bringing the

final concentration of oligonucleotide and gold nanoparticles to ~3.0 μM and ~7.0 nM, respectively. The pH of the solution was adjusted to pH 7.4 by adding $1/10^{th}$ the total volume (~133 μL) of 100 mM phosphate buffer, thus bringing the phosphate buffer concentration to 9 mM. The particles were stabilized by adding sodium dodecyl sulfate (SDS) to the solution and bringing the SDS concentration to 0.1% (g/mL) by using a stock solution of 10% SDS. The particles were successively salted with eight NaCl additions that were spaced 20 min apart using a stock solution of 2.0 M NaCl and 10 mM phosphate buffer. The final NaCl concentration of the DNA AuNP solution was increased to 0.7 M. The first two NaCl additions increased the concentration by 0.05 M increments, while the remaining six NaCl additions increased the NaCl concentration by 0.1 M increments. The particles were immediately sonicated for 10 s after each salt addition to maximize DNA packing, as indicated in literature.[172] Fully salted particles were then incubated overnight, in the dark at room temperature. We found that the 10-23 active catalytic core of the DNAzyme had a tendency to drive the formation of nanoparticle aggregates at 0.7 M NaCl due to partial self-complementarity of sequences. The formation of these aggregates did not result in any observable reduction in the quality of the particles (as measured by UVvis, TEM, DNA density, and ultimately TNF–α knockdown). The particles were stored as a stock solution (high salt and excess DNA) at 4℃ until needed for a maximum duration of 1 month. This was due to diminished activity over time for washed particles stored in Nanopure water as shown in (Figure A3) (no salt or excess DNA). Prior to knockdown studies, particles were centrifuged four times at 13,500 RPM, filtered using a 0.2 μm syringe filter, and reconstituted in PBS. Quantitation of DNAzyme loading density

The commercial Quant-iT$^{TM}$ OliGreen® ssDNA kit was used to determine the total DNAzyme density per particle. The Quant-iT$^{TM}$ OliGreen® ssDNA kit required preparation of a calibration curve by diluting a DNA stock solution (4 μg/mL) composed of the same thiolated oligonucleotide used during particle functionalization to 0.1, 0.2,

0.5, 0.75, 1.0, and 2.0 μg/mL at a final volume of 100 μL in 1x TE buffer. DNAzyme particle solutions were prepared by diluting a ~10 nM stock solution to 0.4, 0.6, and 0.8 nM with TE buffer. The oligonucleotides were then released from the particle through oxidizing/dissolving the gold with potassium cyanide (KCN) by adding 1 μL of a 5 M stock solution of KCN to each well, including the calibration wells to be consistent. The solutions were incubated with KCN for 30 min to ensure complete dissolution. After complete dissolution of the gold nanoparticles, 100 μL of the freshly prepared 1x Quant-iT$^{TM}$ OliGreen® solution was added to each well and fluorescence intensities (485/528 nm excitation/emission) of each well were then measured using a Bio-Tek Synergy HT plate reader to determine the total DNA density.

### 4.2.3 Cell culture

RAW 264.7 macrophages obtained from American Type Culture Collection (ATCC number: TIB-71) were maintained at 37°C under a humidified atmosphere of 5% $CO_2$ in Dulbecco's Modified Eagle's Medium (DMEM) containing 10% (v/v) fetal bovine serum (FBS), supplemented with penicillin (100 U/mL) and streptomycin (100 mg/mL) and 2 mM L-Glutamine. For primary macrophage culture, peritoneal macrophages were isolated from Sprague Dawley rats as described previously [173]. Briefly, cold PBS was infused into the peritoneal cavity of rats and cellular lavage was collected, spun down at 1000 x g at 4°C for 10 minutes, following which cell solution was resuspended in media described above. The cell solution was plated in 24-well plates ($3x10^6$ cells/well) and left to adhere overnight for treatment the following day. Primary single ventricular myocytes culture from Sprague Dawley rat hearts is described in Appendix section A.3.1.

### 4.2.4 Particle uptake by macrophages and myocytes

In order to confirm the intracellular distribution of DNA delivered by DNA modified gold nanoparticles, RAW264.7 macrophages or adult rat cardiomyocytes were

treated with Cy5 labeled DNAzyme functionalized gold particles for 1 hour (5 nM particle concentration equivalent to 666.7 nM DNA concentration) and then washed in PBS three times, fixed in 4% PFA and stained with DAPI for nuclei and calcein for macrophages or FITC Maleimide for cardiomycocytes to delineate the cell surface, and imaged using laser scanning confocal microscopy (Zeiss LSM 510 META) to identify Cy5 fluorescence within the cells to indicate internalization of Cy5-DNA modified gold particles. Further, particle uptake was compared to commercially available Lipofectamine® RNAiMAX reagent (Life Technologies) mediated transfection at 1, 4, 18 and 24 hours using fluorescence microscopy in live cells for macrophages, and in fixed cells at 18 hours for cardiomyocytes.

### *4.2.5* *In vitro* silencing of TNF−α with Dz particles

For TNF−α knockdown studies, peritoneal macrophages were treated with three types of particles: catalytically active TNF−α specific (Dz) or inactive but with antisense binding ability to TNF−α (i-Dz) or active but nonspecific (NS-Dz) at a particle concentration of 10 nM/well (1.3 μM DNA). After 20 hours of treatment, the media was removed and the cells were re-treated with the same concentration of particles while at the same time receiving stimulation with LPS (5 ng/ml) to induce TNF−α production. After 4 hours of stimulation, 100 uL of media was collected from each sample and analyzed for secreted TNF−α via ELISA according to the manufacture's protocol (eBioscience).

### *4.2.6* Cytotoxicity

Cytotoxicity of DNAzyme particles was compared with a commercially available, commonly used transfection reagent, using pro-inflammatory cytokine TNF−α itself as a surrogate cytotoxicity indicator. Primary peritoneal macrophages were transfected with either Lipofectamine® RNAiMAX containing scrambled DNA or NS-Dz for 20 hours,

and stimulated with LPS (5 ng/mL) for 4 hours to induce TNF–α production. Extracellular medium was collected and TNF–α production quantified by ELISA.

### 4.2.7 Myocardial infarction and particle injection

A randomized and blinded study was conducted using adult Sprague Dawley rats. The animals were assigned to treatment groups ($n$=6-9) using a random number generator and the animal surgeon was only given letter codes to identify groups. While one group was subjected to a sham surgery, the other four groups received myocardial infarction via permanent ligation of the left descending artery. Briefly, the animals were anesthetized (1-3% isoflurane) and following tracheal intubation, the heart was exposed by separating the ribs. Myocardial infarction was performed by ligation of the left anterior descending coronary artery. For groups receiving particle injections, immediately after coronary artery ligation, 100 µL of one of the following DNAzyme modified particles were injected into the cyanotic ischemic zone (3 locations) through a 25-gauge needle while the heart was beating: Dz, i-Dz or NS-Dz. The dose of DNAzyme injected was 0.07 mg/kg (100 nM particle concentration). Following injection, the chests were closed and animals were allowed to recover on a heating pad until functional assessments were made 3 days following MI surgery using echocardiography (Acuson Sequoia 512 with a 14 MHz transducer) and invasive pressure-volume hemodynamics (Millar Instruments). These studies conformed to the *Guide for the Care and Use of Laboratory Animals* published by the US National Institutes of Health (NIH Publication No. 85-23, revised 1996) and all animal studies were approved by Emory University Institutional Animal Care and Use Committee.

### 4.2.8 *In vivo* bioimaging

Rats were subjected to MI as described above and Cy5 labeled NS-Dz gold particle conjugates were injected in 3 areas in the border zone surrounding the infarct. Rats were sacrificed and the hearts, liver, spleen and kidneys were harvested and imaged

on days 0, 1, 2, and 3 post-injection (n=1 per time point) using Bruker In-Vivo Xtreme. The Cy5 fluorescent intensity in these organs was plotted as arbitrary fluorescence over time to demonstrate retention of the particles up to 3 days in the heart.

### 4.2.9 Echocardiography and Invasive pressure-volume hemodynamics analysis

In a separate study, rats were subjected to MI surgery and injections as described above, and 3 days post-surgeries and treatment anesthetized rats were subjected to echocardiography (Acuson sequoia 512) and invasive pressure-volume hemodynamics (Millar MPVS instruments) analyses to assess the functional effects of treatment. From echocardiography, short axis values of left ventricular end systolic (ES) and end diastolic (ED) dimensions were obtained. An average of 3 consecutive cardiac cycles was used for each measurement and was performed three times in by a blinded investigator. Fractional shortening was calculated as [(end-diastolic diameter – end-systolic diameter)/(end-diastolic diameter)] and expressed as a percentage. For invasive hemodynamics, the pressure-volume probe was inserted into the left ventricle. After stabilization, baseline left ventricular pressure-volume loops were recorded for at least 10 cardiac cycles and data averaged to get mean values for each animal. Data extracted include +dP/dT, -dP/dT and left-ventricular Ejection Fraction (%EF).

### 4.2.10 *In vivo* gene expression and plasma cytokine analysis

Following functional measurements at 3 days, animals were sacrificed and the left ventricle infarct tissue was harvested and homogenized, which the total RNA contents were isolated using Trizol (Invitrogen) according to the manufacturer's protocol. Complementary DNA (cDNA) was synthesized using SuperScript III kit (Invitrogen) and the quantitative real-time PCR (qRT-PCR) was performed using Power SYBR Green (Invitrogen) master mix with Applied Biosystems StepOnePlus$^{TM}$ real time PCR system. Absolute quantification method was employed to analyze gene expression levels of each of the target genes. Standard curves for each of the primer sets were constructed with

serial dilutions of input DNA templates and validated comparable amplification efficiencies (curve slopes: −3.32 to −3.64). Relative mRNA levels were obtained by extrapolation of Ct values from the slopes of the standard curve for each primer set. Gene expression levels were then normalized to the endogenous housekeeping gene GAPDH and further, expressed as fold changes compared to expression levels in sham animals in order to minimize batch-to-batch variability in tissue processing. Primer sequences used are listed in Appendix section A3.3.

Prior to sacrificing the animals, blood was collected via cardiac puncture, plasma separated from blood cells and stored in -70$^0$C until cytokine analysis using the Luminex multiplex analyzer system (Luminex LX100). A custom cytokine bead panel from ebioscience was used to analyze cytokines IL-12b, IL-1b, IL-6 and IL-10 in the plasma.

### 4.2.11 Statistics

All statistical analyses were performed using Graphpad Prism 5 software. Quantitative results were presented as means ± SEM. Statistical comparisons were performed by one way analysis of variance (ANOVA) followed by the appropriate post-test as described in the figure legends. P values of less than 0.05 were considered significant. To make the variance independent of the mean for gene expression data sets that had significantly different variances according to Bartlett's test (TNF-α, IL-12β and iNOS), statistical analysis was performed after logarithmic transformation

## 4.3 Results

### 4.3.1 Characterization of Gold DNAzyme particles

Citrate stabilized gold nanoparticles were synthesized by reducing chloroauric acid ($HAuCl_4$) with sodium citrate. The resulting particles were very homogeneous and monodisperse with a mean particle diameter of 14± 3 nm as determined by TEM analysis

and the extinction spectra showing a peak absorption at 525 nm correlating to the nanoparticle's surface plasmon resonance (Figure 11B-D). The particles were functionalized with Dz, i-Dz, or NS-Dz (Figure 11A) and had a DNAzyme density of 99±3, 109±7, and 65±2 oligonucleotides per nanoparticles respectively. This equates to a very high surface density ranging from 6 – 9 $nm^2$/DNA, sufficiently high to ensure optimal activity. It should be noted that NS-Dz has a slightly lower DNA density on the particle due to possessing a stable secondary hairpin structure. After washing, the DNAzyme functionalized particles had a strong surface plasmon resonance in the extinction spectra (Figure 11D).

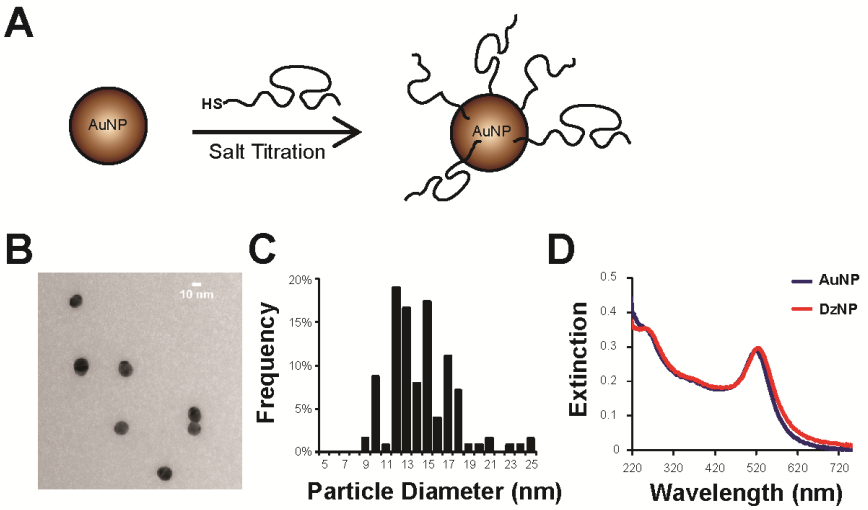


**Figure 11. Synthesis and characterization of DNAzyme-gold particles.**
(A) Schematic showing the approach to synthesize DNAzyme modified gold nanoparticles. Thiolated DNA was mixed with gold nanoparticles and the ionic strength was slowly increased over time. (B) Representative TEM image of the 14 nm citrate stabilized gold nanoparticles, where particle monodispercity was determined through a histogram analysis shown in (C). (D) Extinction spectra of citrate stabilized (AuNP) and DNAzyme functionalized gold nanoparticles (DzNP) showing the surface plasmon resonance at 525 nm.

### 4.3.2 Particle uptake by macrophages and myocytes *in vitro*

Cellular uptake of Cy5-NS-Dz gold nanoparticle conjugates were visualized and compared to cells transfected with the same concentration of DNA using commercially available transfection reagent Lipofectamine® RNAiMAX through a 24 hour period. At

every time point, macrophages transfected with Cy5-NS-Dz modified nanoparticles exhibited superior transfection efficiency compared to Lipofectamine® assisted delivery. Detectable fluorescence within the cells was only observed at 24 hours with Lipofectamine® transfection (Figure 12B, right), compared to the superior transfection by Dz particles as early as 1 hour (Figure 12A & 2B, left), and were continuously being taken up 24 hours later (Data not shown). Further, internalization and cytoplasmic

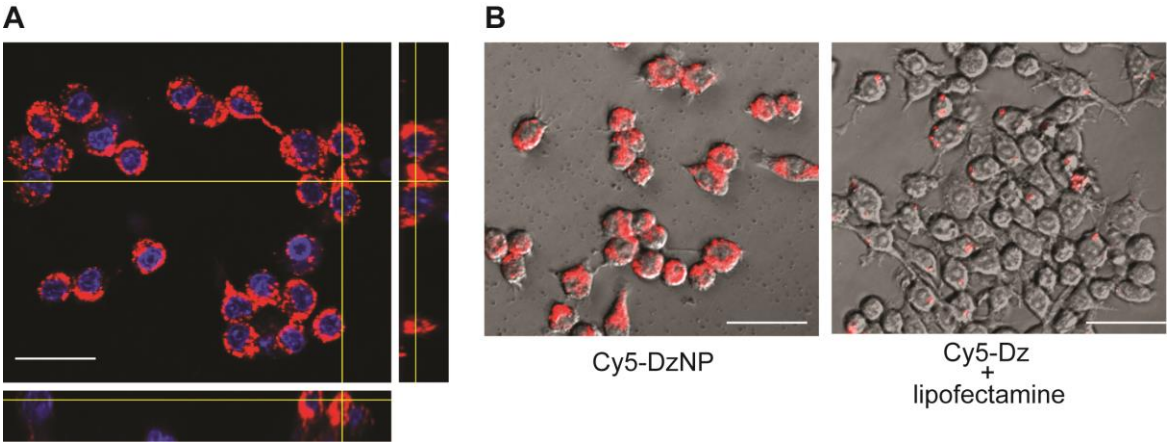


**Figure 12. *In vitro* Cy5-NS-DzNP particle uptake by macrophages.**
RAW 264.7 macrophages were treated with Cy5 labeled NS-DNA modified gold particles. Following 1 hours of treatment, cells were imaged using confocal microscopy to visualize cytoplasmic localization of Cy-5-DNA. (A) Representative Z-stack image confirms internalized DNA within macrophages (scale bar,30μm) (B, left) Uptake efficiency was compared in macrophages treated with Dz-particles at 1 hour and (B, right) lipofectamine® transfection reagent for 24 hours. DNA (red, Cy5), Nucleus (blue, DAPI). (Scale bar, 30μm).

localization within the cells was confirmed via confocal microscopy as shown by the orthogonal Z-slice in Figure A4. Although adult rat cardiomyocytes did not take the particles up as quickly as macrophages at 1 hour (data not shown), they showed internalization at 18 hours (Figure A5, left). At this time point, uptake of fluorescently labeled DNA by myocytes was not observed when Lipofectamine® RNAiMAX was used to transfect the DNA (Figure A5, right). Together, these data demonstrate that gold particles functionalized with DNA exhibit superior uptake efficiency than Lipofectamine® in macrophages and myocytes.

### 4.3.3 *In vitro* protein knockdown and cytotoxicity

To demonstrate the ability of DNAzyme to silence TNF-α expression in macrophages, we treated peritoneal macrophages with particles modified with either active DNAzymes specific towards TNF–α mRNA (Dz), inactive DNAzyme (i-Dz), or active but non-specific DNAzyme (NS-Dz) which were compared to the appropriate untreated controls for 24 hours (Figure 13A). Macrophages were activated with LPS at 20 hours to stimulate the production of TNF–α. Figure 13C shows that treatment of Dz modified nanoparticles resulted in ~50% reduction in TNF–α production as compared to cells that received no treatment with LPS stimulation ($p < 0.05$) or Dz loaded with a non-specific recognition sequence (NS-Dz) ($p < 0.01$). The NS-Dz and i-Dz particle treatment groups did not show any significant difference from the untreated cells stimulated with

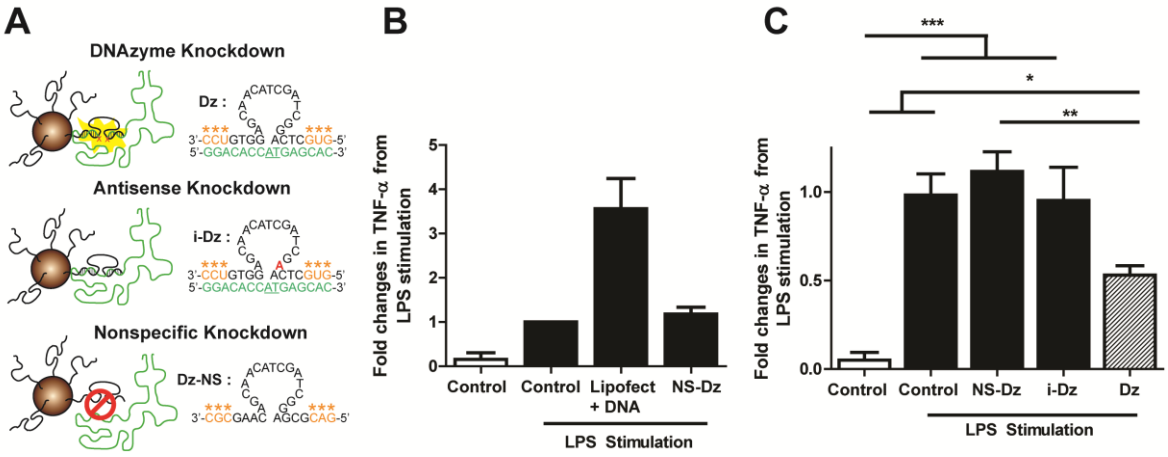


**Figure 13. Biocompatibility of DNAzyme-gold particles and *in vitro* TNF–α knockdown in primary rat peritoneal macrophages.** (A) Schematic of gold particles modified with either active DNAzymes specific towards TNF–α mRNA (Dz), inactive DNAzyme (i-Dz) specific to TNF–α mRNA but non-catalytic, or active but non-specific DNAzyme (NS-Dz). (B) Grouped data (mean ± SEM; n=3) from 1 day following treatment of peritoneal macrophages with commercial lipofectamine® + DNA complex induced several folds of TNF–α upregulation compared to untreated LPS stimulated cells while NS-Dz particles did not induce any additional cytotoxicity (C) Grouped data (mean ± SEM; n=6) showing a significant decrease in TNF–α protein levels in the Dz treatment group compared to the untreated and NS-Dz particle treated groups. Protein levels were measured by ELISA and the results were normalized to untreated LPS stimulated cells and reported as fold changes in TNF–α (*p<0.05, **p<0.01, ***p<0.001; One-way ANOVA followed by Tukey's Multiple Comparison post-test)

LPS. In addition, we discovered that NS-Dz exhibited no additional cytotoxicity, while cells treated with Lipofectamine® loaded with scrambled DNA sequence exhibited TNF–α concentrations that were 3.5 fold higher than with LPS stimulation alone (Figure 13B).

### 4.3.4 *In vivo* biodistribution

Bio-distribution and extent of myocardial retention of DNA-gold particles was examined by ex-vivo fluorescence image analysis in a rat model of MI (Figure 14A). As shown in Figure 14B-C, time course ex-vivo fluorescence imaging indicated that the DNA-gold particles were retained in the heart for up to 3 days, and higher retention was observed in the heart compared to the other organs up to day 2.

### 4.3.5 Cardiac function following myocardial infarction

To determine the effect of sustained Dz delivery on cardiac function following acute MI, echocardiography data and invasive hemodynamics measurements were collected 3 days after MI. As shown in Figure 15A, all groups receiving MI demonstrated significantly reduced cardiac function ($p < 0.001$) as measured in absolute change in fractional shortening 3 days post-injury compared to sham animals. While there was no effect for NS-Dz or i-Dz particle treated groups, Dz particle treatment significantly restored function by ~40% compared to MI ($p < 0.01$). The invasive hemodynamics measurements also indicate a trend towards improvement in % Ejection Faction (%EF) and parameters that measure the rate of change of pressure in the left ventricle chamber (dp/dt) in Dz particle treated group (Figure A6 A-B).

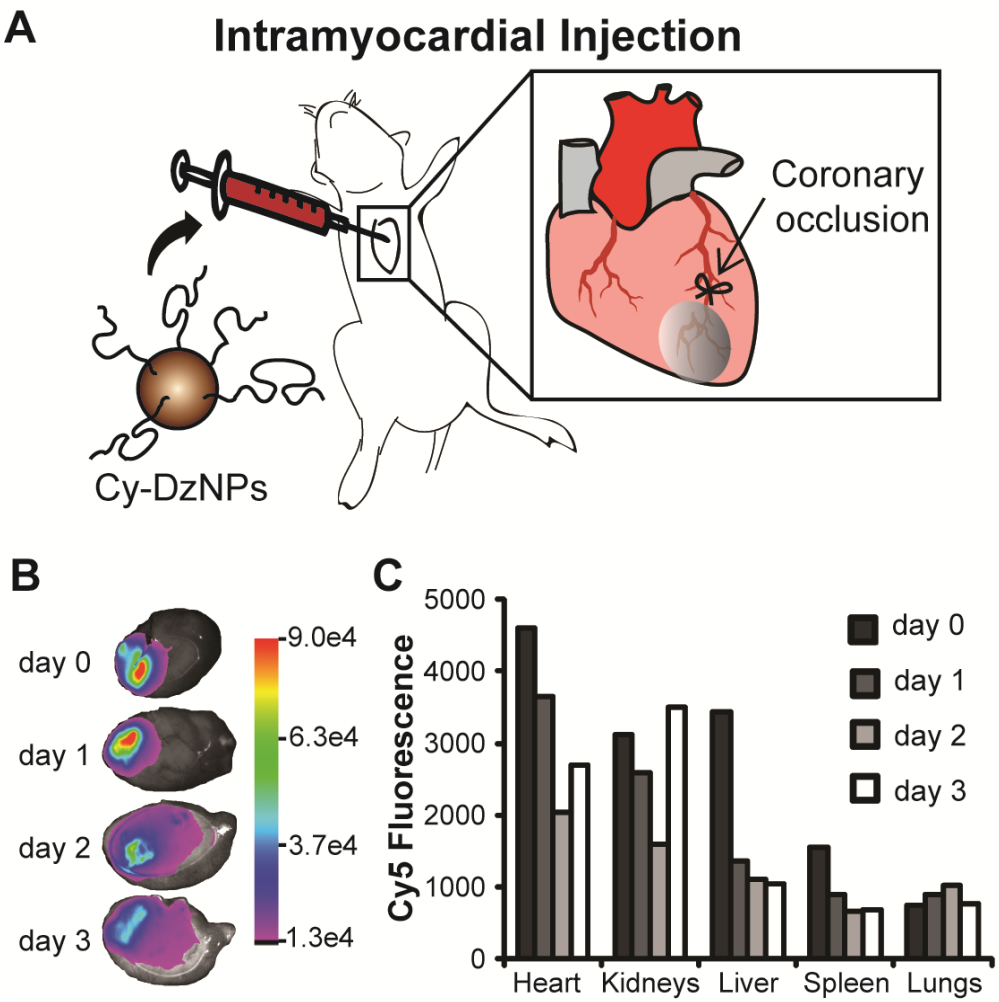


**Figure 14. *Ex-vivo* fluorescence imaging of organs from animals injected with Cy5-NS-DzNP.** (A) Schematic of ligation of the coronary artery to cause permanent ligation MI in rats followed by particle injection. (B) Images of hearts from each day following injection (B) Fluorescence intensity of all organs imaged from days 0, 1, 2 and 3 days (n=1) is expressed as arbitrary units.

### 4.3.6 *In vivo* inflammatory marker expression

At 3-days following injury, the expression of TNF−α at the mRNA level increased significantly ($p < 0.001$) in rats that underwent MI by 3.55±0.54 fold compared to sham rats (Figure 15B). The treatment groups receiving NS-Dz or i-Dz particle injections following MI showed no differences in TNF−α mRNA expression compared to the group receiving MI alone. In contrast, rats receiving Dz particles following MI demonstrated significantly lower levels of TNF−α mRNA expression compared to the MI

group as well as the groups receiving NS-Dz and i-Dz ($P < 0.05$). In order to determine the effects of TNF−α suppression in the infarcted heart, we also determined the gene expression of other inflammatory markers and immediate downstream targets of TNF−α. There was a signnificant upregulation of pro-inflammatory cytokines IL-12β ($p < 0.001$), IL-6 ($p < 0.05$), IL-1β ($p < 0.001$) as well as the enzyme iNOS ($p< 0.05$) following MI compared to sham (Figure 16). We observed a significant reduction in IL-12β ($p < 0.01$), IL-6 ($p < 0.05$), IL-1β ($p < 0.05$) and iNOS ($p < 0.05$) mRNA expression in groups that receied the Dz treatment compared to MI, and a strong trend in reduction in IL-12β and IL-1β ιn the plasma from these animals (Figure A7). We also tested the effect of Dz particles on anti-inflammatory cytokine IL-10, and interestingly there was a signficant upregulation of IL-10 mRNA expression following MI, However, none of the treatment groups showed any statistical difference from the MI group. Although plasma IL-10 levels showed a trend of upregulation with Dz treatment, it was statistically not significant (Figure A8 and A7 D).

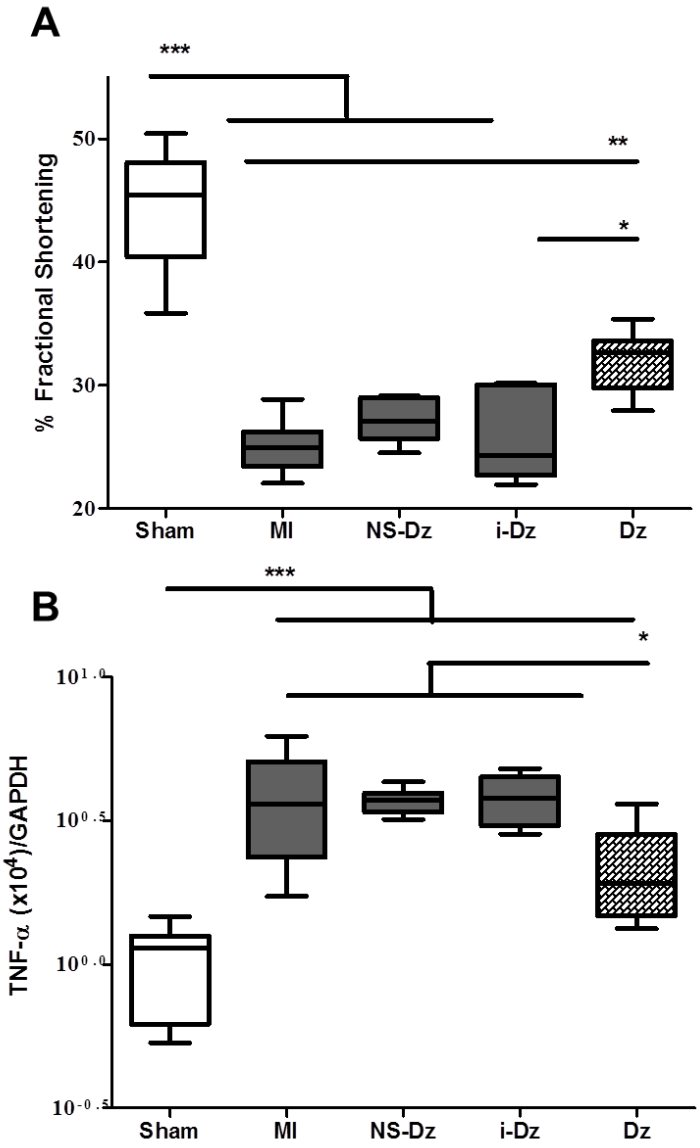


**Figure 15. Effect of *in vivo* delivery of Dz particles on cardiac function and TNF-α gene expression in a rat model of MI.**
Grouped data (mean ± SEM; n=5-9) from 3 days. (A) There was a significant decrease in cardiac function in animals that received an MI compared to sham as demonstrated by % FS. Among treatment groups, there was a significant restoration in function only in the Dz treated rats compared with untreated MI and i-Dz groups. (B) A significant upregulation of TNF−α expression was observed in animals that received an MI compared to sham. There was a significant decrease in mRNA expression in the LV infarct issue only in the Dz treated rats compared with all controls. Gene expression was evaluated by qRT-PCR using the quantitative standard curve method, and the results were normalized to GAPDH levels and reported logrithmic transformation of fold changes in copy number of mRNA levels compared to sham animals (*$p<0.05$; (**$p<0.01$ ***$p<0.001$; one-way ANOVA followed by Tukey's Multiple Comparison post-test).

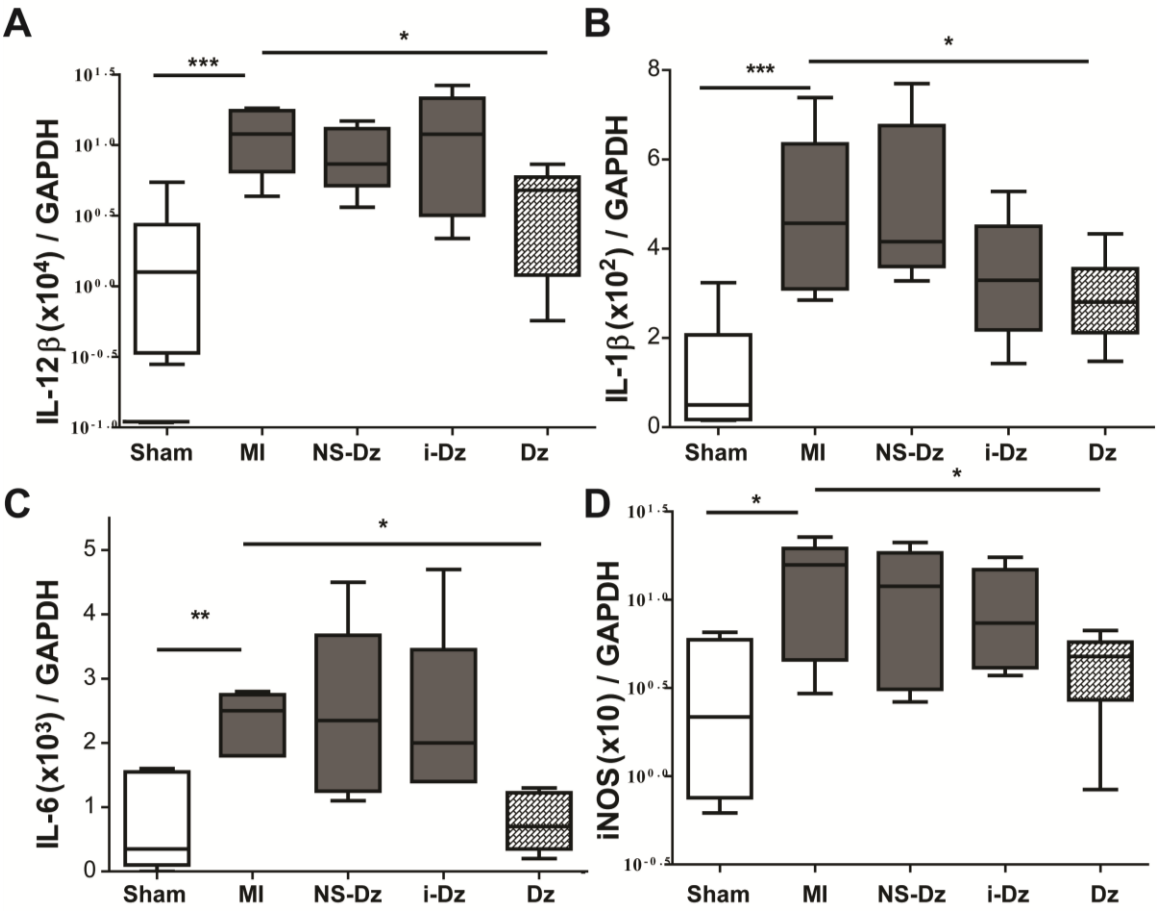


**Figure 16. Downstream effects of inhibiting TNF-α on pro-inflammatory cytokine and iNOS gene expression.**

Grouped data (mean ± SEM; n=5-9) from LV infarct tissue at 3 days following MI and injection. There was a significant upregulation in gene expression of pro-inflammatory cytokines (A) IL-12β, (B) IL-1 β, (C) IL-6 as well as (D) iNOS enzyme in infarct LV tissue compared to sham animals, and was significantly reduced in Dz treated animals. Gene expression was evaluated by qRT-PCR using the quantitative standard curve method, and the results were normalized to GAPDH levels and reported as fold changes in copy number of mRNA levels compared to sham animals. IL-12β and iNOS gene expression data were transformed logrithmically prior to statistical analyses in order to make the variance indpendent of the mean (*$p<0.05$;**$p<0.01$;*** $p<0.001$ vs. MI; one-way ANOVA followed by Dunnett's Multiple Comparison post-test).

## 4.4 Discussion

Over the last few decades, mortality due to MI has decreased due to the optimized reperfusion strategies employing sophisticated designs of stents/balloons, advancements in thrombolytic therapies and neurohormonal inhibitors. Despite these improvements, the incidence of heart failure as a direct consequence of MI remains high, suggesting that the current therapeutic regimen fails to target other key aspects of the pathophysiological mechanisms leading to cardiac dysfunction. Much interest has been devoted to studying the role of inflammation in the progression of heart failure, leading to a large volume of pre-clinical data illustrating the potential of anti-inflammatory therapies in prevention of heart failure post-MI. Interestingly, many pharmacological therapies with demonstrated efficacy for the treatment of acute MI have anti-inflammatory properties distinct from their perceived primary mechanism of action. [6, 41]. Reduced serum cytokine levels and inflammatory markers have been observed in patients receiving neurohormonal ACE inhibitors; statin therapies including simvastatin; and thrombolytic therapies such as aspirin, clopidogrel and GP IIb/IIIa. This suggests modulation of inflammation is a contributing factor to the clinical benefit ascribed to these medications.

The pro-inflammatory cytokine TNF–α is an extensively studied potential therapeutic target implicated in many of the processes involved in the development of heart failure. In the initial inflammatory phase post-MI, physiological levels of TNF–α have been shown to be cardioprotective [68, 70, 82, 83]. However, lingering inflammation and persistent high levels of pro-inflammatory cytokines contribute to unfavorable myocardial remodeling, leading to worsening clinical outcomes. Infusion of TNF–α to rats and dogs with normal cardiac function at levels comparable to that reported in patients with chronic heart failure (CHF) has been shown to depress ventricular function and cause adverse remodeling, recapitulating CHF conditions [64, 72].

Despite the volumes of encouraging pre-clinical data for TNF–α antagonism, human trials employing a soluble TNF–α receptor (etanercept) or a monocolonal antibody (infliximab) designed to neutralize TNF–α have failed to demonstrate long-term clinical benefit in patients with chronic heart failure post-MI. Post-mortem analyses revealed that both biological agents were highly unsuitable for TNF–α antagonism in a heart failure setting. Etanercept was shown to have a stabilizing effect on TNF–α by binding to it, thus accumulating bioactive TNF–α in circulation. Infliximab acts by exerting cytotoxicity to cells expressing TNF–α on the membrane, and while suitable for Crohn's disease where its beneficial to remove activated T-cells, lysing already failing cardiomyocytes during heart failure would be detrimental [160, 174, 175]

Results from these trials demonstrate a clear need for careful selection of the mechanism of TNF–α antagonism, as the nature of inhibition is a crucial factor for an anti-inflammatory therapy in the setting of heart failure. Furthermore, while the past clinical trials have targeted patients with advanced chronic heart failure, mounting evidence suggests the importance of early intervention to contain the initial inflammatory phase post-MI in order to halt the progression of the disease as opposed to treating the symptoms of chronic inflammation at later stages [17]. Ischemic injury leads to systemic as well as an exuberant local inflammation, and therefore designing and evaluating approaches to deliver transient suppression of TNF–α during the critical acute inflammatory stage is an important step towards successfully translating TNF–α antagonism as a treatment strategy for acute MI.

In order to circumvent the above mentioned limitations of the protein based strategies, we investigated a gene knockdown approach to inhibit TNF–α mRNA. Specifically, DNAzymes selective towards TNF–α mRNA were functionalized to gold nanoparticles and delivered to cells. DNAzyme therapies have shown great potential in pre-clinical trials in treating a wide variety of ailments ranging from cancer to spinal cord

injury including myocardial infarction, notably targeting transcription factor c-Jun for knockdown [28, 113, 176-178]. DNAzymes are also currently in human trials for treating nasopharyngeal carcinoma [28, 179]. However, all these studies employ cationic liposomes and are known to stimulate inflammatory pathways and induce cytotoxicity, which is detrimental for treating inflammatory pathologies. In this report, we tested whether DNAzyme functionalized gold nanoparticles could effectively regulate TNF–α expression to be used as an anti-inflammatory therapy for minimizing heart damage following MI, with the ultimate goal of preventing HF.

Intracellular uptake is a key requirement for the successful delivery of nucleic acids [24, 25]. We demonstrate the efficient cellular uptake of these particles by macrophages by measuring fluorescence of RAW 264.1 macrophages treated with Cy5-NS-Dz *in vitro*. We qualitatively compared the particle uptake with the most commonly used commercial transfection reagent Lipofectamine® RNAiMAX through a time course of 24 hours. While the Dz-NPs were taken up by macrophages as early as 1 hour and are continually taken up through 24 hours, Lipofectamine® mediated transfection was mostly only detected inside cells at 24 hours, and in punctate signals indicating possible entrapment within the endosomal compartments (Figure 12, right). We observe non-punctate, diffuse fluorescence inside cells (Figure 12A & Figure A4) in macrophages treated with the Dz-NPs indicating that the DNA is not trapped in endosomes, but diffusely localized in the cytoplasm. Phagocytic cells such as macrophages are difficult to tranfect and achieve gene silencing as they are programmed to take up foreign particles and ingest them, presenting a challenge for drug delivery to these cells. However, the mechanism of particle internalization is dependent on particle size. Particles below 500 nm in size are usually taken up via endocytosis in phagocytic and non-phagocytic cells [143, 144], suggesting endocytosis as the primary mechanism of uptake for our particles (~14 nm), which is a more preferable method of uptake in the context of therapeutic delivery. Accordingly, we further show that these particles are taken up by non-

phagocytic adult rat cardiomyocytes at 18 hours following transfection. Notably, there was no observable fluorescence in cardiomyocytes transfected with Cy5-DNA utilizing lipofectamine® RNAiMAX (Figure A5).

We then investigated whether DNAzyme functionalized gold particles are a biocompatible delivery vehicle and whether we could deliver catalytically active Dz into macrophages and inhibit TNF–α expression *in vitro*. In order to establish an *in vitro* model to demonstrate knockdown of TNF–α, we stimulated primary peritoneal cavity isolated macrophages with bacterial endotoxin LPS following particle treatment to stimulate the production of TNF–α. LPS stimulates TNF–α via activation of the Toll Like Receptor (TLR), orchestrating a potent inflammatory response, and therefore additionally served as a surrogate assay to evaluate cytotoxicity profile of particle uptake compared to the widely used transfection reagent Lipofectamine® RNAiMAX. Upon treatment with Lipofectamine®, macrophages exhibited ~4 fold higher TNF–α levels compared to the basal LPS stimulation, indicating a severe immune response elicited by cationic lipids widely used for nucleic acid delivery. The nonspecific DNAzyme particle (NS-Dz) treatment caused no additional cytotoxicity (Figure 13B) indicating that DNAzyme functionalized particles are biocompatible and highly suitable for applications in an inflammatory disease context.

To determine the intracellular catalytic activity of DNAzyme gold nanoparticle conjugates in this *in vitro* model, active and inactive DNAzymes modified particles were synthesized targeting the start codon (AUG), a region of the TNF–α mRNA with minimal secondary structure. The recognition arms were 7 and 10 base pairs in length, which was designed based on prior literature precedence (Supplemental Table 1) [113]. A single base mutation was made to the 15 base catalytic core to render the i-Dz from RNA hydrolysis activity, thus allowing one to distinguish antisense knockdown from DNAzyme mediated knockdown (Figure 13A). To ensure minimal degradation, four 2'-

methyl ether modifications were added to either end of the recognition arms. Surprisingly, initial tests showed limited DNAzyme mediated knockdown where Dz and i-Dz treated macrophages showed only 14% and 2% knockdown, respectively (Figure A9). We hypothesized that this was caused by product inhibition due to high stability of the 10 base pair length recognition arm. To address this concern, the recognition sequence for this arm was shortened from 10 to 7 in addition to changing the two terminal thymidine bases in the T10 spacer region to two cytodines to ensure minimal interaction with the mRNA. In the optimized design, compared to untreated LPS stimulated cells, only Dz particles showed significant (~50%) reduction in TNF–α levels while NS-Dz and i-Dz particles showed no effect (Figure 13B). Together, these results show that spherical nucleic acids can deliver DNAzyme to macrophages protected from degradation in its catalytically active form and decrease the expression of TNF-α in activated macrophages.

We then investigated the ability of these particles to deliver DNAzymes to the myocardium in a rat model of MI. For these *in vivo* studies, particles were delivered into the heart via intramyocardial injection into the infarct zone of rats immediately following MI surgery. This is clinically relevant in the context of MI as routine interventional procedures, such as PCI following MI, require catheterization and can be leveraged for site-specific therapeutic administration [27]. Initially, to determine the myocardium uptake efficiency and particle retention, Cy-NS-Dz modified gold particles were injected into the myocardium. The time-course *ex-vivo* bioimaging revealed strong Cy5 fluorescence emitting from the heart for all 3 days tested suggesting efficient particle uptake and that these nanoparticles are retained in the myocardium following injection for at least up to 3 days (Figure 14A-C). Due to the pulsatile nature of the heart, as anticipated, the particles are introduced to the blood circulation to a certain extent, and secondary to the heart, they predominantly biodistribute to the kidney and liver, suggesting renal and/or hepatobilary clearance.

To test the potential of DNAzyme functionalized gold particles as anti-inflammatory agents for the treatment of acute MI, we investigated the effect of injecting these particles to the myocardium of rats immediately following experimental MI using cardiac echocardiography and invasive hemodynamics measurements at a 3-day acute time point. A significant improvement in cardiac function was observed in Dz treatment group compared to MI alone with no effect from control treatments (Figure 15A). Corresponding to the functional improvement, delivery of Dz significantly reduced the TNF−α mRNA levels in LV tissue compared to all controls, exhibiting no statistical significance from sham controls (Figure 15B).

We also sought to analyze the impact of knocking down TNF−α gene expression on profiles pro-inflammatory markers involved in myocardial inflammation as well as systemic levels of these cytokines in the plasma collected from treated animals. Dz treatment demonstrated a strong anti-inflammatory effect that disrupted the gene expression of pro-inflammatory mediators IL-12β, IL-1 β, IL-6 as well as iNOS, an inducible form of Nitric oxide (NO) synthase stimulated by cytokines such as TNF−α and IL-1 β [180]. Several studies have illustrated the central role that TNF−α plays in myocardial dysfunction by propagating pro-inflammatory cytokines such as IL-6 and IL-1β that acutely regulate myocyte survival/apoptosis and trigger further cellular inflammation including oxidative stress and recruitment of inflammatory cells to the infarct [24, 78-81]. Furthermore, there is substantial evidence showing that TNF−α and subsequent induction of IL-6 or IL-1β can attenuate myocyte contractility directly through the reduction of systolic cytosolic $Ca^{2+}$ levels via alterations in sarcoplasmic reticulum function [80, 181], down-regulation of contractile proteins, ß–adrenergic receptor uncoupling [78, 182, 183] or indirectly by decreasing myocyte contractility through nitric oxide-dependent attenuation of myofilament $Ca^{2+}$ sensitivity [24, 73, 80, 180, 183] or oxidative effects on the RyR2 [184, 185]. It is well established that the

induced NO production has a negative inotropic effect on cardiac myocytes and that high levels of NO produced by iNOS are cytotoxic [24, 183, 186]. Interestingly, our data also demonstrates reduction of iNOS expression with Dz treatment, suggesting that knocking down TNF−α has beneficial effects on cardiac contractility via direct and indirect mechanisms, potentially contributing to the improvement in cardiac function we observe. We further substantiated this proposed mechanism *in vitro* by recording spatially resolved dyssynchronous $Ca^{2+}$ sparks via line scan confocal imaging upon stimulating primary adult rat cardiomyocytes with LPS to induce TNF−α production followed by treatment with Dz particles. Our data (Figure A10) shows reduction in inhomogenous subcellular $Ca^{2+}$ spark frequency in cardiomyocytes treated Dz particles compared to the untreated LPS stimulated myocytes, thus supporting the potential role that suppression of TNF−α has on preventing myocardial dysfunction.

Systemic levels of these cytokines measured from plasma reflected the local gene expression patterns and exhibited a strong trend of Dz treatment mediated anti-inflammatory effect (Figure A7 A-C). An endogenous anti-inflammatory cytokine IL-10, although did not show any statistically significant changes in local gene expression (Figure A8), exhibits a trend of upregulation in plasma levels with Dz treatment (Figure A8 D). Combined with the trend for downregulation of IL-12 only in the Dz treatment group (Figure A7 A), these results suggest a lower ratio of IL-12/IL-10 in systemic circulation, a surrogate measure of anti-inflammatory response employed in several studies due to the apparent opposing relationship of these cytokines and positive implications in resolution of inflammation [187].

Taken together, we demonstrate potent gene silencing *in vivo* via catalytic DNA particles, and specifically, the striking anti-inflammatory effects brought about as a direct consequence of suppressing the pro-inflammatory cytokine TNF−α in an acute MI setting. While this study shows promising acute functional improvement likely brought

about by the comprehensive anti-inflammatory effect of TNF–α mRNA specific Dz treatment at the initial inflammatory stage post-MI, follow up studies evaluating the chronic effects of this treatment on cardiac remodeling and chronic function are needed to determine whether repeated administrations are necessary to sustain the benefits of transient knockdown of TNF–α. High concentrations of TNF–α is shown to contribute to structural alterations in the failing heart such as cardiomyocyte hypertrophy and cardiac fibrosis and often used as an indicator of CHF as described earlier, and therefore merits further investigation beyond acute modulation [70, 73, 80]. Despite this limitation, this study presents a strong case for early anti-inflammatory intervention and the potential to revive TNF–α blockade as a viable therapeutic avenue for the prevention of chronic heart failure.

# CHAPTER 5 PEG-hydrogel mediated cytokine therapy as a strategy for immunomodulation in the heart

## 5.1 Introduction

The complex myocardial healing process constituting of cellular, morphologic and histological changes to the myocardium takes place in multiple phases [4, 154, 155]. Immediately following MI and the acute cell death, the ensuing acute inflammatory phase involves an influx of phagocytic macrophages and neutrophils that are recruited to the area of infarct to absorb the necrotic tissue [18, 36, 37, 84, 88, 90, 155, 156] following which myofibroblasts appear in the wound and contribute to reconstruction of a new collagen network, ultimately leading to deposition of a collagen-rich scar tissue. Clinical standards today focus on strategies for an optimal reperfusion therapy during the first hours of MI which has proven benefits in reducing the extent of hypoxic myocardial damage, and prevented the rate of mortality following MI [7, 38]. However, prevalence of HF is on the rise in patients that survive acute MI or received reperfusion therapy too late due to infarct expansion that occurs during the wound healing response before scar tissue formation, a process mainly attributed to the extent and quality of the inflammatory response following MI [4, 44].

This delicate equilibrium of the loco-regional myocardial inflammatory response, in conjunction with the post-MI systemic inflammatory reaction is a crucial step for a balanced post-MI healing process, and presents a viable therapeutic target to influence effective cardiac repair [17, 41]. Recent studies have brought to light the role of monocytes/macrophages as key orchestrators of the myocardial healing process. Macrophages play an apparently paradoxical role, one in which they conduct destructive processes including release of inflammatory mediators and reactive oxygen radicals in the process of absorbing the damaged myocardium, and another where they promote

angiogenesis and proliferation of myofibroblasts to aid in infarct stabilization [18, 90, 157, 188, 189]. Several studies have now definitively reported distinct macrophage populations that are responsible for these biphasic functions. In the initial inflammatory phase following MI (days 1-4), pro-inflammatory or classically activated macrophages, commonly known as M1 macrophages dominate the infarct and clear the wound, while reparative or alternatively activated of macrophages, known as M2, are present during the resolution of inflammation phase and propagate repair (days 4-8). Often however, prolonged pro-inflammatory responses stall resolution of inflammation and hamper the reparative functions of M2 macrophages essential for the formation of a stable scar [35, 41, 44, 61, 62, 157]. There is significant evidence for the benefits of mitigating the influx of pro-inflammatory monocytes/macrophages in the initial injury response in multiple cardiac disease models including acute MI and atherosclerosis [16, 17, 190, 191]. Herein, we investigate an alternate therapeutic approach that can modulate the function of pro-inflammatory macrophages to bring about inflammation resolution. This approach can mediate an effective repair process while at the same time suppressing the pro-inflammatory response rather than depleting it. The strength in our approach is that even if the number of macrophages impacted is small, they have the ability to produce more anti-inflammatory and pro-regenerative factors that amplify the desired signals and improve the quality of healing.

While this system of classifying macrophages as distinct M1 or M2 phenotype is antiquated in light of studies attributing a spectrum of multiple functional phenotypes to macrophages based on activation type, it provides an operationally useful, simple framework to study the role of macrophages and form hypotheses that can then inform viable therapeutic applications *in vivo*. In an *in vitro* context, a classical activation is brought about by stimulation of macrophages or monocytes with pro-inflammatory cytokine IFN-γ and bacterial endotoxin LPS stimulation, and alternative activation is brought about by cytokine IL-4, IL-10 or IL-13 [192-195]. In the context of

immunomodulation for a regenerative application, of particular interest is IL-4, a cytokine that has emerged as a powerful mediator for regeneration in muscle and liver [196, 197] by directly acting on progenitor cells. Further, on a peripheral nerve injury model, IL-4 delivery demonstrates a regenerative bias brought about by its ability to promote a reparative macrophage phenotype [25].

One of the key challenges for molecular therapies targeted to the heart is controlled delivery [12]. Especially with a small 14 kDa protein such as IL-4, direct bolus delivery to the myocardium will be highly inefficient as it will be carried away in the highly vascularized and pulsatile cardiac tissue. In recent published work from our laboratory, we had utilized a protease cleavable 4-arm PEG-Maleimide (PEG-MAL) hydrogel for the safe and efficacious dual release of growth factors to the infarct of rats [32]. In this study, this injectable hydrogel is employed as an immunomodulatory material to delivers IL-4 to macrophages in the infarct site. We evaluate the functional effects of the delivery *in vivo* and propose strategies to optimize this immunomodulatory approach for future studies.

## 5.2 Materials and Methods

### 5.2.1 Cell culture

A mouse macrophage cell line RAW 264.7 from American Type Culture Collection (ATCC number: TIB-71) was maintained at 37 $^{0}$C under a humidified atmosphere of 5% $CO_2$ in Dulbecco's Modified Eagle's Medium (DMEM) (Cellgro) containing 10% (v/v) fetal bovine serum (FBS) (Hyclone), supplemented with penicillin (100 U/mL) and streptomycin (100 mg/mL) and 2 mM L-Glutamine (Invitrogen). For primary macrophage culture, bone marrow-derived macrophages (BMMs) were isolated from Sprague Dawley rats as described previously [198]. Briefly, bone marrow cells were obtained by flushing the femurs with HBSS+. The bone marrow derived precursor cells were grown in 100mm$^2$ cell culture dishes for 7 days in RPMI 1640 (Cellgro) media

containing 10% FBS supplemented with 10ng/mL of mouse colony stimulation factor (M-CSF, Miltenyi Biotec) which directed the cell proliferation towards a purer population of BMMs. Media on the dishes was doubled on day 3 during the culture. The adherent cells at the end of 7 days were scraped and used for subsequent experiments, and confirmed as macrophages by immunofluorescence staining for pan-macrophage marker CD68 using mouse anti-CD68 (abcam). For endothelial cells, either immortalized mouse aortic endothelial cells (iMAECs) (a kind gift from Dr. Hanjoong Jo's laboratory) or rat primary cardiac microvascular endothelial cells (CECs) (Cell Biologics R2111) were cultured in gelatin coated cell culture flasks with low-glucose DMEM (GIBCO) supplemented with 10% v/v FBS, penicillin/streptomycin at the same concentrations described above, 50 μg/ml ECGS (Sigma), MNEAA 100X (GIBCO). For cardiac progenitor cell culture, c-kit-positive cells from the rat myocardium isolated as described previously [199] were cultured in growth media consisting of Ham's F-12 media (Cellgro) supplemented with 10% (v/v) FBS, L-glutamine/ penicillin/streptomycin as described above, 10ng/mL leukemia inhibitory factor and 10ng/mL basic fibroblast growth factor (Sigma). Before commencing the experiments, the cells were grown to 80% confluence, serum starved in starvation media containing Ham's F-12 media supplemented with L-glutamine, insulin/transferrin/selenium (ITS) serum supplement (Cellgro), and penicillin/streptomycin.

### 5.2.2 Macrophage polarization studies

RAW 264.1 macrophages were either treated with IL-4 (10ng/mL) or IFN-γ (10ng/mL) and LPS (5ng/mL) for 24 hours in order to alternately or classically activate macrophages. Following treatment, RNA was isolated from cells for gene expression analysis via qRT-PCR for expression of pro-inflammatory cytokine TNF-α as an M1 marker and Mannose receptor 1 (MRC-1) as M2 marker. Furthermore, the nitrite production by activated macrophages (as a surrogate for nitric oxide (NO) produced by a

characteristic M1 marker iNOS) was measured from the conditioned media (CM) using Griess reagent system (Promega). The M2 marker Arginase 1 (Arg1) activity was measured by a colorimetric enzymatic assay that measures the conversion of substrate L-arginine to urea catalyzed by Arg1 using a chromogen that complexes with urea to form color [200]. Briefly, cells were washed in PBS and lysed in 70µL of 0.1% Triton X-100 containing 1x protease inhibitor cocktail (AbD Serotec). The mixture was then incubated with shaking for 20 minutes at room temperature. After the cells were lysed, 50µL of 10 mM $MnC1_2$, 50 mM Tris-HCl, pH 7.5 were added to 50µL of the cell lysate and the enzyme was then activated for 10 minutes at 55°C. Arginine hydrolysis was carried out in Eppendorf tubes and was initiated by the addition of 50µL of 0.5M arginine, pH 9.7 to the previously activated lysate. Incubation was performed at 37°C for 60 minutes and the reaction stopped by the addition of 400 µl of an acid mixture containing $H_2SO_4$, $H_3PO_4$ and $H_2O$ (1:3:7). Then 25µL of 9% alpha-isonitro (ISPF) dissolved in 100% ethanol was added to the mixture and heated at 100°C for 45 minutes. After 10 minutes of further incubation in the dark, the urea formed was colorimetrically quantified at 540 nm in a microplate reader (Biotek Synergy 2) using 200µL aliquots/per well. A calibration curve was prepared with increasing amounts of urea between 1.5 and 30µg. In this case to 100µL of urea solution at the appropriate concentrations, 400µL of the acid mixture and 25µL ISPF were added, and the procedure followed as described above.

For polarization studies where we attempted to steer macrophages already activated towards an M1 state towards an M2 functional phenotype, RAW 264.7 macrophages or BMMs were either simultaneously treated with M1 (IFN-γ and LPS) stimuli and M2 (IL-4) stimuli in a simultaneous activation pattern or first treated with M1 stimuli for 24 hours, following which the media was simply changed again without any additional treatment as a control, or changed to M2 stimuli in a staggered activation pattern. Post-treatments, conditioned media was harvested for NO measurements (M1 marker) and cells lysed for Arg1 assay (M2 marker).

### 5.2.3 *In vitro* tube formation studies

The capacity of macrophage secreted factors to stimulate angiogenesis was assessed using a growth factor-reduced Geltrex (Invitrogen) assay. M1 or M2 conditioned media from RAW 24.7 macrophages in a ratio of 1:1 conditioned media and endothelial treatment media (2% of growth media described above) was applied to mouse endothelial cells (iMAECs) plated at $1x10^6$ cells/well in a 6-well plate for 24 hours. Cells were then lifted and counted so that 15,000 cells from each treatment group in endothelial treatment media could be plated onto 120 μl thick Geltrex gels in 96-well plates. The cells were then incubated for 6 hours and imaged using phase contrast and the cumulative tube length was quantified in 3 fields of view from each well using ImageJ software analysis. For tube formation studies with rat BMM conditioned media, rat primary cardiac microvascular endothelial cells (CECs) were quiesced in treatment media overnight and seeded onto a 96-well plate coated with 120 μL of Geltrex in media containing 2:1 ratio of the treatment media and M1 or M2 BBM conditioned media. Additional groups containing just the M1 (IFN-γ + LPS) or M2 (IL-4) stimuli in the treatment media were also added to the experiment to control for the added stimuli present in the conditioned media. Following 6 hours of treatment, cells were stained with 4μM Calcein AM dye (Invitrogen) and imaged with a fluorescent microscope (Olympus IX71) and the tube length was quantified as above. In a separate study, the same procedure was performed on plates coated with gels made from rat tail collagen (Invitrogen) to mimic a growth factor deprived 3-D environment to clearly assess the effect of differentially activated BMM conditioned media on endothelial cell spreading and aggregation and results quantified using Cell Profiler.

### *5.2.4 In vitro* cell migration

The ability of conditioned media from macrophages to recruit cardiac progenitor cells (CPCs) was assessed using a modified Boyden chamber trans-well migration assay.

Cell Tracker Orange CMRA (Life Technologies) labeled CPCs were seeded in the top well of the Boyden chamber (Corning) at a density of 100,000 cells/ well and allowed to adhere to the wells. Conditioned media obtained from untreated and M1 or M2 polarized macrophages as well as plain media or media containing M1 or M2 stimuli was added to the bottom chamber. After 12 hours, the inside of the Boyden chamber was aspirated and wiped clean, and the bottom side of the chamber was incubated in cell-dissociation buffer while shaking for 1 hour in a $37^0$C to get migrated cells in solution. The extent of cell migration through the insert was then quantified by measuring CMRA fluorescence on a microplate reader (BioTek Synergy 2). A standard curve of CMRA fluorescence to cell number was used to calculate the percent of migrated cells, and reported as percent changes in cell-migration over appropriate untreated controls.

### 5.2.5 Preparation and characterization of PEG-MAL hydrogel

A protease-cleavable hydrogel system with a 4-arm PEG macromer end-functionalized with Maleimide groups (PEG-MAL) was prepared as previously described [32]. PEG-MAL macromers (20 and 10 kDa, 0.95% maleimide functionalization; Laysan Bio) were pre-functionalized with GRGDSPC (RGD) adhesion peptide in 1.0 mM triethanolamine (TEA) solution at pH 7.4 by allowing the PEG-MAL macromers to react with the cysteine groups of the RGD peptide for 30 minutes in $37^0$C. The cytokine IL-4 (1% v/v) (Antigenix America) was then mixed in with the precursor solution to be encapsulated within when the solution is cross-linked into a hydrogel by addition of a cysteine-flanked protease-degradable peptide sequence GCRD**VPM**SMRGGDRCG (VPM) [32, 33]. Since IL-4 does not have any free cysteines, it is not expected to be physically tethered to the hydrogel. PEG polymer density used in animal studies was 5% w/v and RGD density was 2.0 mM. The final concentration of cytokine delivered was 1 μg IL-4 per 50 μL hydrogel.

Mass swelling ratio of 10 kDa PEG-MAL hydrogels at weight percentages of 5%, 6% and 7% PEG was characterized. Firstly, hydrogels were formed (n=6 per group) in coverslips coated in Sigmacote® (Sigma-Aldrich). After cross-linking, hydrogels were allowed to freely swell in PBS for 24 hours and the swollen hydrogel mass measured. Hydrogels were then snap-frozen in liquid $N_2$ and lyophilized followed by dry mass measurement. The mass swelling ratio is reported as the ratio of swollen mass to dry mass.

### 5.2.6 *In vitro* release study

In order to characterize the passive and enzyme mediated release of IL-4, the protein was tagged with Alexa Fluor 488, Carboxylic Acid, Succinimidyl Ester, mixed isomers (Invitrogen) according to manufacturer's instructions. Briefly, protein was incubated at 0.1 mg/mL at a 1:50 protein to dye molar ratio in sodium bicarbonate buffer for 2 hours at $37^0$C, and purified into PBS by 3 passes through a desalting spin column (Zeba Spin Desalting Column, Pierce, 7K MWCO). Labeled protein was stored at 4-$8^0$C for short-term until use. PEG-MAL macromers of 10 kDa and 20 kDa at varying weight percentages (5, 6, 7 and 12%) were tested. Furthermore, in order to place the release characteristics in context of previously published work utilizing this gel, we compared the release profile of IL-4, which is only 14 kDa to that of a larger protein such as IgG (150 kDa). Gels were incubated in PBS alone or with 0.1 mg/mL or 0.075 mg/mL collagenase Type 1 (Worthington Biochemical, 385U/mg activity) for 3 days at $37^0$C. Individual hydrogel volumes were 50 μL and 5 μL of tagged protein.

In order to confirm release of bioactive IL-4 from the hydrogel, RAW 264.7 macrophages were stimulated with 100ng/mL LPS in the presence of either empty or IL-4 encapsulating hydrogel with Collagenase I at 0.1mg/mL over 48 hours to degrade the gels and release IL-4. The NO production in the media at 48 hours was determined to confirm the activity of IL-4 against LPS-activated macrophages.

### 5.2.7 Animal studies

MI was induced via permanent ligation of the left anterior descending artery in adult male Sprague Dawley rats. Briefly, the animals were anesthetized (1-3% isoflurane) and following tracheal intubation, the heart was exposed by separating the ribs. Then ligation of the left anterior descending coronary artery was carried out and appropriate injections were administered in 3 areas of the ischemic zone. Following injection, the chests were closed and animals were allowed to recover on a heating pad until appropriate assessments were made at later time points. Three different randomized and blinded animal studies were conducted as follows: e*x vivo* bioimaging study, acute and chronic functional study with immunohistological evaluation at the chronic time point, and gene expression analysis study. In all studies, the animals were assigned to treatment groups using a random number generator and the animal surgeon was only given letter codes to identify groups. These studies conformed to the *Guide for the Care and Use of Laboratory Animals* published by the US National Institutes of Health (NIH Publication No. 85-23, revised 1996) and all animal studies were approved by Emory University Institutional Animal Care and Use Committee.

### 5.2.8 *Ex-vivo* bioimaging

Rats were subjected to MI as described above and DyLight 800 (Invitrogen) labeled IL-4 encapsulated hydrogel or bolus IL-4 (50μL) was injected in 3 areas in the border zone surrounding the infarct. Rats were sacrificed and the hearts, liver, spleen and kidneys were harvested and imaged on days 0, 1, 2, 3 and 7 post-injection (n=3 per time point) using Bruker In-Vivo Xtreme using the same imaging settings and reported as arbitrary fluorescence units plotted over time.

### 5.2.9 Echocardiography and invasive pressure-volume hemodynamics analysis

For the animal study designed to evaluate cardiac function and immunohistological analyses to assess cardiac repair, one group of animals received

sham surgery while four other groups received MI surgery. For groups receiving injections, immediately after coronary artery ligation, 50 μL injection of either an empty hydrogel or bolus IL-4 injection or IL-4 hydrogel (containing 1μg IL-4) was administered into the cyanotic ischemic zone (3 locations) through a 25-gauge needle while the heart was beating. Functional assessments were made 7 and 21 days following MI surgery using echocardiography (Acuson Sequoia 512 with a 14 MHz transducer) and additionally on day 21 using invasive pressure-volume hemodynamics (Millar MPVS Instruments). From echocardiography, short axis values of left ventricular end systolic (ES) and end diastolic (ED) dimensions were obtained. An average of 3 consecutive cardiac cycles was used for each measurement and was performed three times in by a blinded investigator. Fractional shortening was calculated as [(end-diastolic diameter – end-systolic diameter)/(end-diastolic diameter)] and expressed as a percentage. For invasive hemodynamics, the pressure-volume probe was inserted into the left ventricle. After stabilization, baseline left ventricular pressure-volume loops were recorded for at least 10 cardiac cycles and data averaged to get mean values for each animal. Parameters extracted include left-ventricular Ejection Fraction (%EF), +dP/dT and -dP/dT.

### 5.2.10 Immunohistochemistry

Following functional assessments on day 21, the animals were sacrificed and the hearts were fixed in 4% paraformaldehyde, dehydrated and embedded in paraffin and sectioned to 5 μm sections and adhered to a glass slide. Following rehydration, tissue sections were probed with Alexa fluor 647-labeled isolectin B4 (Invitrogen) to stain endothelial cells for angiogenesis/arteriogenesis determination and imaged using fluorescence microscopy. For quantification, 3 non-serial sections from each animal were analyzed by a blinded investigator using a custom written Matlab code that identified percent red pixels in the infarcted regions (identified as regions lacking auto-fluorescence which is normally exhibited by healthy myocardium in the green channel) [201].

Additionally, collagen deposition was determined by picrosirius red (Sigma) staining as previously described [124]. Briefly, 5 μm tissue sections were stained with Sirius Red and imaged at 5x objective using a light microscope. Overlapping images were taken and then stitched together using Adobe Photoshop to generate an image of the entire heart. Total collagen area (red staining) was normalized to total left ventricular area in 3 separate sections per animal using a custom written Matlab program.

### 5.2.11 *In vivo* gene expression and plasma cytokine analysis

In order to assess whether IL-4 hydrogel delivery resulted in the transformation of M1 like macrophages towards M2 like macrophages even at acute time points (prior to the pre-determined shifts reported in the literature), we conducted a study spanning several acute time points with only two groups of main concern. Both of these groups underwent MI, while only one of those groups received the IL-4-hydrogel injection (n=3). At days 1, 2, 3 and 7 days following MI, animals were sacrificed and the left ventricle infarct tissue was harvested and homogenized from which the total RNA contents were isolated using Trizol (Invitrogen) according to the manufacturer's protocol. Complementary DNA (cDNA) was synthesized using SuperScript III kit (Invitrogen) and qRT-PCR performed using Power SYBR Green (Invitrogen) master mix with Applied Biosystems StepOnePlus$^{TM}$ real time PCR system. Comparative $\Delta\Delta C_t$ method was employed to analyze gene expression levels of each of the target genes. Gene expression levels were then normalized to the endogenous housekeeping gene GAPDH. Primer sequences used are listed in Appendix section A3.3.

Prior to sacrificing the animals, blood was collected via cardiac puncture, plasma separated from blood cells and stored in -70$^0$C until cytokine analysis using the Luminex multiplex analyzer system (Luminex LX100). A custom cytokine bead panel from ebioscience was used to analyze cytokines IL-12β and MCP-1 in the plasma.

### 5.2.12 Statistics

All statistical analyses were performed using Graphpad Prism 5 software. Quantitative results were presented as means ± SEM. Statistical comparisons were performed by one way analysis of variance (ANOVA) followed by the appropriate post-test as described in the figure legends. P values of less than 0.05 were considered significant.

## 5.3 Results

### 5.3.1 Effect of polarized macrophages on endothelial cell survival and tube formation and cardiac progenitor cell migration *in vitro*

A cell line of macrophages (RAW 264.7) treated with IL-4 upregulated M2 marker MRC-1 and showed increased Arg1 activity, indicative of polarization towards an M2 functional phenotype (Figure 17 D-E). Similarly, IFN-γ and LPS treated cells exhibit polarization towards an M1 phenotype indicated by the increase in NO production induced by the classical M1 marker iNOS and upregulation of the pro-inflammatory cytokine TNF-α gene expression (Figure 17 B-C). RAW 264.7 macrophages polarized towards an M2 functional phenotype induced favorable aortic endothelial tube formation in iMAECs in a Geltrex® tube formation assay (Figure 18A). Furthermore, on growth factor deprived collagen gels, IL-4 polarized BMM (M2) conditioned media (M2 CM) treated CECs exhibited significant improvements in cell viability and cell spreading (captured in a single metric of area of cells occupied) compared to cells treated with M1 or untreated BMM conditioned media or media containing the polarizing stimuli IL-4 or IFN-γ + LPS alone (Figure 18B). In fact, it would seem that endothelial cells treated with conditioned media from M1 polarized macrophages (M1 CM) fare poorly compared to even untreated macrophage conditioned media, although not statistically significantly different. Furthermore, only M2 CM treated endothelial cells on collagen gels migrated towards each other and formed aggregate structures, potentially pre-cursors to tube

formation (Figure A12). Furthermore, M2 CM from RAW 264.7 macrophages attracted cardiac progenitor cells (CPSs) to a greater extent compared to other conditioned media controls ($p<0.001$ vs untreated CM, $p<0.01$ vs M1 CM), or media containing cytokine stimuli (Figure 19A-B).

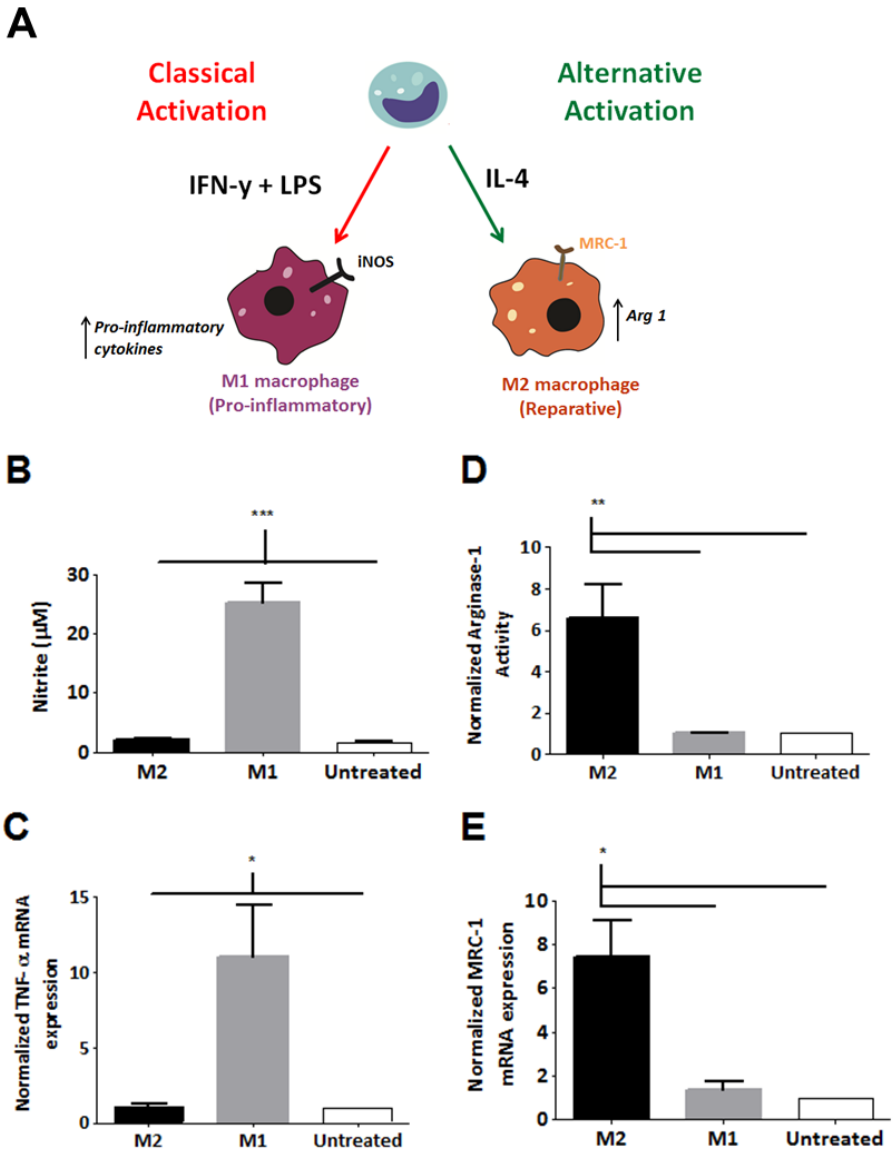


**Figure 17. Characterization of polarized macrophages** (A) Schematic of classical (M1) and alternate activation (M2) of macrophages represented by red and green arrows respectively. (B) Nitric oxide levels (C) TNF-α mRNA (D) Arg 1 activity (E) MRC-1 mRNA were assessed following activation of macrophages with either LPS + IFN-γ or IL-4. All mRNA expression was normalized to housekeeping gene hprt1 (Grouped data,

mean ± SEM; n=3-5*p<0.05, **p<0.01, ***p<0.001; One-way ANOVA followed by Tukey's Multiple Comparison post-test)

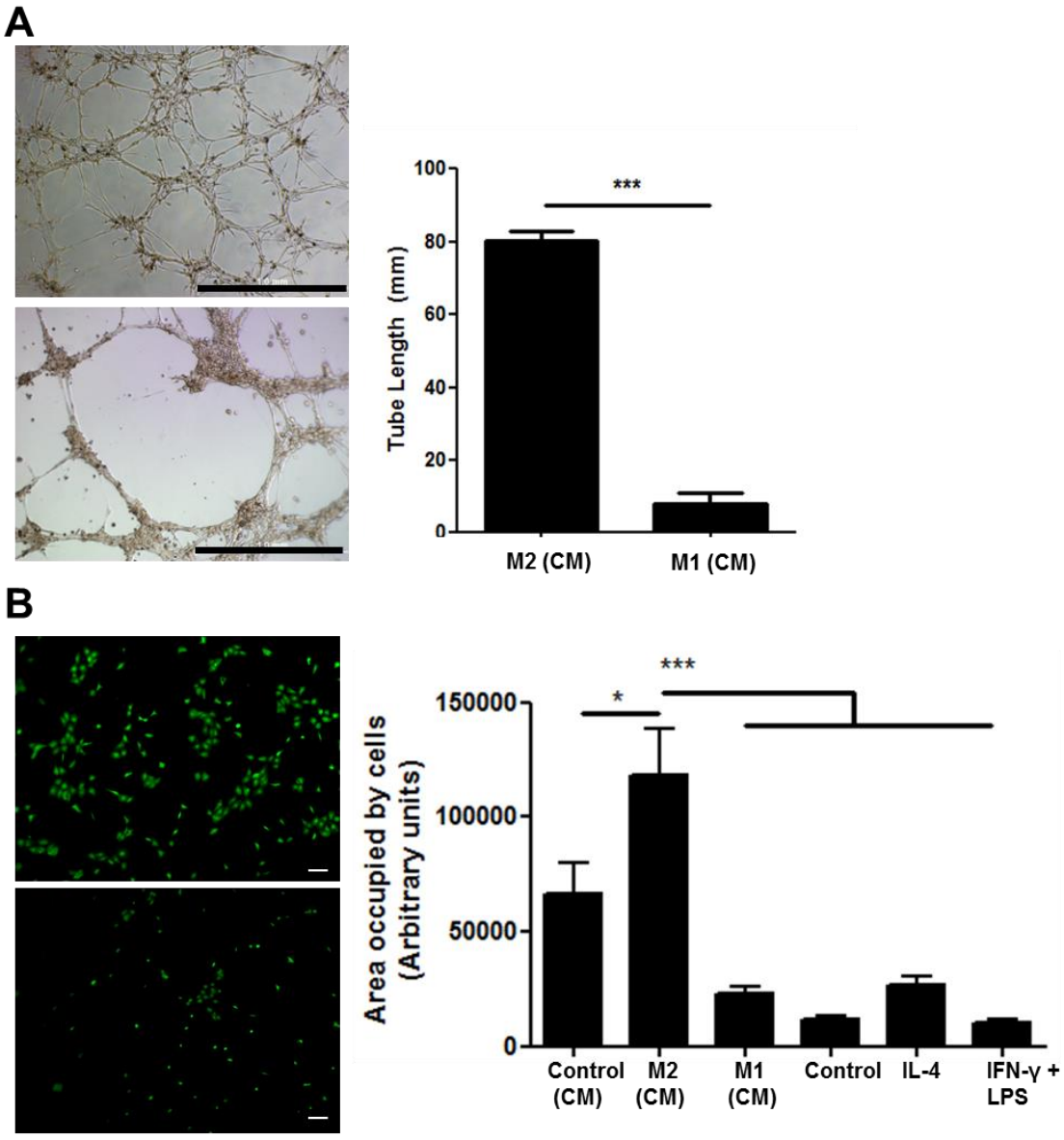


**Figure 18. M2 polarized macrophages influence *in vitro* tube formation and cell survival in endothelial cells via paracrine mechanisms.** Grouped data, mean ± SEM; n=4-6**.** (A) Tube formation of iMAECS in Geltrex® matrix upon treatment with M2 (top, left) or M1 (bottom, left) activated RAW 24.7 macrophage conditioned media, and tube length quantified (right) (scale bar, 1mm). (B) Cell spreading/count of CECs in rat tail collagen gels upon treatment with M2 (top, left) or M1 (bottom, left) activated macrophage conditioned media, and area occupied by cells quantified (right). Images taken in 10x objective, cells (green, Calcein) (scale bar, 100μm) (*p<0.05, ***p<0.001; One-way ANOVA followed by Tukey's Multiple Comparison post-test)

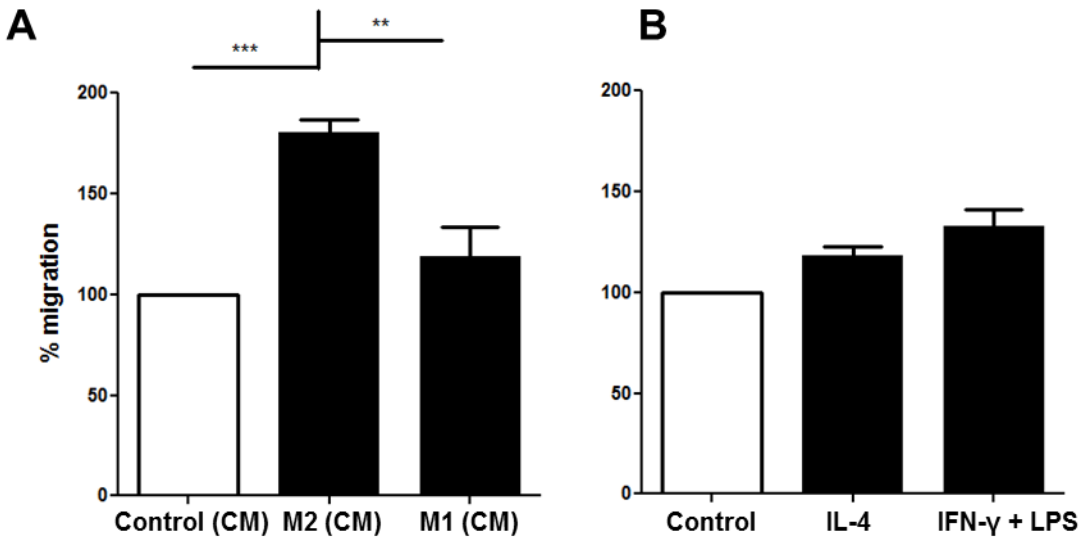


**Figure 19. Effect of M2 polarized macrophages on migraton of cardiac progenitor cells *in vitro*.** (A) Migration of CPCs labeled with CellTracker Orange dye through the Boyden chamber insert towards conditioned media from either untreated or M1 or M2 polarized RAW 24.7 macrophages or (B) migration towards plain media or media containing the polarizing stimuli IL-4 or LPS + IFN-γ. (Grouped data, mean ± SEM; n=4-6 *p<0.05, **p<0.01, ***p<0.001; One-way ANOVA followed by Tukey's Multiple Comparison post-test)

.

### 5.3.2 Plasticity characteristics of macrophages

In order to determine the ability of macrophages to change their functional phenotypes depending on their environmental cues despite their disposition towards a certain phenotype, we either primed them towards an M1 phenotype first (IFN-γ + LPS) followed by M2 stimulation (IL-4) in subsequent days (staggered activation), or simultaneously activated them with M1 and M2 stimuli (IFN-γ + LPS and IL-4) for 2 days. Simultaneous activation exhibits a hybrid phenotype that favors M2 activation, as shown by the significant suppression of NO production and increased Arg1 activity (Figure 20A-B, Figure A13). On the other hand, staggered activation pattern showed little to no tendency to revert to an M2 polarization status from M1 functional phenotype (Figure A13).

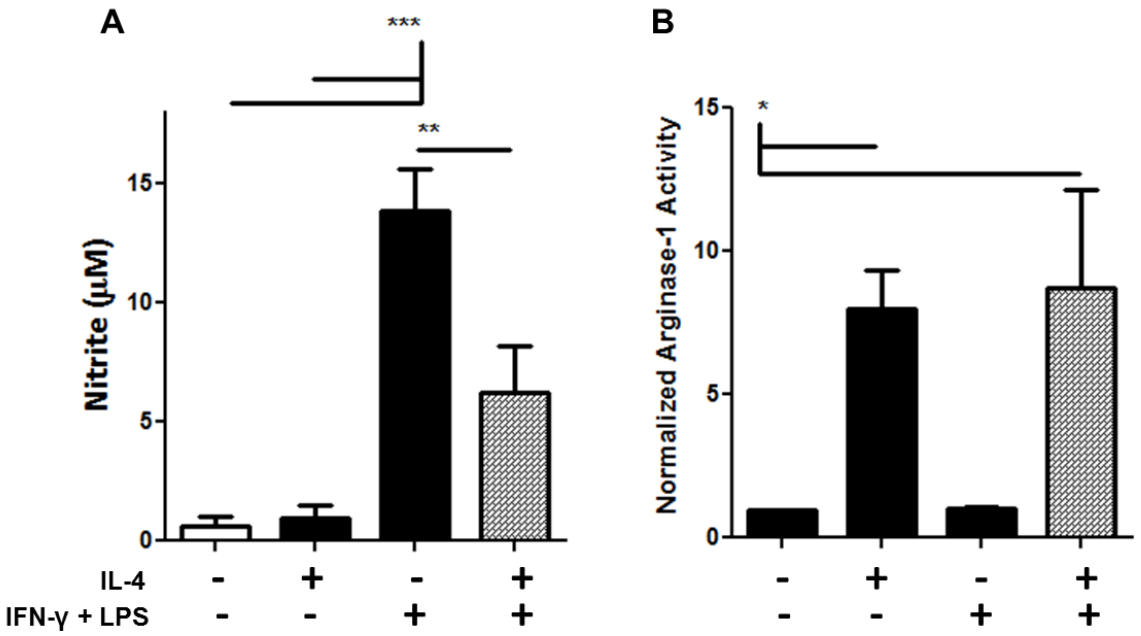


**Figure 20. Simultaneous M1 and M2 polarizing stimuli on macrophage activation.** Characterization of (A) NO production and (B) Arg1 activity following simultaneous activation of RAW 24.7 macrophages with IFN-γ + LPS and IL-4 treatment IL-4 for 24 hours (Grouped data, mean ± SEM; n=5-6, *p<0.05, **p<0.01, ***p<0.001; one-way ANOVA followed by Dunnett's Multiple Comparison post-test)

### 5.3.3 Characterization of protein release from PEG-MAL hydrogel

To determine release of IL-4 *in vitro*, fluorescently-labeled IL-4 was encapsulated into the PEG-MAL hydrogels (Figure 21A). Firstly, the release profile of IL-4 (14 kDa) from 5% (w/v) PEG-MAL gel of 10 and 20 kDa molecular weight was compared to that of release of Alexa Fluor 488-labeled antibody IgG (150 kDa) from these gels (Figure A14). The results demonstrate a more sustained release of the larger protein IgG and pronounced differences in release rate due to the differing mesh sizes formed by the 10 kDa vs 20 kDa PEG-MAL hydrogels. The 10 kDa macromers form tighter networks and therefore smaller mesh sizes and thus higher entrapment and slower release. These differences in mesh sizes had no significant effect on the

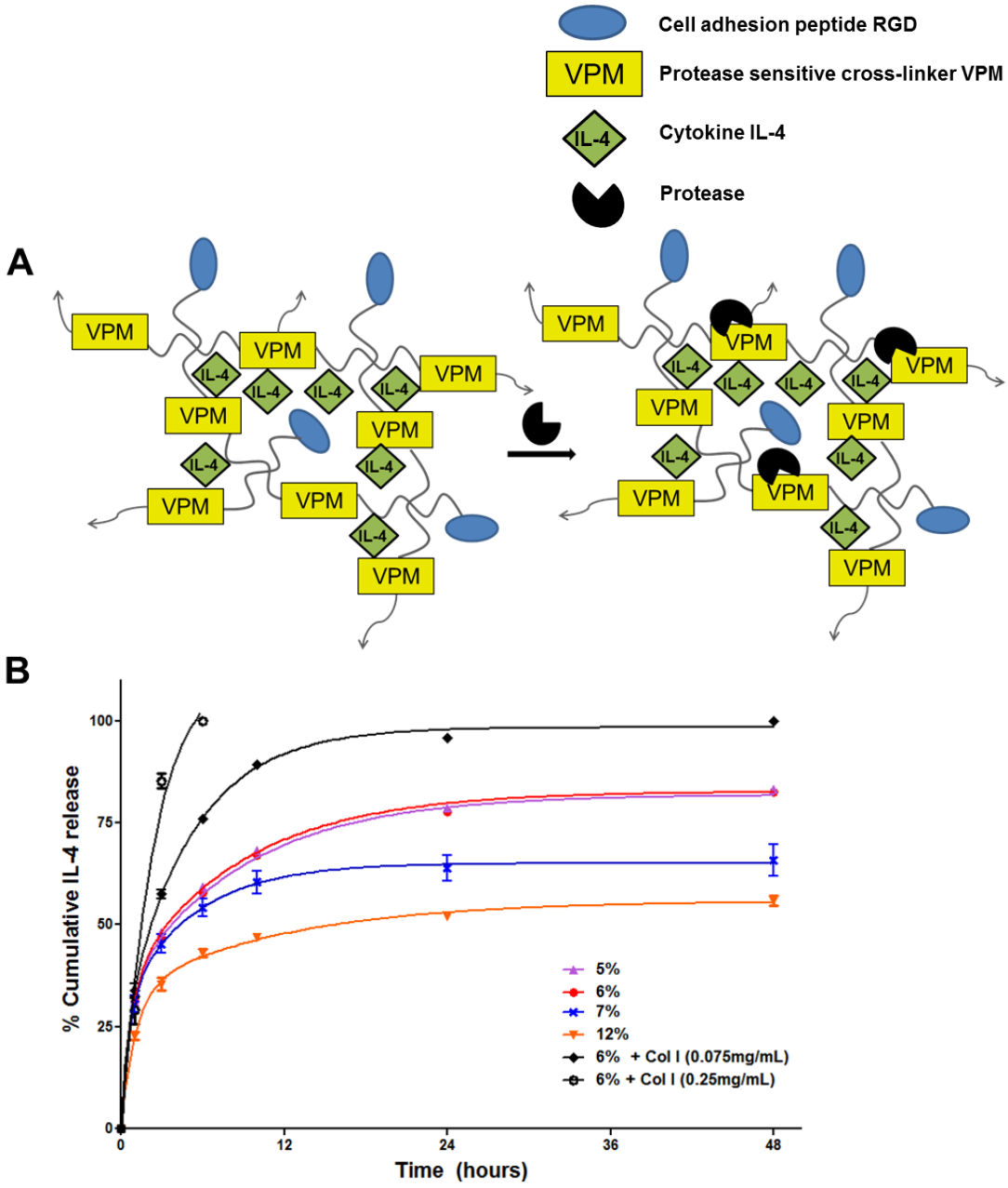


**Figure 21. Hydrogel design and release studies.** A) PEG-maleimide (PEG-MAL) 4-arm macromers of 10 kDa were pre-functionalized with RGD adhesion peptide and IL-4 was encapsulated. The precursor molecules were cross-linked into a hydrogel by addition of cysteine-flanked protease- degradable peptide sequence GCRDVPMSMRGGDRCG (VPM). B) Fluorescently tagged IL-4 released from varying weight percentages of PEG-MAL hydrogel (5%, 6%, 7% and 12%) swelled in either PBS or 2 different doses of collagenase Type 1 as measured by fluorescent plate reader sampling of incubation media. Grouped data were fitted with a two-phase exponential best-fit curve.

release of the small cytokine IL-4, although 10 kDa PEG-MAL hydrogels led to slightly slower overall release of IL-4. Further characterization of the IL-4 release profile from varying weight percentages (5, 6, 7 and 12%) of the 10 kDa PEG-MAL hydrogel was then performed to investigate potential for better controlled release of IL-4 (Figure 21B). Hydrogels subjected to higher collagenase I (Col I) treatment (0.25mg/mL) were observed to degrade and release loaded IL-4 rapidly within the first 6 hours after treatment, and a lower concentration of Col I (0.075mg/mL) treatment released IL-4 slower, but degraded the hydrogels completely within 24 hours, demonstrating a protease-dependent release of IL-4 in these bioactive hydrogels. Hydrogels encapsulating IL-4 and placed in PBS released IL-4 slower overall, although there was burst release observed during the first 10 hours, and a slower sustained release profile in the latter phase. This is substantiated by the two-phase exponential best-fit line that yielded $R^2 \geq 0.98$ for all curves. The amount of IL-4 released varied inversely with the % weight of PEG in the hydrogel, with ~45% release in 12% PEG hydrogel in the initial 10 hours compared to 65% in 5% gel. Furthermore, in all weight percentages of hydrogels, beyond the burst release, there is a perceived inflection point at around 10 hours (Figure A16) beyond which the rate of release slows incredibly, with only 10-15% more IL-4 released from all gels. Interestingly, the release profile between 5 and 6% hydrogel was very similar through both phases of the release profile. As shown in Figure A15, the mass swelling ratio (related to the average distance between cross-links, and thus a measure of loose vs tight hydrogel network structure [32]) of 5, 6 and 7% hydrogels made from 10kDa PEG-MAL macromers differ significantly from each other, but very moderately, which could partially explain the very little differences observed in the release of IL-4 within these 3 weight percentage gels in the initial burst release phase.

Furthermore, Figure A17 demonstrates the ability of the PEG-MAL gel to encapsulate and release IL-4 in its bioactive form by the significant reduction in NO levels observed in the IL-4-hydrogel treated group which is comparable to the 50%

reduction in NO levels compared to LPS stimulation alone that is observed in all experiments conducted in this study where LPS and IL-4 were simultaneously used to co-stimulate macrophages.

### 5.3.4 *In vivo* IL-4 release characterization

*In vivo* biodistribution and retention of fluorescently tagged IL-4 in the heart upon IL-4-hydrogel (5% weight percentage of 10 kDa PEG-MAL macromere) or bolus IL-4 delivery to the heart was determined using ex-vivo fluorescence imaging of the internal organs at days 0, 1, 2, 3 and 7 following MI surgery and injection (n=3). Due to imaging artifacts on day 1 in the bolus IL-4 injection group, this time point was excluded from the dataset. As shown in Figure 22, IL-4-hydrogel injection exhibited greater than 3 times the fluorescence to that of bolus IL-4 injection in the heart on day 0 immediately after the injection (within 5 minutes of injection, the rat was sacrificed and heart excised for imaging) , and sustained a 2 times higher fluorescence intensity through day 3. At day 7, the fluorescence levels in IL-4-hydrogel injected group decreased to below detected levels (Figure 22A, right). Higher retention was observed in the heart than any other organs in IL-4-hydrogel injected group (Figure 22A, right). Secondary to the heart, levels of fluorescence was highest in the kidneys and it is uncertain whether it is the cleaved fluorophore or the protein that is being eliminated from the kidney. Similar lower levels of fluorescence were observed in all organs in the bolus IL-4 injection group (Figure 22B, left).

### 5.3.5 Cardiac function following myocardial infarction

To determine the *in vivo* efficiency of IL-4 delivery utilizing PEG-MAL hydrogel, adult male Sprague Dawley rats were randomized into 5 treatment groups. The injected hydrogels were composed of 5% (w/v) PEG-MAL from 10 kDa macromer, and the injections were of 50μL volume with or without 1μg IL-4. While one group was subjected to sham surgery, the other four groups received MI surgeries followed by either

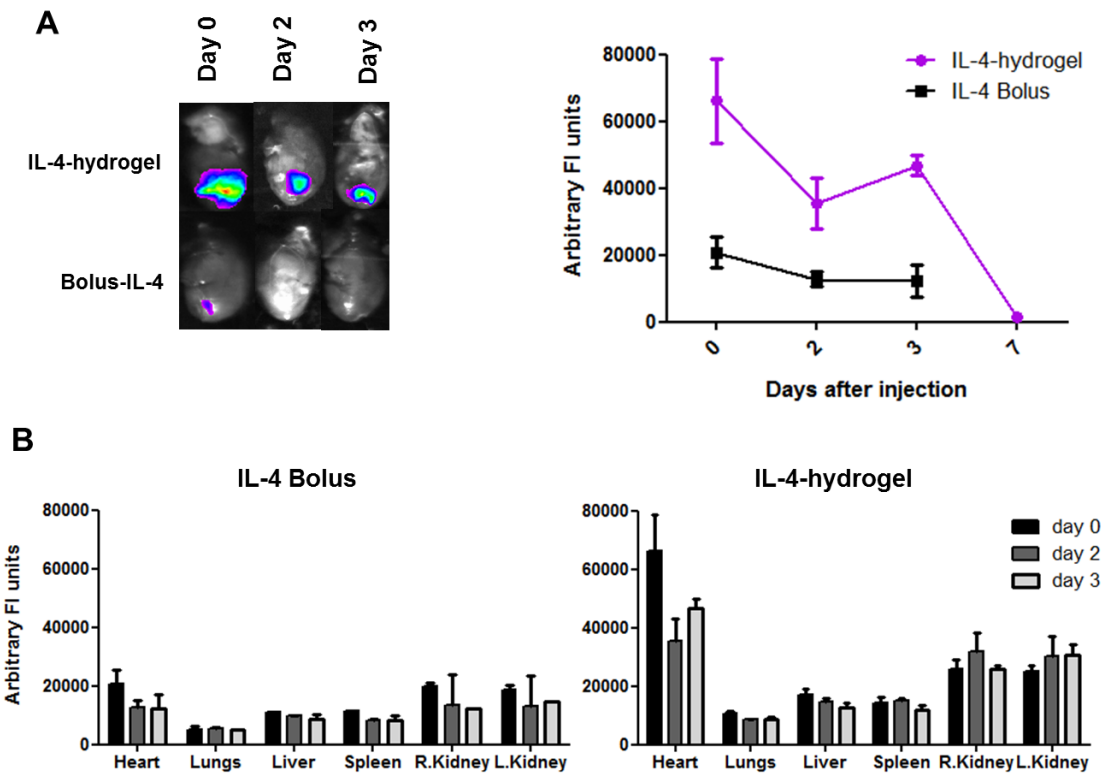


**Figure 22. Ex-vivo fluorescence imaging upon IL-4 delivery to the myocardium.** (A) Representative mages of hearts from day 0, 2 and 3 following either a bolus IL-4 or IL-4-hydrogl injection (left) and mean fluorescent intensity for the heart expressed in arbitrary fluorescent units through day 7 (right) (B) Fluoresent mean intensity of all organs expressed as mean arbitrary fluorescent intensity units for bolus IL-4 injection (left) and IL-4 hydrogel injection (right) (Grouped data, mean ± SEM; n=3)

no injections (MI) or injections of either empty hydrogel, bolus IL-4 (50μL with 1μg IL-4) or hydrogel encapsulating IL-4 ($n$=5-9 for each group, $n$=40 total). At the acute 7 day time point following surgery and injection, all groups receiving MI demonstrated significantly reduced cardiac function ($p < 0.001$) as measured in absolute change in percent fractional shortening (%FS) compared to sham animals, and only the IL-4-hydrogel treated animals showed about 30% restoration in function compared to MI ($p < 0.001$) as well as the empty hydrogel ($p<0.001$) and IL-4 bolus ($p<0.05$) injected groups (Figure 23). However, this improvement is lost at the chronic 21 day time point in terms of %FS (Figure 24A), although the invasive hemodynamics measurement derived %

Ejection Fraction values suggest perhaps a moderate improvement in function compared to the MI and empty hydrogel groups (Figure 24B).

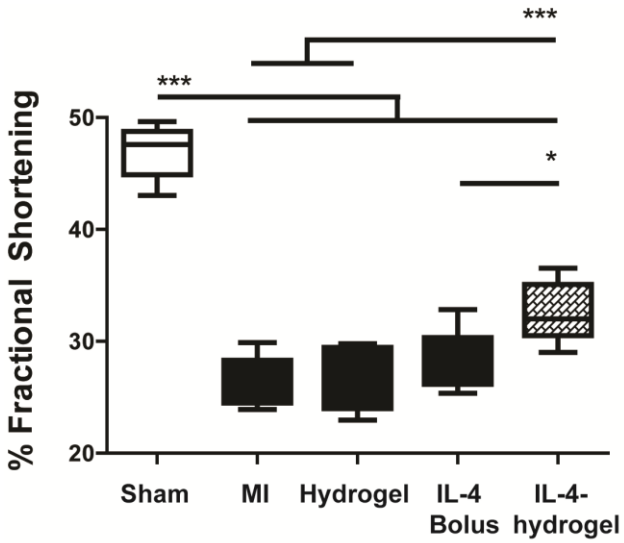


**Figure 23. Effect of *in vivo* delivery of IL-4-hydrogel delivery on acute cardiac function in a rat model of MI.** Grouped data (mean ± SEM; n=6-9) at day 7 following MI and injections. Cardiac function was evaluated by echocardiography using % fractional shortenting measurements. (*p<0.05; **p<0.01; ***p<0.001; one-way ANOVA followed by Tukey's Multiple Comparison post-test).

### 5.3.6 Fibrosis

To determine levels of fibrosis following MI, tissue sections were stained with picrosirius red 21 days following MI and fibrotic area was normalized to total heart tissue section on each respective slide. Animals that received no treatment had a fibrotic area of 56.3±20% (Mean ± SD) of total area (Figure 25A), although the variability in this group was the highest leading to no statistically significant differences in any of the treatment groups despite the trend of reduced fibrosis in groups treated with bolus IL-4 or IL-4-hydrogel.

### 5.3.7 Angiogenesis

To determine levels of angiogenesis, sections were probed with an Alexa Fluor 647-labeled isolectin conjugate and percentage of the infarcted tissue section showing staining for endothelial cells/vessels was quantified to determine percent changes in

angiogenesis in the IL-4-hydrogel treated animals compared to untreated animals that underwent MI. IL-4-hydrogel treated animals exhibited a trend towards increased percent vessel formation in the infarct area than the untreated animals (Figure 25B) suggesting the potential of IL-4 encapsulated PEG hydrogel to enhance angiogenesis following MI.

### 5.3.8 *In vivo* acute gene expression profile and plasma cytokine levels

In order to determine whether IL-4-hydrogel delivery contributed to changes in the inflammatory milieu of the infarct, at 1, 2, 3 and 7 days following MI and IL-4-hydrogel injections (n=3 at each time point), the gene expression levels of classic M1 macrophage markers pro-inflammatory cytokines TNF-α, IL-1β, chemokine MCP-1 as well as iNOS enzyme was evaluated and expressed as fold changes in gene expression from sham levels (Figure 26). Although this study is a survey of gene expression and not powered enough to reliably perform statistical analyses (ongoing studies thoroughly characterize them in these 2 groups as well as the bolus IL-4 delivery group) there is a general overall trend for the reduction of TNF-α in IL-4 hydrogel treated group compared to untreated animals and perhaps of IL-1β on day 7 and MCP-1 on day 3 and 7. Other genes examined did not show any notable trends (Figure A18).

We further analyzed the plasma obtained from day 3 in these animals for the chemokine MCP-1 and pro-inflammatory cytokine IL-12β levels and show a strong trend for reduced levels of IL-12β and significant reduction in MCP-1 levels ($p<0.05$) in the IL-4-hydrogel treated animals (Figure 27).

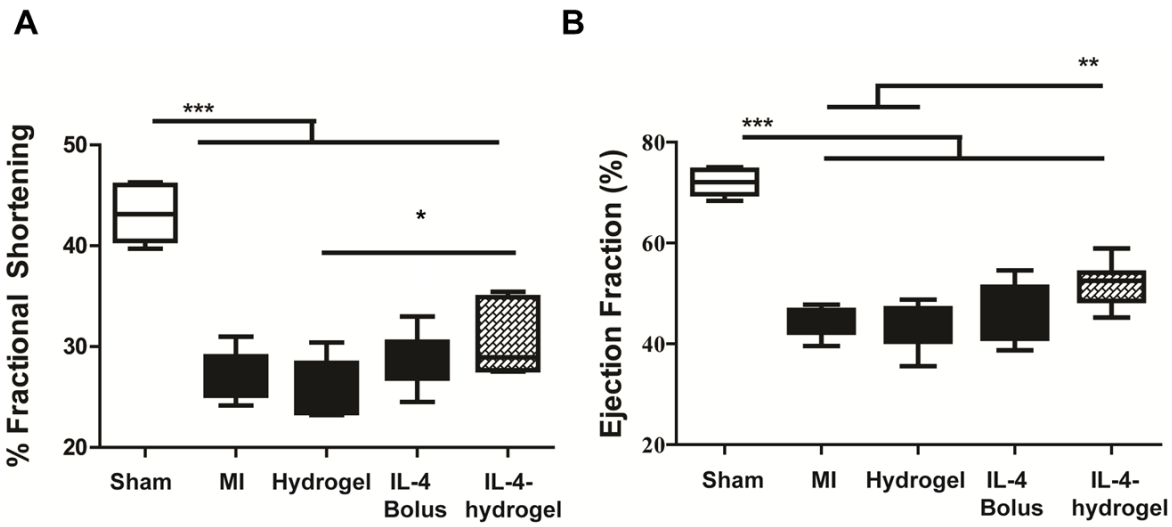


**Figure 24. Effect of IL-4 hydrogel delivery on chronic function**. Grouped data (mean ± SEM; n=6-9) at day 21 following MI and injections. Cardiac function was evaluated by echocardiography using (A) % Fractional shortenting measurements and (B) % Ejection fraction from invasive-hemodynamics measurements (*p<0.05; **p<0.01; ***p<0.001; one-way ANOVA followed by Tukey's Multiple Comparison post-test).

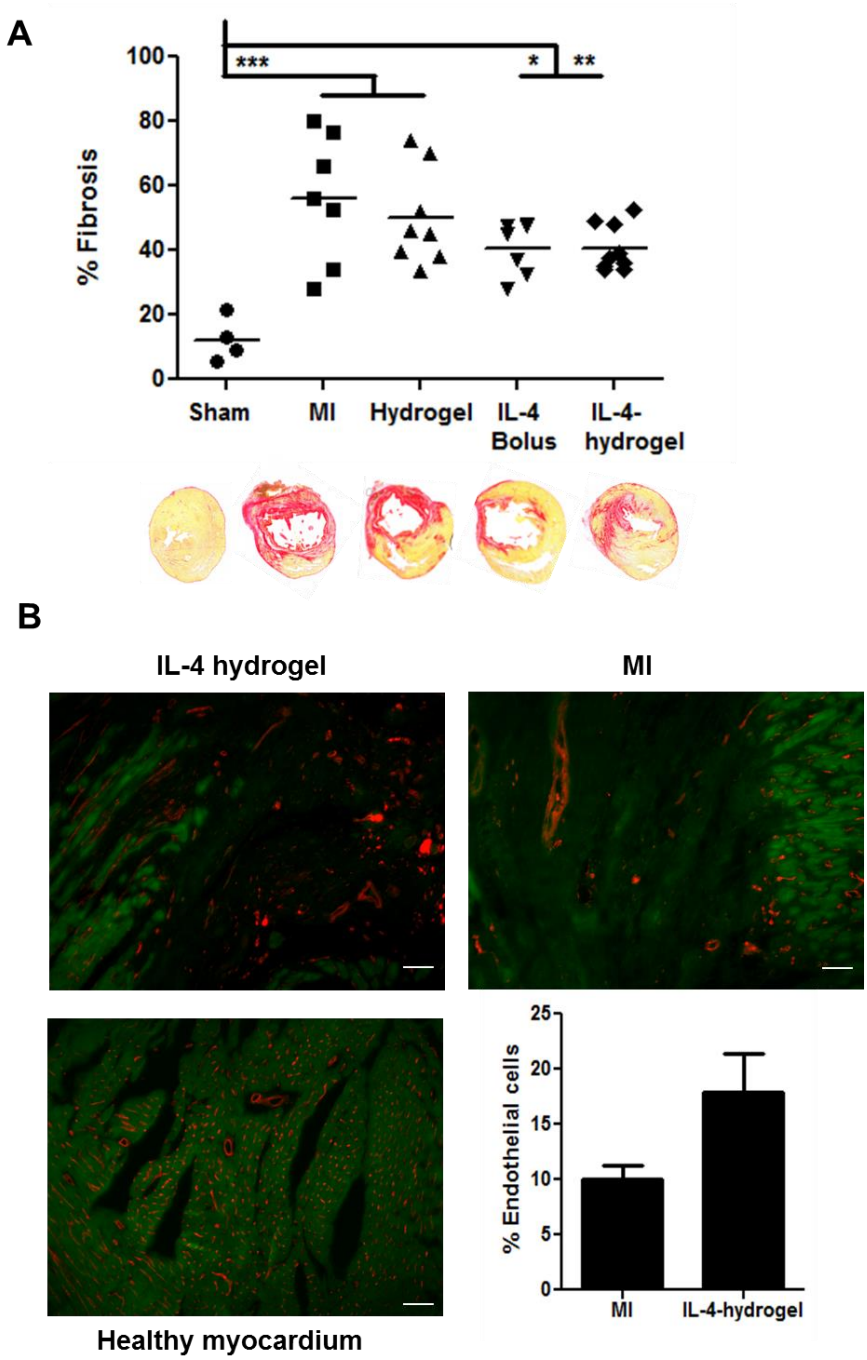


**Figure 25. Evaluation of cardiac repair following in vivo delivery of IL-4-hydrogel.** Grouped data (mean ± SEM; n=6-9) from immunohistological analysis at day 21 following MI and injections. (A) Fibrosis was measured by staining for collagen using picrosirius red (red stain, images taken at 4x magnification). (B) % Area of isolectin staining was calculated as a measure of new vessel density (red stain) (Scale bar, 50μm) (*p<0.05; **p<0.01; ***p<0.001; one-way ANOVA followed by Tukey's Multiple Comparison post-test).

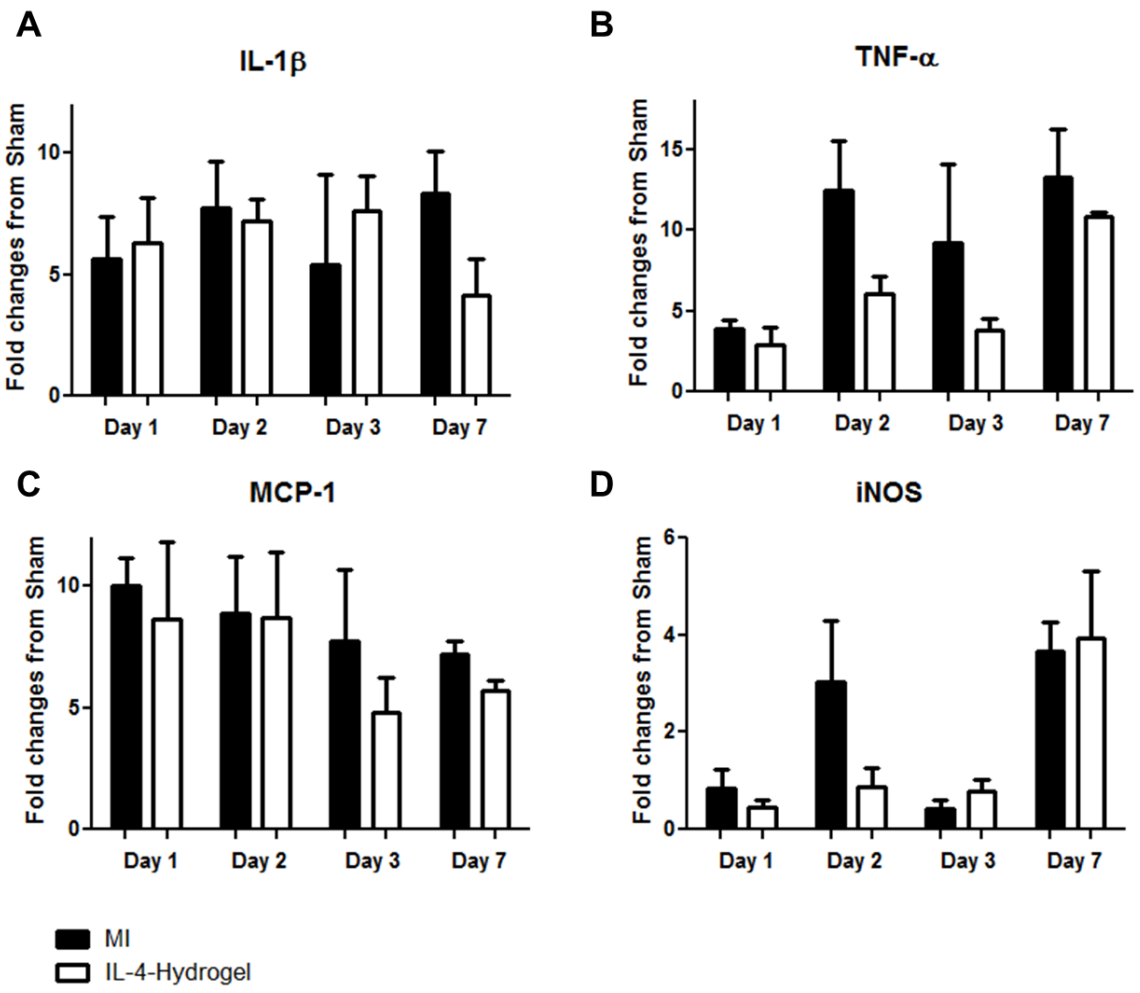


**Figure 26. Effect of IL-4-hydrogel delivery on pro-inflammatory cytokine gene expression levels over a course of a week.** Grouped data (mean ± SEM; n=3 per group) LV infarct tissue gene expression of (A) IL-1β, (B) TNF-α, (C) MCP-1 as well as (D) iNOS from animals on days 1,2,3 and 7 after MI with or without IL-4 hydrogel treatment. Gene expression was evaluated by qRT-PCR using the comparative Ct method and the results were normalized to GAPDH levels and reported as fold changes in copy number of mRNA levels compared to sham animals.

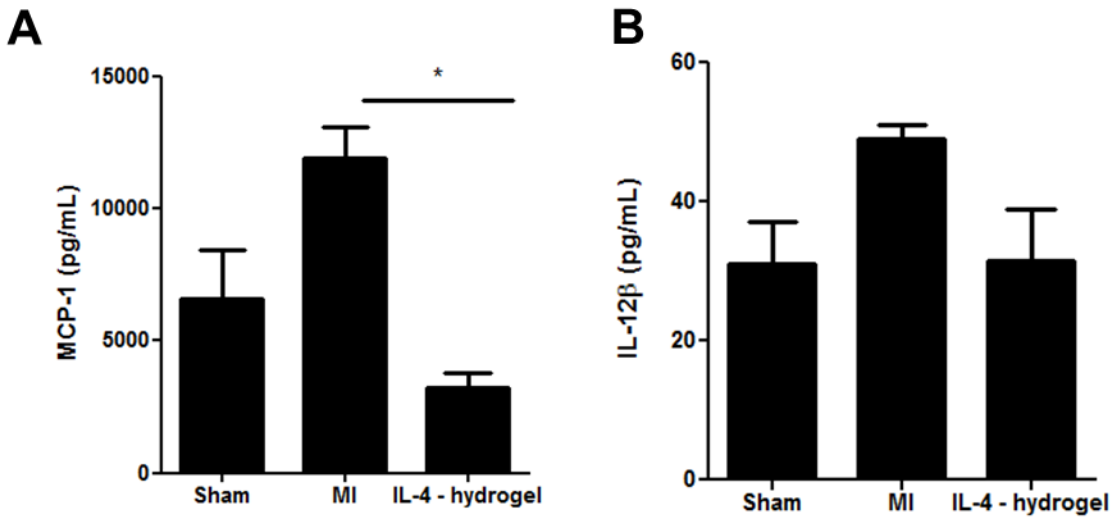


**Figure 27. Effect of IL-4-hydrogel on plasma levels of MCP-1 and IL-12β.**
Grouped data (mean ± SEM; n=3 per group) from plasma at 3 days. Levels of chemokine (A) MCP-1 and cytokine (B) IL-12β determined from Luminex Multiplex system and reported as plasma cytokine concentrations quantitatively derived from standard curves of each cytokine. (*$p<0.05$; one-way ANOVA followed by Tukey's Multiple Comparison post-test).

## 5.4 Discussion

Current regenerative approaches to prevent cardiac dysfunction following MI focus largely on stem cell therapy or molecular therapies aimed at enhancing the regenerative capacity of the heart, an organ long thought to be terminally differentiated. Even with recently found niches of endogenous cardiac stem-cells capable of differentiating into many cardiac lineages, human heart is no zebra fish or adult newt heart with enviable cardiac regenerative capacity. While the ideal therapy for cardiac dysfunction would bring about complete cardiac regeneration, it is imperative in the meantime to explore processes that can influence and improve cardiac wound healing. Interventions to enhance wound healing may open up a new therapeutic window between the few hours that may be used to limit necrosis by reperfusion and an irreversible cardiac scar that can better respond to other promising regenerative interventions.

Much interest has been devoted to studying inflammatory pathways as therapeutic targets to halt the progression of heart failure, specifically the role of

monocytes/macrophages and several immunomodulatory strategies have emerged in the field [191, 202-204]. A notable example is work from Nahrendorf's group where chemokine receptor CCR2 that localizes the pro-inflammatory Ly-6C$^{high}$ monocyte subset to the site of infarct was targeted for therapeutic silencing. This subset of monocytes gives rise to the pro-inflammatory M1 macrophages following MI, and reducing their influx to sites of injury by suppressing CCR2 attenuated their accumulation in atherosclerotic plaques and reduced infarct size after MI in mice [191]. However, in light of recent evidence demonstrating that biphasic macrophage responses likely derive from the same recruited pool of Ly6C$^{hi}$ monocytes regulated by a nuclear hormone receptor switch (Nr4a1) [89], the previous theory of sequential recruitment of the biphasic macrophage population has been revised. This new direction for the field would suggest providing local biochemical cues to differentiate pro-inflammatory monocytes/macrophages towards a reparative phenotype rather than reducing the influx of monocytes to the site of infarct to be a more suitable approach to aid balanced and effective cardiac repair. An approach in line with this thought process exploited the anti-inflammatory propagating properties of apoptotic cells by devising liposomes that mimic apoptotic cells. Delivery of these liposomes augmented anti-inflammatory response while suppressing pro-inflammatory response rats following MI, bringing about inflammation resolution and preventing infarct expansion [203]. Similarly, our approach aims to induce classically activated pro-inflammatory monocytes/macrophages to switch to an alternately activated reparative phenotype by delivering the polarizing cytokine IL-4 to the infarcted myocardium, with the ultimate goal of creating a balanced inflammatory environment that can influence cardiac wound healing in a favorable manner.

One of the hallmarks of regeneration is revascularization of injured tissue, and role of macrophages in angiogenesis is extensively studied and several reports have implicated them as key contributors to the process of angiogenesis [87, 205] and our in vitro results confirm that the IL-4 treated alternately activated macrophages enhance tube

formation in endothelial cells. Further, in a serum/growth factor limited (1% serum), 3D collagen environment, paracrine factors secreted from alternatively activated macrophages contribute significantly to cell viability, spreading and tube pre-cursor structures of endothelial cells. This is an indicator of angiogenic potential crucial to effective cardiac repair. Another important aspect of wound healing is the recruitment of progenitor/stem cells to the area of injury and the modulation of stem cell populations to promote repair. An elegant study conducted in adult salamanders that possess extraordinary regenerative capacity shows lack of limb regeneration when macrophages were depleted from their system [206]. The authors speculate a potential mechanism whereby macrophages promote dedifferentiation and formation of the progenitor pool that contributed to regeneration. Furthermore, several studies have suggested a critical role for macrophages in the beneficial outcomes observed from stem-cell therapy to treat the infarct [207-209]. Taken together, there is compelling evidence suggesting a crucial interplay between macrophages and progenitor cell populations in a regenerative environment. A majority of studies exploring this phenomenon only tested the hypothesis that mesenchymal stem cells influence macrophage phenotype in favor of effective cardiac repair [207, 210, 211]. While it has been shown that alternately activated (M2) macrophages promote MSC growth and viability [212], in our study we sought to explore the possibility of macrophages influencing stem cell recruitment. Our *in vitro* migration studies demonstrate enhanced migration of Cardiac Progenitor Cells (CPCs) towards conditioned media from M2 differentiated macrophage. While this study did not provide a mechanism for paracrine effects involved in this increased migration of stem cells observed, future studies could build on these encouraging results to further explore the roles M2 macrophages may have on endogenous stem cell populations in the heart, and the recruitment of mobilized bone-marrow derived stem-cell populations.

Macrophage plasticity has been an interesting area of study with implications in many disease areas. From the M2 like tumor-associated macrophages to deleterious

effects of M1 macropahges in atherosclerosis, to our very interest in the biphasic nature of macrophage role after MI, the two-faced characteristics of macrophages has raised several questions as to the plasticity of macrophages in the interest of therapeutic modulation [90, 156, 157, 188, 189, 213-216]. Monocyte/macrophage lineage is generally thought to be plastic with remarkable abilities to change their activation type based on external microenvironmental cues [194, 195, 217, 218]. However, various studies have shown mixed results in the ability of macrophages to completely switch phenotypes in a sequential manner, and the jury is still out on definitive outcomes [219-221]. The general consensus is that macrophages exist in a continuum of a spectrum of activation states with M1 and M2 phenotypes being the extremes [193-195, 217, 222]. Re-polarization studies in our hands in both RAW 264.7 macrophages and BMM macrophages demonstrate that sequential activation from M1 to M2 has little effect on reversing the M1 characteristics, while simultaneous activation suppresses the M1 characteristics and promotes M2 activation, suggesting the possibility of achieving a hybrid functional phenotype of macrophages favoring M2 activation from a therapeutic strategy that attempts to provide IL-4 as a cue to re-polarize pro-inflammatory macrophages towards a reparative phenotype. These results make a case for earlier presence of IL-4 in the pro-inflammatory myocardial environment to achieve such modulatory efforts, and this has several implications for the design criteria for the delivery system, especially that of temporal control of release. Furthermore, monocyte kinetics studies following MI suggest rapid turnover of the monocyte/macrophage populations recruited to the infarct, with a continuous flux and an average of 20 hours at the infarct for each wave of recruited cells. Taken together, an ideal delivery system for the desired application would release IL-4 in a controlled manner starting at the time of injection following MI over a period of 3-4 days during which the pro-inflammatory response peaks.

We evaluated the PEG-MAL hydrogel cross-linked with protease cleavable linkers for their ability to release IL-4 in a controlled manner with and without the enzymatic trigger in the form of Collagenase I enzyme. Hydrogels formed from 5 and 6% in either the 10 kDa or 20 kDa exhibited similar release profiles for IL-4 (~14kDa). In comparison, the 10x larger IgG (150 kDa) displayed more controlled and distinct release profiles when weight percentages or the molecular weight of the PEG macromere was altered. These differences suggest that the mesh size of the PEG-MAL hydrogel may be too large to enable controlled delivery of IL-4 from this material. However, interestingly, the release tapers off after the first 10 hours to only release 10-15% more of the IL-4 in the span of the next 38 hours. This suggests an interior pocket of tightly cross-linked hydrogel that traps the protein tightly, thus causing an inflection point in the release profile when this region is just about tapped. Enzymatically triggered release would be ideal at this layer to release this remaining depot of trapped IL-4. However, to make the best use out of the enzymatic trigger, the burst release from the hydrogel would need to be controlled to leave a larger percentage of the IL-4 remaining, so that even when proteases secreted by macrophages during the initial inflammatory phase during MI act on the gel, the release would be controlled, and not bulk release. One of the many ways to achieve this outcome would be to engineer fusion proteins of IL-4 with a cysteine group that can then be physically tethered to the gel. Another strategy would be to functionalize the hydrogel with biotinylated peptides that can then use the streptavidin-biotin linkages to tether IL-4 to the hydrogel. An alternate strategy could, for instance, encapsulate IL-4 in polymeric microspheres or present IL-4 on the surface of the particles, and the hydrogel could encapsulate these particles, affording a multi-layered controlled release. Further studies would build upon these strategies to optimize the delivery system, and in the meanwhile, we seek to gain proof-of-concept from this initial *in vivo* study with a 5% PEG-MAL hydrogel encapsulating IL-4.

Other important criteria for the successful implementation of biomaterials for delivery of proteins to the myocardium include preservation of bioactivity and biocompatibility. Our *in vitro* studies confirm that IL-4 is released from the PEG-MAL hydrogel in bioactive form (Figure A17). Additionally, previous studies from our group have shown active release of growth factors from the PEG-MAL hydrogel *in* vivo and the hydrogel has not shown any adverse immunological reaction in the myocardium [33], which is substantiated by the extensive characterization of PEG hydrogels for a variety of biomedical applications that show these materials to be non-fouling, inert and non-immunogenic [32, 97, 223, 224].

Delivery of IL-4 from the PEG-MAL hydrogel was compared to bolus IL-4 delivery into the myocardium of a rat model of MI. The time-course *ex-vivo* bioimaging revealed strong fluorescence signals in the hearts for 3 days in the animals receiving IL-4 hydrogel injection, suggesting retention of the delivery system in the heart. The fluorescence signals were 2-3 times higher in the heart than the bolus IL-4 delivery approach, and very minimal fluorescence was observed in other organs with the hydrogel mediated IL-4 delivery. We investigated the effect of IL-4 delivery on cardiac function. At an acute 7-day time point, there was a significant improvement in cardiac function in the IL-4 hydrogel treated group compared to all controls including the bolus IL-4 delivery. Interestingly this improvement is not as definitively sustained at the chronic 21-day time point. Histological analysis of new vessel formation at this chronic time point shows only a modest trend of increased percentage of endothelial vessels in the IL-4 hydrogel treated group compared to rats that received no treatment post-MI. In addition, there were no changes in levels of fibrosis in any of the treatment groups as compared to untreated MI group. These results are in contrast to our original hypothesis that effective IL-4 delivery to the heart during an earlier window through the inflammatory process could stimulate a balanced cardiac repair process resulting in chronic functional improvement. However, the initial acute improvement in function is encouraging, and

although there were no significant changes in the local inflammatory gene expression profile upon IL-4 hydrogel delivery in this low powered pilot exploratory survey, there were some encouraging trends in reduction of pro-inflammatory mediators. One such trend within 2-3 days post-MI is of pro-inflammatory cytokine TNF-α (Figure 26), a powerful upstream inflammatory mediator of many of the pathophysiological processes that take place in the progression of cardiac dysfunction [37]. Another notable decreasing trend is the expression levels of MCP-1 from day 3-7, the chemokine responsible for the recruitment of monocytes to the infarct [37]. This reduction in MCP-1 levels was corroborated by a significant reduction in the plasma MCP-1 levels at day 3 (Figure 27).

While these results potentially give support to the merits of IL-4 delivery to exert anti-inflammatory effects at the very least, the lack of improvement in chronic function raises two possibilities: one possibility is that the modest anti-inflammatory effects and other untested mechanisms through which IL-4 potentially acted to provide acute functional improvement may not have been sufficient to enhance the wound healing process as originally hypothesized; another possibility is that the delivery system was not ideally suited to deliver IL-4 in sufficient quantities to effect the changes desired in macrophage phenotype. While IL-4-hydrogel delivery better retained IL-4 in the myocardium, it is possible that during the bulk of the release of IL-4 in the first 12 hours (as suggested by the *in vitro* release studies with 5% PEG hydrogel), the inflammatory phagocytes were not present in abundance to effect sufficient functional modulation of the monocyte/macrophage phenotype to translate to functional cardiac repair. Furthermore, as suggested by the bioimaging study, the hydrogel likely degraded by day 7, and perhaps employing a less protease-sensitive cross-linker could minimize the protease-mediated degradation and allow the gel to remain in the heart longer, affording mechanical support which has been shown to be beneficial in cardiac remodeling following MI [96]. Taken together, our *in vivo* study employing IL-4-hydrogel delivery suggests that the retention of IL-4 in the heart is higher than with bolus IL-4 delivery, and

that there is promising acute functional improvement and potential ant-inflammatory effects induced by IL-4 hydrogel delivery which warrants further study and thorough characterization of gene expression at these acute time points in comparison with bolus IL-4 delivery. While chronic functional improvement or improved cardiac remodeling are not observed, optimization of the hydrogel delivery system to achieve a more controlled delivery of IL-4 to the heart could potentially elicit a stronger polarizing effect on the macrophage population and the inflammatory milieu.

# CHAPTER 6 CONCLUSIONS AND FUTURE DIRECTIONS

## 6.1 Polyketal-siRNA delivery for antioxidant therapy

Antioxidant therapy has shown promise in battling the excessive ROS production caused by infiltrating neutrophils and macrophages during the initial stages of inflammation post-MI in pre-clinical models. However, to date none has been clinically translated to successful treatment options. Identification of appropriate therapeutics, temporal window of administration as well as delivery hurdles have all contributed to lack of translation. Chapter 3 describes polyketal nanoparticles as a viable system for the local delivery of siRNA against a major oxidant enzyme Nox2-NADPH in the heart following MI. We were able to demonstrate their intracellular localization in macrophages *in vitro* and the ability to knockdown Nox2-NADPH oxidase at the genetic and protein levels *in vitro*. At a low dose of 5μg siRNA/kg, the delivery of Nox2-siRNA by polyketal particles was able to restore acute cardiac function following MI injury in mice. These results point to the potential of Nox2-NADPH as a therapeutic target in acute-MI and consideration of polyketal particles as siRNA delivery vehicles for future large-animal studies.

The infarcted heart is an inflammatory environment and special care should be devoted in designing drug delivery approaches that do not exacerbate those conditions. The major strength of PK3 polymers for siRNA delivery in the context of MI is their biocompatibility, especially in light of the alternative approaches of cationic lipids that can generate cytotoxicity. However, a cationic lipid DOTAP was used to ion-pair to siRNAs in order to charge neutralize them prior to formulation, and while the cationic residues are not exposed on the surface of the particles, it would be ideal to eliminate these from the formulation process. Future generations of this delivery system could explore the use of biological cationic molecules such as spermidine for efficient complexation of siRNA [225].

Polyketal polymeric particles are also ideal vehicles for intracellular delivery of therapeutics to target phagocytic macrophages, as they are taken up efficiently by these cells. Further, since PK3 polymers are synthesized using acid degradable ketal linkages, they enable design of nanoparticles with pH sensitive degradation properties, and in the setting of siRNA delivery following endocytosis/phagocytosis, this represents a unique opportunity [122, 226]. When a nanoparticle formulation is endocytosed, intracellular trafficking begins in early endosomal vesicles which subsequently fuse with sorting endosomes, which in turn transfer their contents to the late endosomes (pH of 5-6) The late endosomal content is then relocated to the lysosomes (pH ~4.5) and contain various nucleases that could degrade the siRNAs. To avoid lysosomal degradation, siRNAs must escape from the endosome into the cytosol, in order to associate with the RNAi machinery. In the field of nucleic acid delivery, endosomal escape is thought to be the rate-limiting step, and one of the most challenging barriers for efficient siRNA delivery [164]. As our particles are acid sensitive, they potentially degrade in the moderately acidified endosomes and enable release of siRNA. In order to ensure faster degradation of the particles, we incorporated another pH sensitive small molecule chloroquine to the formulation. However, there is potential to further engineer the polyketal polymers to afford even better spatial and temporal control of degradation without the incorporation of chloroquine, for instance, by synthesizing polyketal polymers that are highly sensitive to changes in pH so that they degrade faster, even at the slightly acidified pH of 6, ensuring protection of siRNA from nucleases of the late endosomal/lysosomal compartments.

Furthermore, in terms of endosomal escape, there can be many other potential improvements to the system. A recent study tracked endosomal trafficking of siRNA Lipid Nanoparticles (LNPs) and found that only a very minor fraction (1–2%) of siRNAs were released from endosomes [164]. Further, the authors found that the bulk of these siRNAs were released from moderately acidified early endosomal compartments, and

interestingly they were not released due to bursting of endosomes or permeabilization of the limiting membrane of endosomal compartments, but rather from individual siRNAs escaping from multiple endosomal compartments. This concerning fraction of only 1-2% of siRNA reaching the cytosol necessitates re-thinking of the nucleic acid delivery problem in terms of design of delivery vehicles. We incorporated the chloroquine into the particles not only to enhance pH-mediated degradation, but also to aid in endosomal escape. As a weak base, chloroquine gets protonated in the acidic environment of endo/phagosomal compartments, which can trigger swelling and destabilization of their membranes to facilitate release of siRNA into the cytoplasm [149]. However, it is not clear whether the endosomal contents are released at once due to endosomes bursting, or the effect is more destabilization of the compartment, permeabilizing the membranes to allow for siRNA to leak out of the endosome, somewhat similar to that demonstrated in the study describing LNP tracking. Further studies would have to be done to ensure the mechanism of endosomal escape and to optimize the system to obtain even lower therapeutic concentrations. Incorporation of fusogenic lipids or membrane interacting peptides with high buffering capacity to the polyketals could contribute to rapid endosomal escape and warrants further study. .

A variation of the polyketal polymers that contain thioketal linkages sensitive to ROS has been used to encapsulate pro-inflammatory cytokine TNF-α targeted siRNA in a similar manner as in our study. When orally delivered to an intestinal inflammation mouse model, these particles degraded in response to the high levels of ROS in the intestine, knocked down TNF- α and protected mice from ulcerative colitis. This study illustrates the versatility to engineer these polymers to respond to various stimuli such as pH and ROS and substantiates the utility of polyketals as nucleic acid delivery vehicles in an inflammatory disease application. Future studies could incorporate antioxidants (small molecules, proteins or nucleic acids) in polythioketals to deliver to the myocardium as an on-demand delivery system that degrades in the presence of ROS, to suppress ROS.

In a related study employing polyketals, Seshadri, et al. delivered antioxidant protein superoxide dismutase (SOD) to the rat myocardium of an ischemia-reperfusion (IR) model of MI. This study was similar in the nature of modulation (antioxidant therapy) and acute time point of assessment (day 3 post-MI), and demonstrated sustained release of SOD as well as the ability to scavenge both intra- and extra-cellular superoxide in the myocardium following IR. This contributed to a four-fold reduction in cardiac myocyte apoptosis compared to IR-surgeries alone at an acute day-3 time point, which reflected in restored cardiac function. While our study employing PK-siNox2 did not investigate the mechanistic aspect for the beneficial restoration in cardiac function observed, the study delivering PK-SOD suggests that prevention of apoptosis could be one of the mechanisms of action. Interestingly, the SOD delivery did not sustain functional improvement in the chronic time point, and using a second polyketal-based therapy to target chronic inflammation (PK-p38i microparticles) had synergistic effects as animals that were treated with both PK-SOD and PK-p38i achieved significant improvement in chronic function [121, 124]. Our study did not assess the chronic effects of Nox2-siRNA delivery such as its effect on fibrosis as well as long-term functional improvement, and in light of results from the PK-SOD study, it is imperative to conduct these chronic studies to determine whether higher dosage or repeated injections or other synergistic therapies that target long-term chronic inflammation are necessary to sustain benefits of knocking down Nox2 at the initial inflammatory stage following MI. Further, oxidative stress markers (lipid and protein peroxidation markers) should be assessed as well, to confirm the direct antioxidant mechanism of action.

Further, our study did not confirm *in vivo* knockdown of Nox2 mRNA expression to be primarily in macrophages, although in previous studies, non-modified PK particles have not shown effective uptake by non-phagocytic cell types [123, 227]. However, while the infiltrating inflammatory cells represent a large source of $O_2^-$ following infarction, Nox2 is also expressed on other cardiac cell types, and is indeed

overexpressed in cardiomyocytes following infarction. It is possible that for long-term functional improvement other cell types will need to be targeted. A recent publication from our laboratory demonstrates that PKs modified to present N-acetylglucosamine ligands on the surface are taken up by cardiomyocytes, and this could allow for dual targeting of Nox2 in other cell types [227]. Studies to assess the efficacy of this approach would be an exciting possibility to further polyketals as targeted siRNA delivery vehicles to the myocardium, potentially even extending this approach to a completely non-invasive I.V delivery route. This approach then widens the scope of nucleic acid delivery mediated by polyketal nanoparticles to non-phagocytic cells, and especially to mycocyte, a cell type that scarcely takes up foreign particles, and is of utmost interest to the field of regenerative cardiology in terms of drug delivery.

Finally, use of polyketals for nucleic acid delivery can extend beyond inflammatory disease applications. *In vitro,* phagocytic bone marrow derived mononuclear cells derived from the hematopoietic linage were able to express pluripotent gene expression when a cocktail of embryonic stem cell specific microRNAs were delivered to them via PK3 polyeketal nanoparticles [228]. The application of these particles was well tolerated by these primary mononuclear cells and opens up the possibility to use polyketals as effective reprogramming tools with implications in the field of regenerative medicine and stem cell technologies.

### 6.2 Spherical nucleic acid delivery for anti-inflammatory therapy

Chapter 4 describes an efficient gene silencing methodology for anti-inflammatory therapy in a rat model of MI. Catalytic DNA (DNAzyme) targeted against mRNA of pro-inflammatory TNF-$\alpha$ was functionalized to gold particles in a spherical nanostructure to impart enhanced substrate binding, stability and cellular uptake. The advantages of this system include stability and low cost of DNA over RNA for gene silencing, and the simple synthesis scheme employing the gold-sulfur self-assembly

technology. A significant advantage of this system is the non-inflammatory nature of the gold-DNA conjugates that make them ideal nucleic acid delivery vehicles in the context of the inflammatory post-MI environment, and this is demonstrated by our comparative studies with widely used cationic lipid particles. *In vitro* results from our studies show efficient uptake of DNAzyme particles by primary macrophages (as well as myocytes) and 50% knockdown of TNF-α at the protein level. *In vivo* studies demonstrate significant anti-inflammatory effects conferred by the knockdown TNF-α by DNAzyme particles and significant improvement in acute cardiac function compared to untreated rats.

While these results are promising, it is important to keep in mind that the inflammatory cascade that follows MI is a complex network of molecular events dictated by cellular, spatial and temporal variables and mediated by molecules with pleiotropic effects such as chemokines and cytokines. Further, cytokines in an inflammatory disease state exhibit redundancy, synergistic activity and antagonistic effects upon each other. Therefore while these inflammatory mediators such as TNF-α appear to be appropriate therapeutic targets when considering their deleterious effects in the early stages of the inflammatory response, it may also be necessary to carefully consider their roles as regulators of cardiac repair [37]. In the case of TNF-α, it may very well be the case that complete or prolonged inhibition of this critical inflammatory mediator may be dangerous for the progression of HF, albeit crucial to modulate in the earlier stages. This was the rationale for utilizing transient gene silencing in the early stages of MI in this study as the first step in a long road to reviving such an anti-inflammatory therapy to the clinics.

The next step in this process is to explore the optimal temporal window to employ TNF-α antagonism, and a few modifications to the current drug delivery system could be used to test this possibility in a minimally invasive manner. The DNAzyme orientation on

the gold particle is shown to be important for the catalytic activity, and in previous work published, it has been shown that DNAzyme anchored through the 5' terminus were inactive. Gold particles functionalized in this fashion were photoactivated by irradiation with a 532nm pulsed laser to partially release the DNAzyme to trigger catalytic activity [31]. Such a mechanism could be used deliver the therapeutic particles to the myocardium following MI surgery as was done in this study, and systematically trigger the release at various time points to induce TNF-α suppression, enabling a wealth of information with regard to the effects of temporal control of release.

Further *in vitro* studies could accompany and lend support to this approach to achieve temporal control of silencing activity. Kinetic studies evaluating the catalytic activity through a time course of 1 hour to 72 hours would be ideal to evaluate the earliest time of knockdown following particle uptake and the temporal window of maximum knockdown. The biggest challenge to this study is establishing a model of TNF-α upregulation, as even macrophages do not produce TNF-α unless subjected to injury. We have been employing bacterial endotoxin LPS to stimulate TNF-α production, and for these kinetics studies planned, the kinetics of TNF-α production upon LPS stimulation would have to be determined at an appropriate concentration in order to provide a steady-state level of TNF-α in the *in vitro* model to then apply the DNAzyme particles for the kinetic study. Multiple dosages should also be evaluated in this study, and extended to *in vivo* studies as well in order to determine the optimal therapeutic levels of DNAzyme particles for maximum desired biological effects (silencing and anti-inflammatory and functional measures).

Implementing the optimal temporal window and therapeutic dosage, future studies should entail evaluating the efficacy of these particles in chronic functional studies. In addition to cardiac function, immunohistochemical analyses evaluating extent of cardiac fibrosis and angiogenesis should be evaluated to assess the effect of TNF-α antagonism

on cardiac repair. These studies would definitively address whether other therapeutic mechanism should supplement regulation of TNF-α to achieve effective cardiac repair and prevent progression of HF.

Often touched on, but not explored further in my thesis work is the ischemia-reperfusion (IR) model of MI, arguably the more clinically relevant model for the study of post-MI treatment strategies as early reperfusion therapies are the gold standard in the management of MI. As discussed in various section of my thesis, the paradoxical reperfusion injury stimulates ROS and vascular inflammation. TNF-α is an established regulator of ROS production and directly implicated in many of the processes associated with vascular inflammation such as upregulation of leukocyte adhesion molecules [70, 77, 229], and therefore employing IR models of MI to test gene silencing by DNAzyme particles may be of significance to move this approach along towards translation.

### 6.3 Bioactive PEG-hydrogel for immunomodulation

The overall objective of the study described in chapter 5 was to deliver polarizing cytokine IL-4 to the heart to alternately activate monocytes/macrophages recruited to the infarct following MI, and assess the effect of this strategy on the inflammatory environment in the myocardium, cardiac repair and functional recovery. We validated this approach *in vitro* by polarizing primary and immortalized cell line of macrophages and testing the beneficial paracrine effects of conditioned media from alternatively activated macrophages on endothelial cell survival, tube formation and cardiac progenitor migration. In order to demonstrate proof-of-concept of this strategy *in vivo*, we utilized an injectable polyethylene glycol (PEG) based hydrogel end-functionalized with maleimide groups (PEG-MAL hydrogel) to allow for functionalization with cysteine containing peptides or proteins. This allows the incorporation of a protease cleavable peptide cross-linker, thus enabling a protease degradable delivery system. Macrophages upregulate proteases in the myocardium during the initial inflammatory phase following MI, and

could potentially trigger degradation of the gel to release IL-4 in an on-demand fashion. However, *in vitro* release characteristics of IL-4 from most variations of the PEG-MAL hydrogel compositions indicate high levels of burst release of this small cytokine (14kDa) and therefore indicate further need for optimization of the delivery system for this application. *In vivo* evaluation of IL-4-hydrogel delivery conferred acute functional improvement and trends of low levels of pro-inflammatory markers TNF-α and MCP-1, although chronic functional study (day 21) did not show any significant improvement in function. This accompanied by lack of significant improvement in fibrosis or angiogenesis indicate the need to carry on future studies that can investigate mechanisms to sustain the initial improvement in cardiac function observed with the IL-4 hdyrogel delivery. One of the primary efforts would be focused on optimizing the delivery system and some of the potential strategies to optimize the release profile of IL-4 from the PEG-MAL hydrogel to prevent burst release and sustain controlled release were outlined in the discussion of chapter 5. Further alternative strategies are discussed here along with other potential materials to consider for this immunomodulatory application as well as other potential parallel or synergistic approaches to IL-4 delivery.

With the PEG-MAL hydrogel, an alternative strategy to intramyocardial injection would be to design a multifunctional hydrogel scaffold that could be applied as a patch, with non-uniform loading distribution, accentuating what we already see with the tightly trapped inner layer. For instance, a center layer of hydrogel could be made up of a high wt% such as 12% PEG-MAL in order to minimize the mesh size and encapsulate IL-4, which is then re-encapsulated by another layer of the hydrogel, preventing burst release and allowing for controlled release. This strategy could also allow for truly on-demand enzymatic release when macrophages infiltrate the hydrogel and release proteases to degrade the gel. Further, several studies demonstrate that hydrogels themselves can acutely improve function due to mechanical support of the LV wall [96] and therefore an application of a patch for drug delivery could lend the additional benefit of mechanical

support, to further enhance cardiac repair. Alternately, microgels formed from PEG-MAL hydrogel, previously used for cell microencapsulation [230], could be utilized to microencapsulate IL-4 and then re-encapsulated by the hydrogel to allow for controlled release via this multilayered system. This hydrogel could be cross-linked with peptide linkers less sensitive to proteases so as to slow down the enzymatically-triggered release as well.

While PEG is a material desirable for many biomedical applications due to their non-fouling surface characteristics, in an application where the goal is to modulate the immune response to achieve a certain regenerative outcome, a biomaterial with known immunomodulatory properties may even be more ideal. Chitin is a non-toxic, biodegradable and biocompatible natural polymer (amino polysaccharide) used in various biomedical applications. Notably they have been used to create tissue engineering hydrogel scaffolds and as wound dressing material due to their ability exert Th2 like, anti-inflammatory effects on immune cells including macrophages [231-234]. Recent advances in chitosan chemistry have proposed numerous controllable gelation methodologies for these materials, and would be an interesting avenue to test out their ability to induce M2 polarization to enhance myocardial wound healing. Self-ssembling peptides are another class of materials that have found numerous tissue engineering and protein delivery applications for myocardial regeneration, and possess numerous inherent advantages amenable to protein delivery, especially that of programmability that allows for incorporation of small fusion proteins [235] as well as assembly triggers [236] and stimuli-responsive degradation properties such as MMP cleavable sites [237]. Further, as peptides, they provide numerous functional moieties to facilitate physical tethering of cytokines/growth factors to these injectable peptide nanofiber gels.

While our existing knowledge of the M1/M2 paradigm has expanded in the recent years, further understanding the regulatory mediators that facilitate the M1 to M2 shift in following MI needs to be explored further. Several studies have definitively shown that

the spleen deploys the pro-inflammatory monocytic population ($Ly6C^{high}$) to the site of infarct immediately following MI in response to the release of chemokine MCP-1 in the myocardium. IL-4-hydrogel treated group exhibited lower local and systemic MCP-1 levels, and this suggests a crucial role MCP-1 may play in preventing further recruitment of pro-inflammatory monocytes to the infarct upon exposure to IL-4. This also signifies chemokine MCP-1 as a potential target for immunomodulation, and careful inhibition of MCP-1 in the initial inflammatory phase might pave way to a controlled inflammatory response. This approach however, would be very similar to that of knocking down the CCR2 receptor in the splenic monocytes that reduced the influx of inflammatory cells and resulted in decreased infarct size following MI [191]. However, the MCP-1 downregulation could be targeted to the myocardium or delivered systemically. Strategies as such aiming to reduce the influx of monocytes, however, should be deployed with care as inflammatory cells are a crucial step in the wound healing process, and absence of these inflammatory mediators may even lead to infarct destabilization and cardiac rupture [17, 157]. Furthermore, the sequential recruitment theory of the pro-inflammatory $Ly6C^{hi}$ monocytes followed by the reparative $Ly6C^{low}$ to the infarct has been somewhat disproven, with new evidence demonstrating a role for a nuclear hormone receptor switch (Nr4a1) in modulating the pro-inflammatory $Ly6C^{hi}$ monocytes to differentiate towards the reparative or M2 macrophage phenotype found in the wound healing phase following MI (day 4-8) [89]. The role of chemokine Fractalkine ($CX_3CL1$) in the recruitment of the $Ly6C^{low}$monocytes has been well established. However, in light of these new turn of events with Nr4a1 emerging as a new target for the modulation of macrophage phenotype towards M2, the role of $Ly6C^{low}$ monocytes is unclear in terms of the role these monocytes play. However, further studies should be performed to confirm whether delivery of Fractalkine may serve as a trigger for the recruitment or local polarization towards a reparative macrophages without hindering the recruitment of pro-inflammatory $Ly6C^{hi}$ monocytes.

Our study looked at only the effects of IL-4 delivery. While there is a strong rationale for evaluating ability of IL-4 to polarize macrophages *in vivo*, other modes of macrophage activation such as the regulatory functional phenotype of macrophages activated by IL-10 merit further investigation. Numerous studies have shown the strong anti-inflammatory effects induced by IL-10 and its role in bringing about inflammation resolution [37, 174, 238, 239]. Further, an IL-10 mimetic peptide is available [240] which makes incorporation into a biomaterial scaffold such as PEG-MAL or self-assembling peptides a simple process, and a rational next step to test out synergistic effects of encapsulated IL-4 and tethered IL-10 on the inflammatory response in the myocardium. Our data from this study, and from previous work employing antioxidant SOD delivery to the myocardium [121] discussed in section 6.1, it is clear that immunomodulation therapy of a singular kind may not be the "magic bullet" to improve cardiac repair, and rather, synergistic effects with another therapeutic may enhance the cardiac repair process. With cardiac regeneration as the ultimate goal for regenerative cardiology, an immune modulatory therapy could enhance stem-cell therapy by creating a pro-regenerative environment that improves cell survival and stimulates endogenous cues to differentiate stem-cells.

It could not be denied that conditions accompanying or preceding MI in humans, such as obesity, atherosclerosis and diabetes have inflammatory components that disrupt the balanced inflammatory response following MI, causing impaired healing [204, 241]. Many of these factors cannot be easily replicated in rodent animal models. Further, part of the wealth of information on the inflammatory response post-MI comes from animal models that underwent permanent occlusion MI while some others from ischemia-reperfusion (IR) models. While both are valid and accepted models in the field, the nature of the inflammatory response is likely different, and it is difficult to reconcile these data to draw the appropriate conclusions regarding targets for modulation as well as outcomes of such attempts. Inflammation induced by the reperfusion-injury in IR may influence the

healing process differently than the permanent occlusion model, not to mention the variability in animal models and surgical procedures that would likely affect the inflammatory milieu from one study to another. Therefore, it is critical to fully characterize the inflammatory response in the animal model we work with prior to reconciling information in the field to create testable hypotheses regarding modulating that immune response. These would not only include temporally resolved local gene expression analyses of macrophage markers, but also local and systemic cytokine and chemokine levels in order to accurately assess the inflammatory network of events, as it is not uncommon for macrophages characterized as M1 to stimulate production of anti-inflammatory cytokines and vice versa [242]. The cytokine and chemokine milieu may represent the inflammation and inflammation resolution phases following MI more accurately than the extreme classifications of macrophage markers.

## 6.4 Perspective

The immune system is closely tied to the development of many chronic diseases we are faced with today, whether it is cancer where the immune system is defective or heart disease where it is often the culprit for worsening conditions. Scientists have for a while now recognized the immune system as an avenue for therapeutic modulation. Given this knowledge, the lack of effective therapies that target the immune system for the treatment of acute MI is significant. This is in some part due to heart being a difficult organ to achieve effective drug delivery. While drug delivery to the heart has come a long way, the future biomaterial designs need to be bolder and more comprehensive in order to tackle the immune system, the regenerative aspects as well as the mechanical aspects of the heart. Further, many limitations exist when drawing comparisons from rodents to humans in the progression of disease and even the nature of drug delivery is a different beast in humans vs rodents. Biomaterials are much more amenable to testing in large animals than rodent models. My thesis work described three strategies to modulate the

immune response in the infarct using biomaterials based delivery systems, progressively choosing therapeutic targets that are key regulators of the disease. However, from a translational point of view, the disease characteristics need to be studied much more intensively in more clinically relevant larger animal models, especially the immune system with regard to heart disease, as the wealth of information that exists is for mice models of the disease. Then, a multidisciplinary approach to careful selection of network regulators and design of multifunctional materials should be applied to move promising therapies to large animal studies sooner than later.

# APPENDIX

## A.1. Supplemental Figures

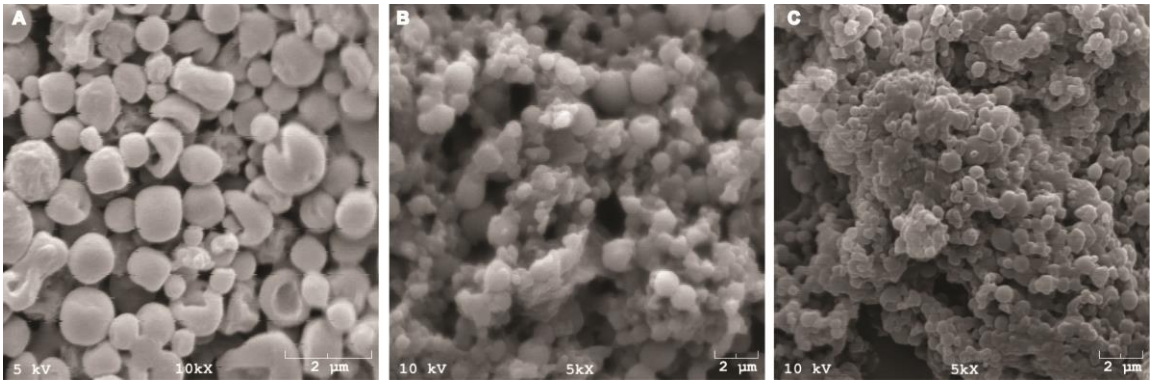


**Figure A1. Modified particle sizes depending on homegenization speeds.**
A) Lower magnification image of particles generated with only homegenization for 60 sec and no sonication (d=1.36 ± 0.43µm). B) Particles generated with sonication at intermediate speeds (d=0.83 ± 0.30µm). C) SEM of particles generated with sonication at higher speeds (d=0.56 ± 0.21µm). Scale bar = 2µm.

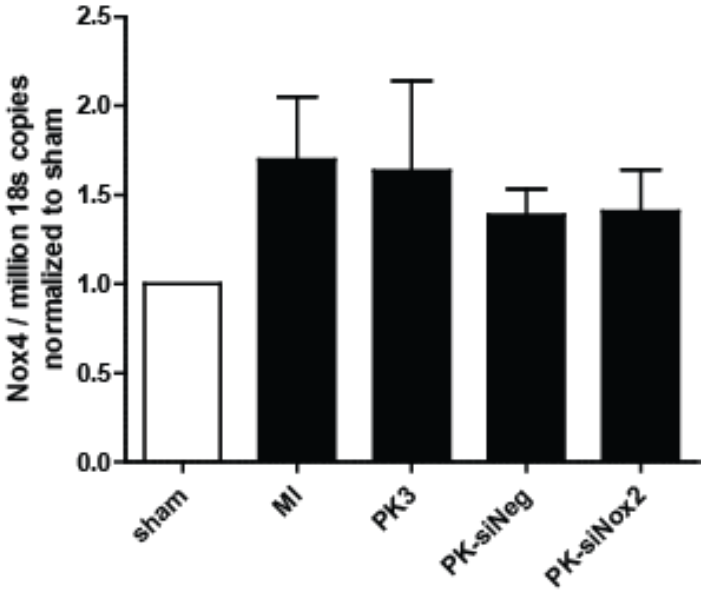


**Figure A2. In vivo Nox4 mRNA expression. Grouped data (mean ± SEM; n≥8 per** group) from 3 days. There was a trend towards an increase in Nox4 mRNA expression in animals that received MI although not statistically significant. In animals that received MI and PK-siNox2 treatment, there was no observed knockdown of Nox4 mRNA expression. Gene expression was evaluated by qRT-PCR using the quantitative standard curve method, and the results were normalized to 18S levels and reported as fold changes in copy number of mRNA levels compared to sham animals (One-way ANOVA followed by Dunnett's Multiple Comparison post-test).

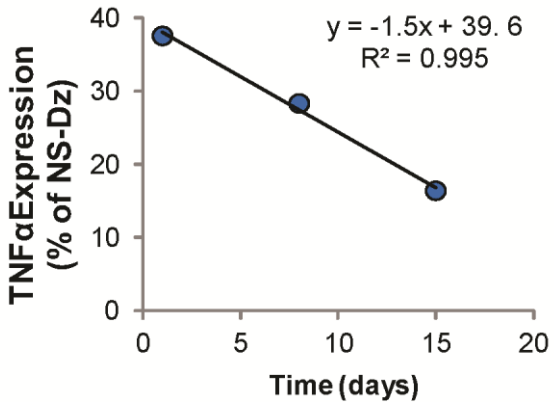


**Figure A3. DNA stability in water.** A plot showing Dz (7/7 b.p. recogntion arms) mediated *in vitro* TNF–α knockdown in primary macrophages for cells treated with particles that were stored in Nanopure water for varied amounts of time (*t*= 1d, 8d, and 15d). Cells were treated with 10 nM particle concentration for 20 h. TNF–α expression was measured by ELISA and the results were normalized to NS-Dz treated cells and reported as percent TNF–α expression. Approximately 1.5% decrease in particle activity per day was observed due to instability of the particles stored in Nanopure water. For *in vitro* and *in vivo* studies, freshly modified particles were used and were stored in the reaction solution (*excess DNA and high salt concentration*) rather than Nanopure water.

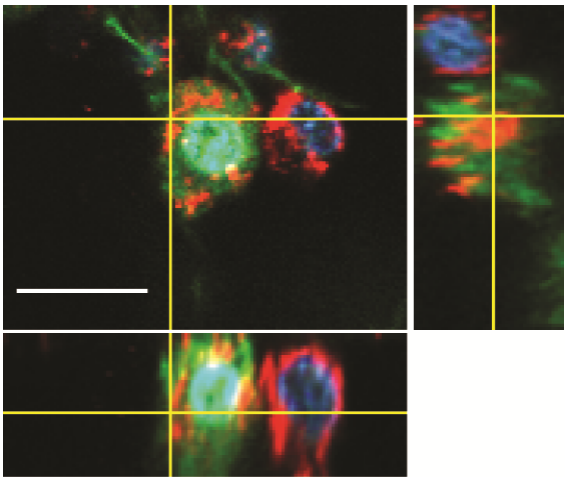

**Figure A4. Cy5-NS-DzNP internalization by macrophages.**
RAW 264.7 macrophages were transfected with 5 nM Cy5 labeled NS-DNA. Following 1 hour of treatment, cells were imaged using confocal microscopy and representative orthoganol Z-stack slice allows visualization of internalized Cy5-DNA modified gold particles. DNA (red, Cy5), Nucleus (blue, DAPI), cellular morphology stain (green, Calcein) (Scale bar, 20μm).

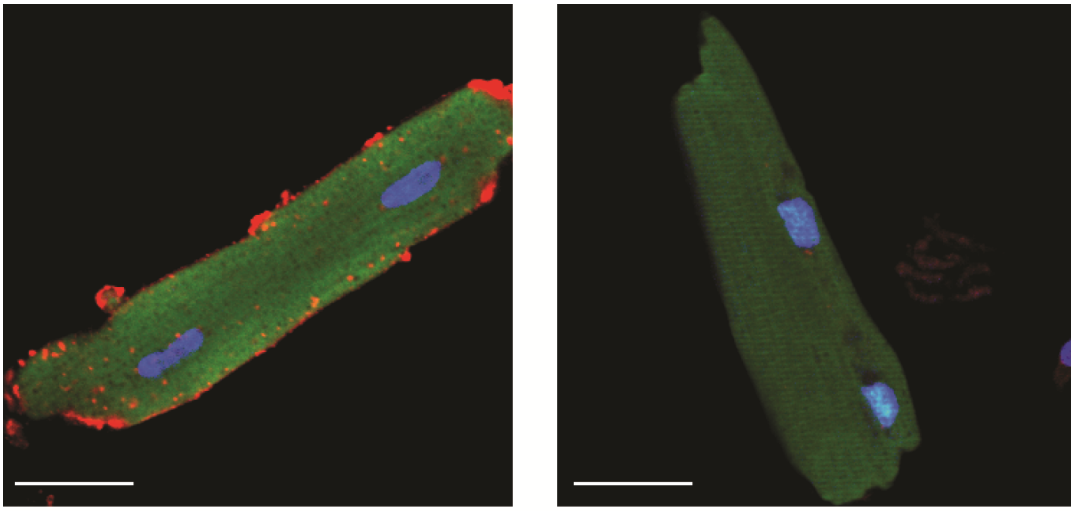


**Figure A5. Cy5-NS-DzNP uptake by primary adult rat cardiomyocytes.**
Adult rat cardiomyocytes were fixed and imaged 18 hours post-transfection with 5 nM Cy5 labeled DNA by (left) Cy5-dzNPs or (right) Lipofectamine® mediated transfection. DNA (red, Cy5), Nucleus (blue, DAPI), cellular morphology stain (green, FITC-Maleimide) (Scale bar, 30μm).

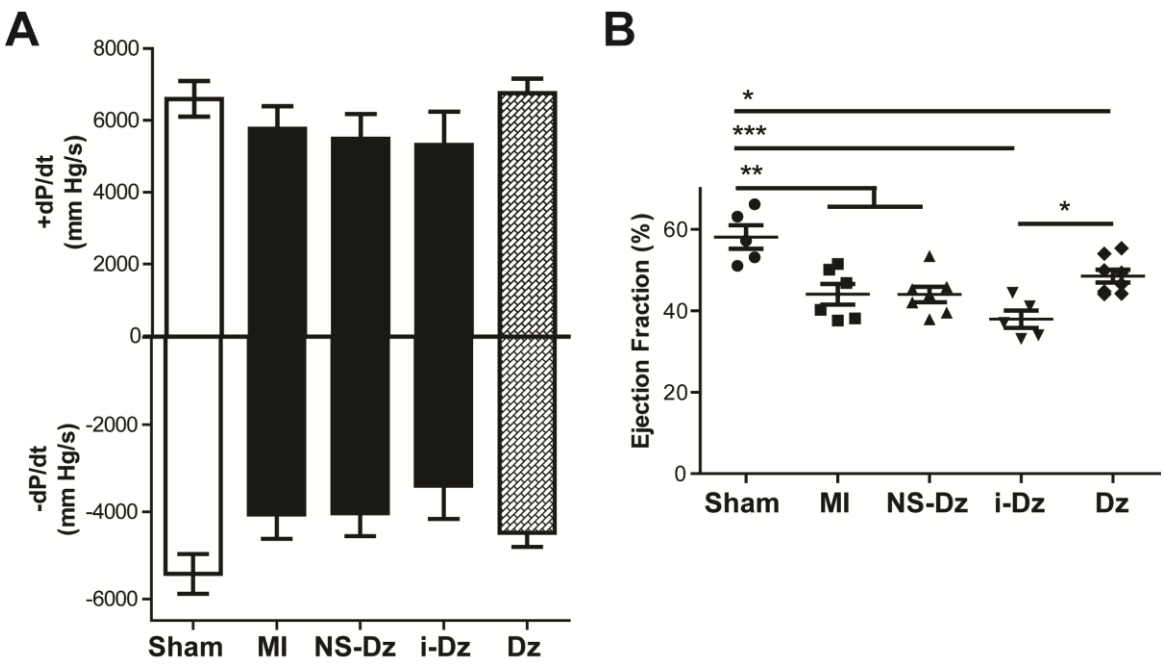


**Figure A6. Effect of *in vivo* delivery of TNF-Dz particles on invasive hemodynamics Pressure-Volume (PV) measurements.** Grouped data (mean ± SEM; *n*=5-9 for each group, *n*=41 total) from 3 days. (A) There was a trend towards depression of function using the dp/dt parameter in all animals that underwent MI except for the Dz treated group. However, there was no statistical significance in these parameters in any of these groups. (B) A significant reduction in % Ejection Fraction (%EF) was observed in all animals that underwent MI compared to sham animals. Although not statistically significant compared to MI group, Dz treated group showed a trend of improved %EF (*$p<0.05$; **$p<0.001$; one-way ANOVA followed by Tukey's Multiple Comparison post-test).

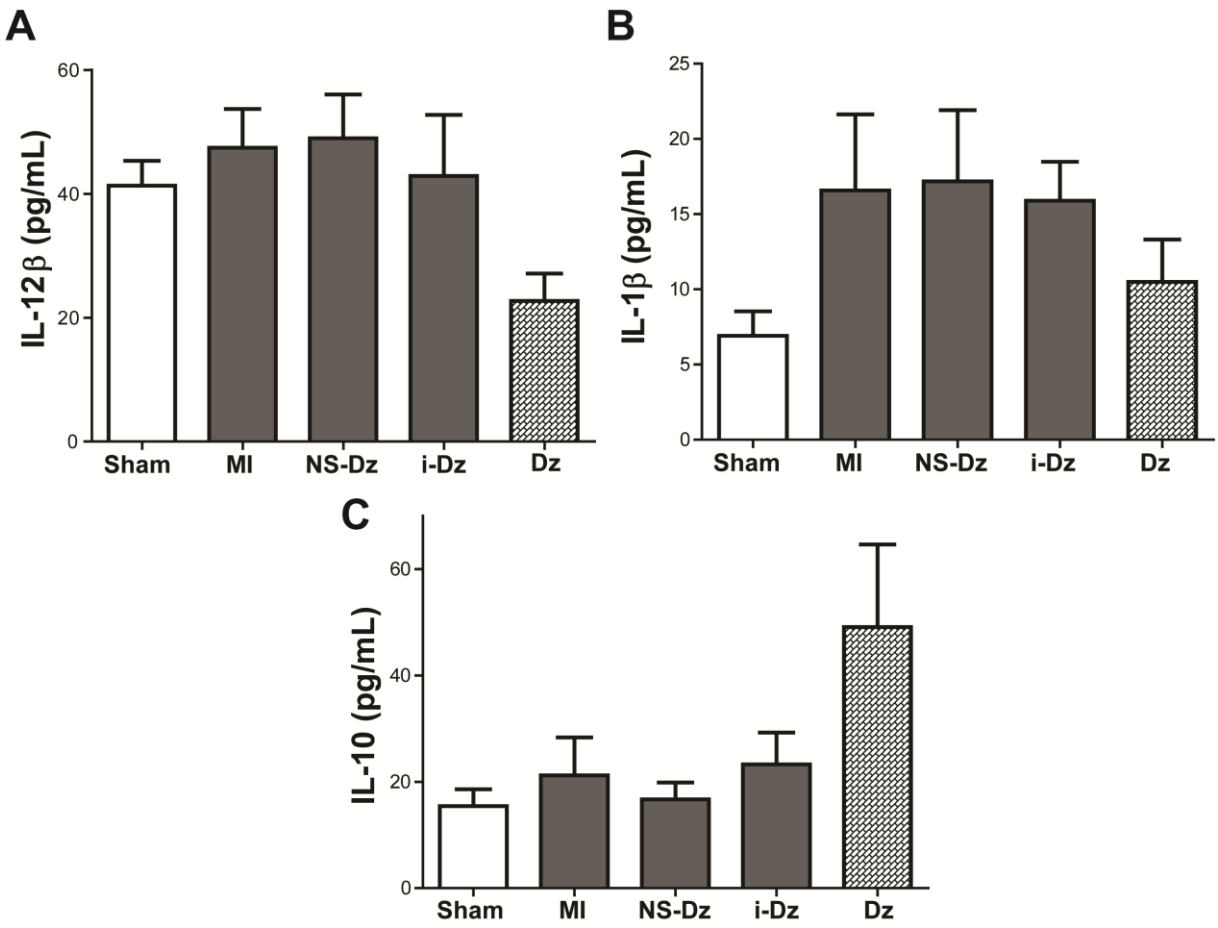


**Figure A7. Effect of TNF-Dz delivery on plasma levels of inflammatory and anti-inflammatory cytokines.** Grouped data (mean ± SEM; n=3-9 per group) from plasma at 3 days. Although there was no statistically significant differences in any of the groups, there were consistent trends towards downregulation of pro-inflammatory cytokines (A) IL-12β, (B) IL-1 β and potential trend towards an increase in anti-inflammatory cytokine (C) IL-10 in the plasma of Dz treatment groups. Data was analyzed using the Luminex Multiplex system and reported as plasma cytokine concentrations, quantitatively derived from standard curves of each cytokine.

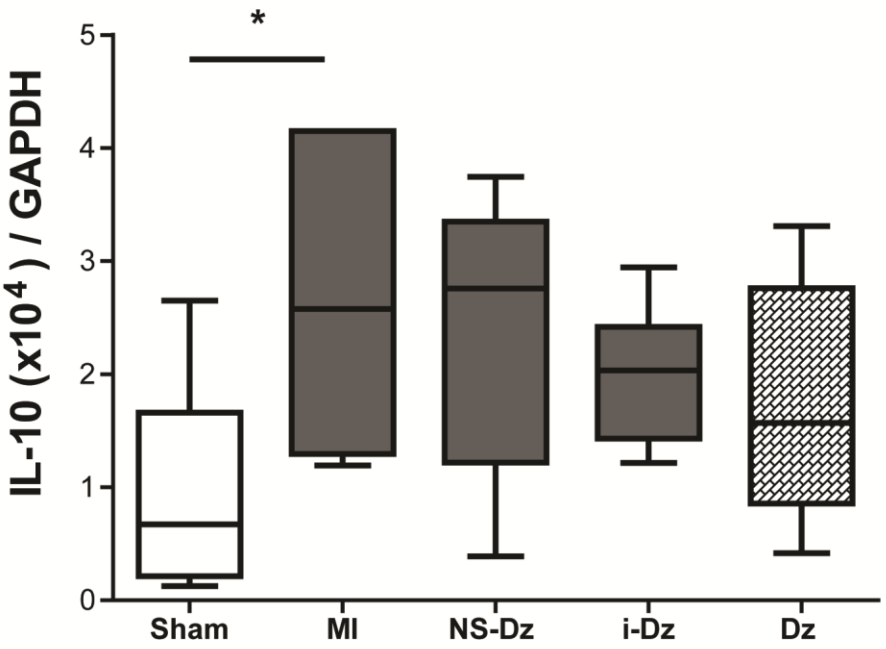


**Figure A8. Effect of TNF-Dz delivery on anti-inflammatory cytokine IL-10 gene expression.** Grouped data (mean ± SEM; n=5-9 per group) from LV infarct tissue at 3 days. A significant upregulation of IL-10 expression was observed in animals that received an MI compared to sham, and no significant changes in IL-10 mRNA expression in any of the treatment groups. Gene expression was evaluated by qRT-PCR using the quantitative standard curve method and the results were normalized to GAPDH levels and reported as fold changes in copy number of mRNA levels compared to sham animals (*$p<0.05$ vs. MI; one-way ANOVA followed by Dunnett's Multiple Comparison post-test).

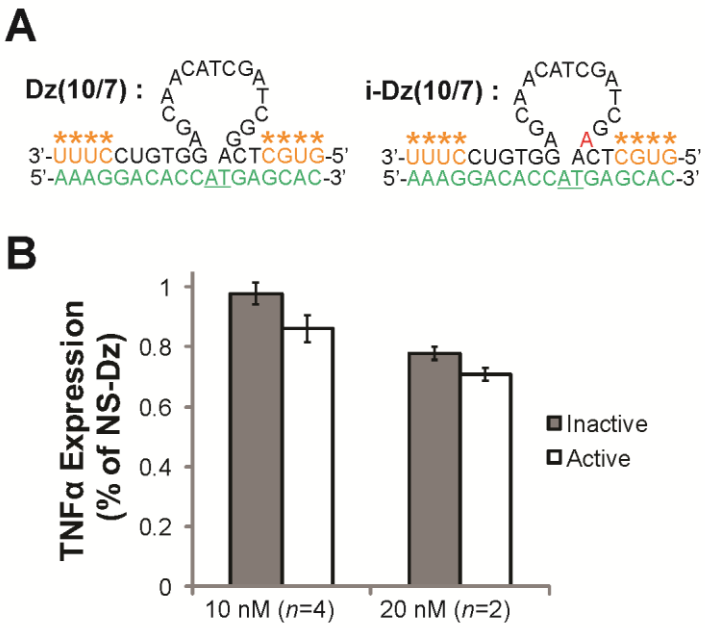


**Figure A9. DNAzyme 7/10 arm.** (A) Schematic showing the original DNAzyme design targeting TNF−α mRNA (green) with recognition arm lengths of 10 and 7 baseparis and eight 2' methyl ether modifications (*, yellow) to enhance stability. The inactive DNAzyme has a single base mutation shown in red to inhibit RNA hydrolysis. (B) *In vitro* TNF−α knockdown in primary macrophages where cells were treated with either active (Dz), inactive (i-Dz), or non-specific (NS-Dz) DNAzyme modified gold nanoparticles at 10 nM or 20 nM concentrations. TNF−α expression was measured by ELISA and the results were normalized to NS-Dz treated cells and reported as percent TNF−α expression. Little knockdown (2% and 14% for Dz and i-Dz, respectively) was observed for cells treated with particles at 10 nM concentration where higher knockdown (23% and 30% for Dz and i-Dz, respectively) was observed for cells treated with 20 nM concentration. At both concentrations, little difference was observed between Dz and i-Dz modified particles due to product inhibition. In the optimized design, the 10 base pair recognition sequence was decreased to 7 base pairs, which significantly increased knockdown and difference in knockdown for Dz and i-Dz modified partices (Figure 3. ~50% and ~0% TNF−α knockdown for Dz and i-Dz treated macrophages at 10 nM particle concentration, respectively).

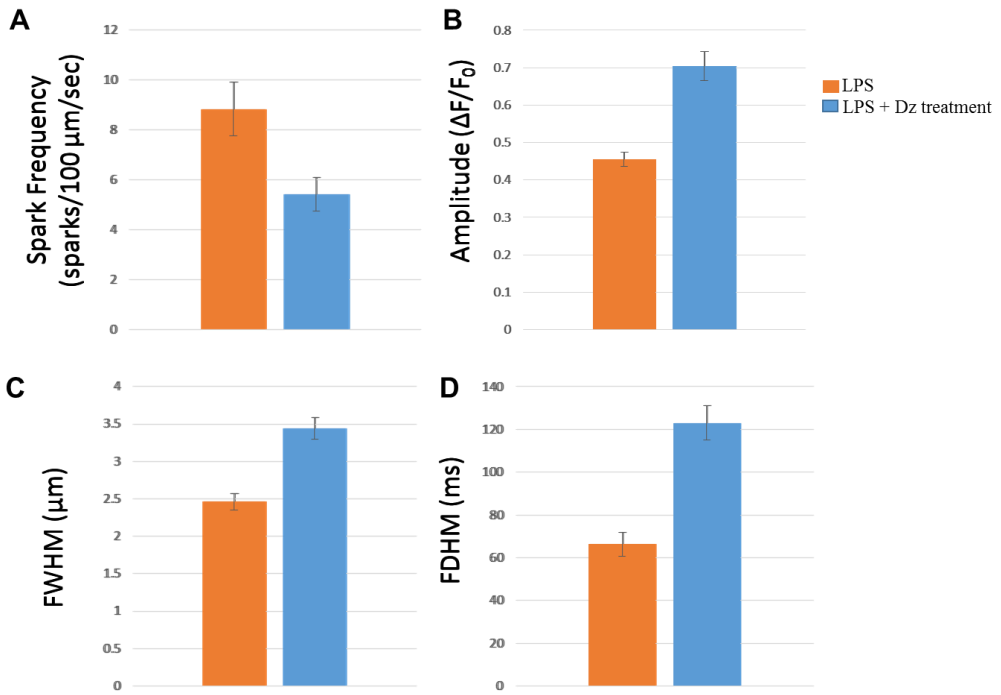


**Figure A10. $Ca^{2+}$ sparks characteristics in adult rat cardiomyocytes following LPS stimulation and Dz particle treatment.** $Ca^{2+}$ sparks are elementary SR $Ca^{2+}$-release events through a cluster of ryanodine receptors (RyR2s) that occur spontaneously during diastole and summate in time and space during systole to form the global $Ca^{2+}$ transient during E-C coupling. To monitor $Ca^{2+}$ sparks, we utilized line scans via laser scanning confocal microscopy to enable visualization of rapid fluorescence intensity changes with time on myocytes treated with Dz particles following LPS stimulation. (A) Frequency of release events decreased with particle treatment (blue bars), and increased in (B) Amplitude, width (FWHM), and duration (FDHM) indicative of a higher SR load that can be attributed to the observed decreased frequency of diastolic release with particle treatment. These data indicate that the knockdown of TNF-α with the particles is able to decreasing aberrant diastolic $Ca^{2+}$ release (Grouped data from n=1, 6-8 cells per group, particle treated group is significantly different from the untreated group by one-way ANOVA, tukey post-hoc test, $p<0.05$ for all measured parameters)

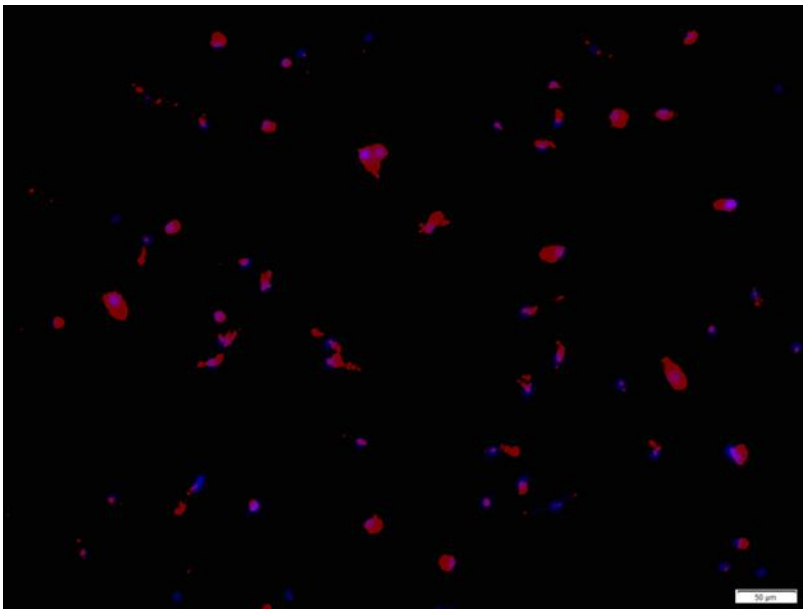

**Figure A11. Bone-marrow derived macrophages (BMM) stained for pan-macrophage marker CD68.** Macrophages (Red, CD68), Nucleus (blue, DAPI). (Scale bar = 50μm)

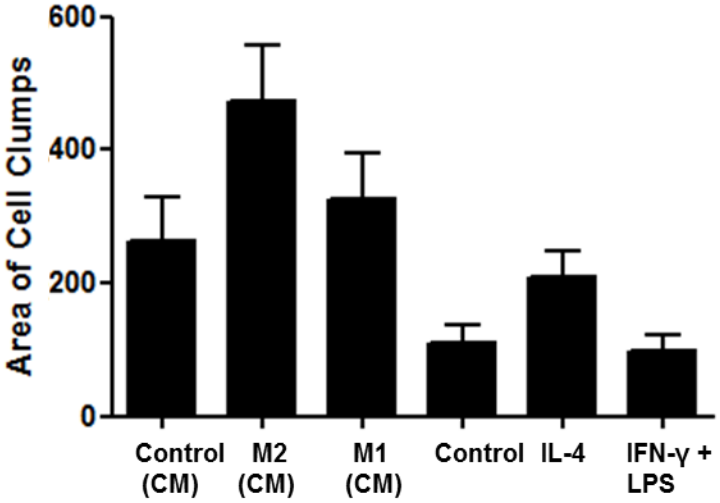


**Figure A12. Endothelial cell migratory/aggregatory behavior on collagen gels.**
CECs treated with M2 macrophage conditioned media treatment showed an increased tendency to migrate towards each other and form aggregates, a possible pre-cursor to tube-like structures.

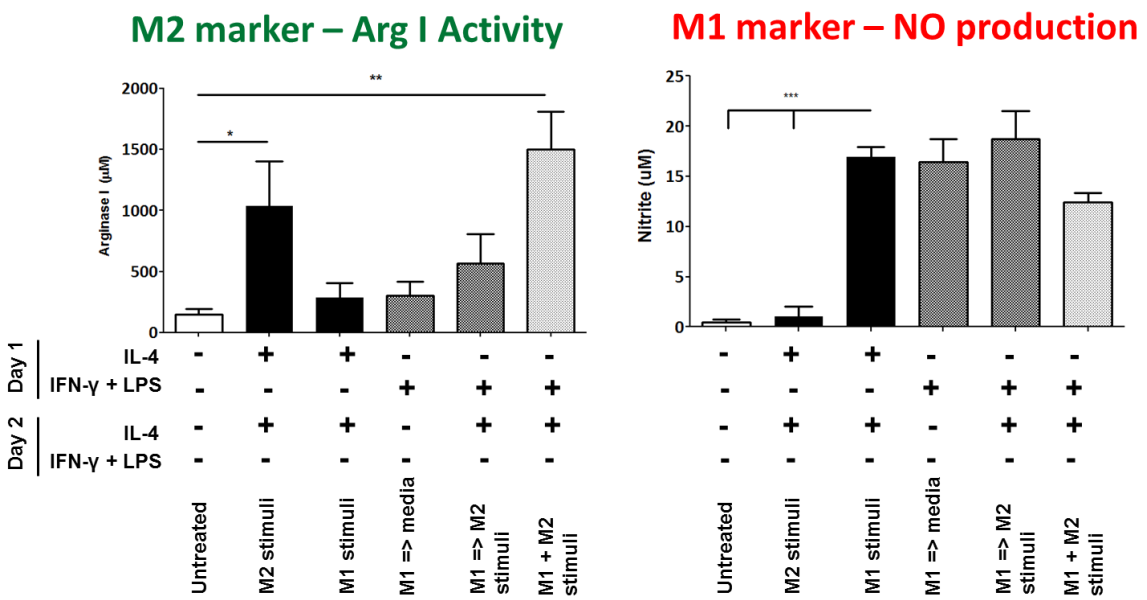


**Figure A13**. **Staggered vs simultaneous M1 and M2 polarizing stimuli on BMM macrophages.** Characterization of (A) Arg1 activity and (B) NO production following staggered (IFN-γ + LPS on day 1, stimuli removal and IL-4 addition on day 2) or simultaneous (IFN-γ + LPS and IL-4 combined for 2 consequtive days) activation of BMM (Grouped data, mean ± SEM; n=5-6, *p<0.05, **p<0.01, ***p<0.001; one-way ANOVA followed by Dunnett's Multiple Comparison post-test). Simultaneous activation shows better tendency for reversal of M1 characteristics, possibly indicating a hybrid functional phenotype.

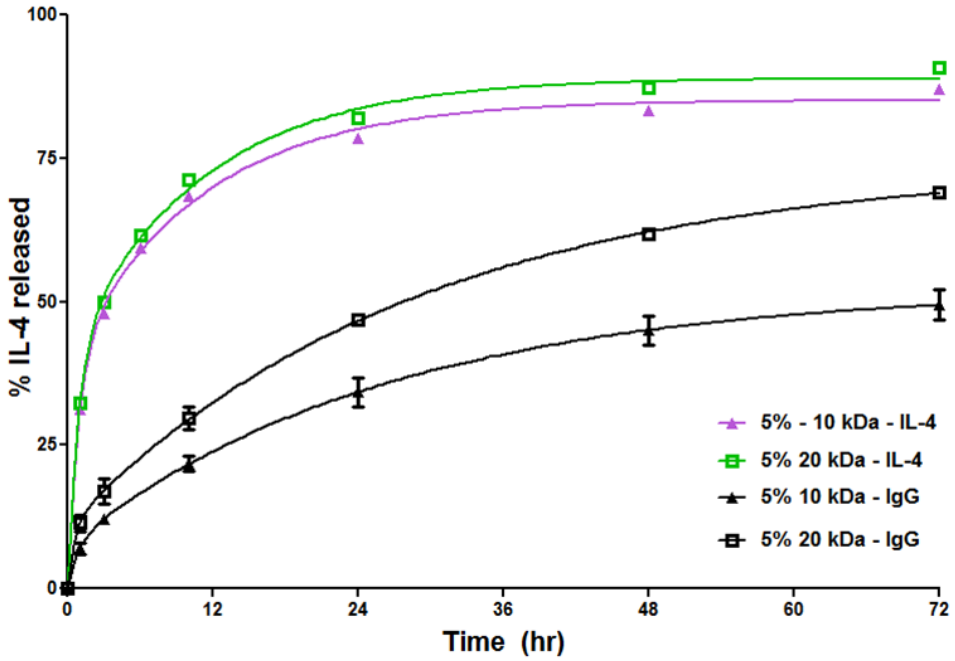


**Figure A14. Comparison of relase of IL-4 with IgG from PEG-MAL gels.**
Fluorescently tagged IL-4 (~14kDa) or IgG (150kDa) released from 5% weight percentage of PEG-MAL hydrogels of two different molecular wieghts, 10 and 20 kDa swelled in PBS by fluorescent plate reader sampling of incubation media.

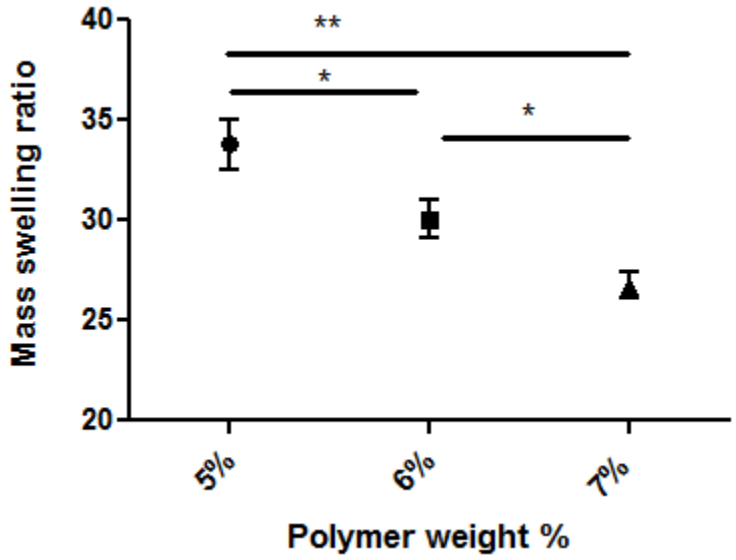


**Figure A15. Mass swelling ratio of 10kDa PEG-MAL hydrogels.**
Influence of polymer weight percentage on equilibrium swelling ratio for hydrogels made from 5, and 7% PEG-MAL of 10kDa MW. Grouped data, mean ± SEM; n=4 *p<0.05, **p<0.01, one-way ANOVA followed by Tukey's Multiple Comparison post-test).

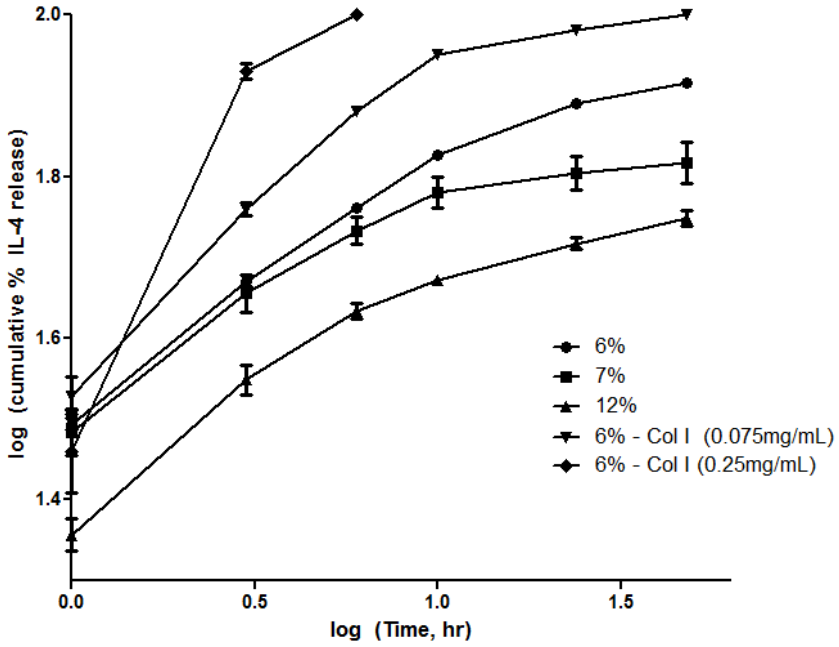


**Figure A16. Log transformation of release study shown in Figure 21.** Fluorescently tagged IL-4 released from 6 ,7 and 12% PEG-MAL hydrogels compared to collagenase mediated release of 2 different concentrations over a 48 hour period. Two phases (burst and slow release) of the release profile are clearer to observe in this scale.

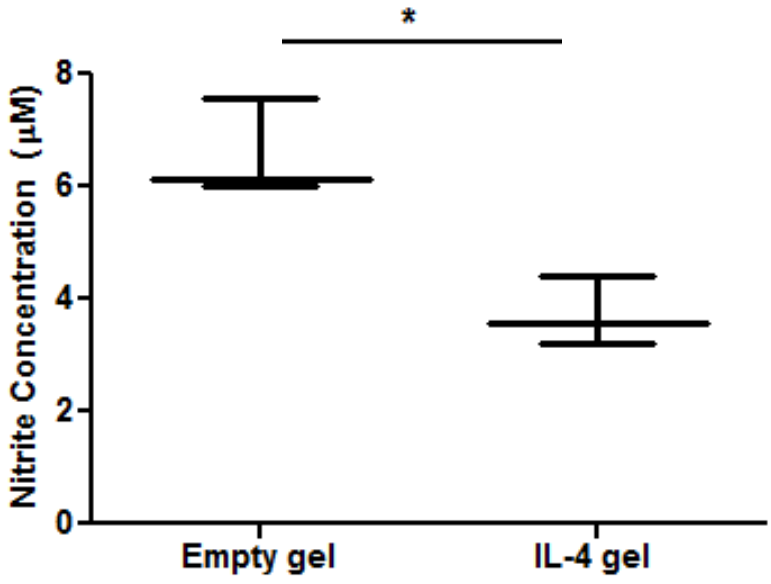


**Figure A17. Bioactive IL-4 release from PEG-MAL hydrogel.** NO production in LPS stimulated macrophages in the presence of empty or IL-4 encapsulating PEG-MAL hydrogel degraded by COL-I application through day 2. (n=3, t-test, *$p<0.05$)

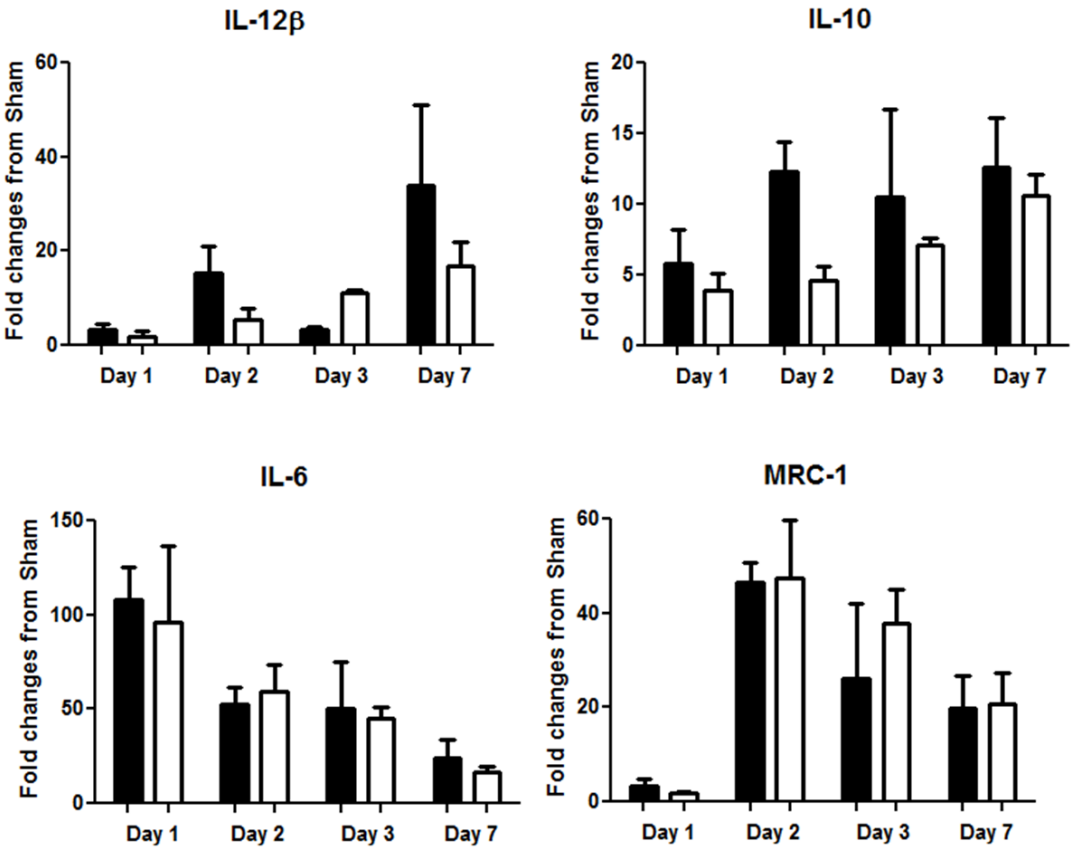


**Figure A18. Effect of IL-4-hdyrogel on a plannael of genes of significance for inflammation.** Grouped gene expression data (mean ± SEM; n=3 per group) over a course of a week after MI with or without IL-4 hydrogel treatment. Gene expression was evaluated by qRT-PCR using the comparative Ct method and the results were normalized to GAPDH levels and reported as fold changes compared to sham animals.

## A.2. Supplemental Results

### A.2.1. Effect of Dz treatment on $Ca^{2+}$ transients on LPS-treated adult rat cardiomyocytes

It has been well established that TNF–α and subsequent induction of other pro-inflammatory cytokines IL-6, IL-1β or ROS generation in cardiac myocytes leads to a high frequency of $Ca^{2+}$ sparks. These effects can attenuate myocyte contractility directly through the reduction of systolic cytosolic $Ca^{2+}$ levels via alterations in sarcoplasmic reticulum function [80, 181], down-regulation of contractile proteins, ß–adrenergic receptor uncoupling [78, 182, 183] or indirectly by decreasing myocyte contractility through nitric oxide-dependent attenuation of myofilament $Ca^{2+}$ sensitivity [24, 73, 80, 180, 183] or oxidative effects on the RyR2 [184, 185]. In Chapter 4 we have shown that knocking down TNF–α in the myocardium utilizing Dz particles following MI resulted in downregulation of several pro-inflammatory cytokines and iNOS, and we wanted to test whether Dz particles can reverse dysregulation of calcium transients.

$Ca^{2+}$ sparks are elementary SR $Ca^{2+}$-release events through a cluster of ryanodine receptors (RyR2s) that occur spontaneously during diastole and summate in time and space during systole to form the global $Ca^{2+}$ transient during E-C coupling. To monitor rapidly changing phenomena such as fluorescence signals from $Ca^{2+}$ sparks, laser scanning confocal microscopy can be utilized and these line scans enable visualization of rapid fluorescence intensity changes with time. We pre-treated myocytes with Dz particles (20nM particle concentration for 12 hours) and stimulated with LPS (50ng/mL) for 1 hour, and observed that the spark frequency was significantly decreased compared to cells not pre-treated with particles. These data indicate that the particles are able to prevent the production of ROS intracellularly (potentially iNOS and others), thus decreasing aberrant diastolic $Ca^{2+}$ release. We hypothesize that the main mechanism for

this observation may be that knockdown of TNF-α in cardiomyocytes lessen the extent of oxidation of the RyR2. Although release events became less frequent with particle treatment (blue bars), they were of increased amplitude, width (FWHM), and duration (FDHM) indicative of a higher SR load that can be attributed to the observed decreased frequency of diastolic release with particle treatment. The properties of the recorded $Ca^{2+}$ sparks were analyzed and summarized in Figure A10.

### A.2.2. Superoxide levels acutely upregulated following MI and IR 7 days after MI or IR surgery (n = 3-4, assessed by DHE-HPLC)

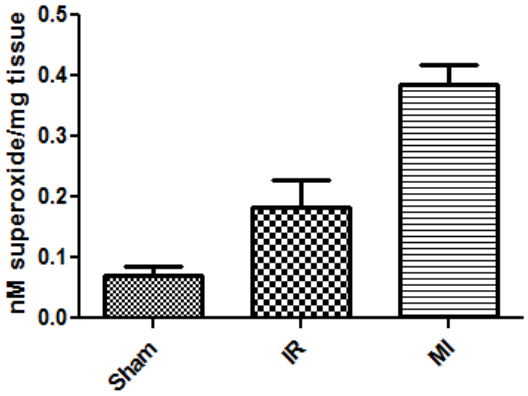


### A.2.3. Nox2-NADPH oxidase levels stay upregulated 7-days after MI (n=7, gene expression using qRT-PCR)

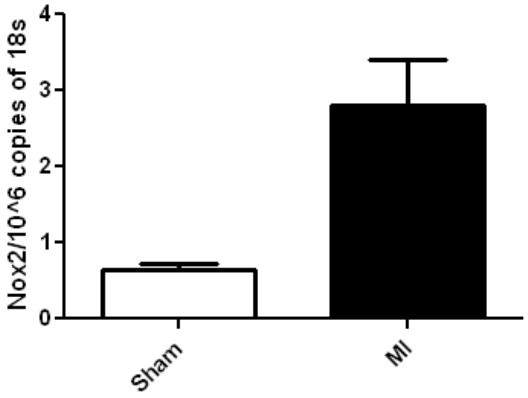

## A.3. Supplemental Methods

### A.3.1. Adult rat cardiomyocyte culture

Single ventricular myocytes were isolated from male Sprague-dawley rats. Rats were anesthetized with ketamine (1 mg/g) and xylezene (0.1 mg/g), and hearts were excised and mounted on a Langendorff apparatus. Hearts were retrogradely perfused with nominally $Ca^{2+}$-free Tyrode's solution for 5 min followed by minimal essential medium Eagle (MEM) solution containing 20 µM $Ca^{2+}$ and 22.5 µg/mL Liberase Blendzyme TH (Roche Applied Science, Indianapolis, IN) for 20-25 min at 37°C. The right ventricular free wall was removed from the heart, minced, filtered, and washed in MEM solution containing 50 µM $Ca^{2+}$ and 10 mg/mL BSA. Isolated cells were kept in MEM solution with 50 µM $Ca^{2+}$ at room temperature (22-24°C) until indicator dye loading and subsequent experimentation. All protocols were approved by the Institutional Animal Care and Use Committee.

### A.3.2. $Ca^{2+}$ sparks imaging

Confocal microscopy (FV1000, Olympus) was used to image $Ca^{2+}$ sparks, with excitation at 488nm and emission collected at >500nm. Cardiac myocytes were loaded with 20 µm fluo-4/AM for 20 min at room temperature (RT), followed by a 20 min wash in 2mM $Ca^{2+}$ Tyrode's at RT. $Ca^{2+}$ spark measurements were acquired from intact myocytes perfused with 2 mM $Ca^{2+}$ Tyrode's solution during rest after 1 Hz stimulation in line scan mode at 2 ms/line with a pixel size of 0.155 µm. All fluorescent signals were background subtracted. Changes in $[Ca^{2+}]i$ are expressed as $\Delta F/F0$, where $\Delta F$ is the change in fluorescence [measured fluorescence (F) – F0] and F0 is resting baseline fluo-4 fluorescence. For all subsequent $Ca^{2+}$ imaging experiments, cells were placed on laminin-coated coverslips. Action potentials and global Ca transients were elicited by electrical field stimulation using a pair of platinum electrodes. Experiments were conducted at room temperature (22-24°C)

### A.3.3. List of primers

| Gene | Species | Sequence (5' => 3') |
|---|---|---|
| Hprt1 | Rat | F: GCTGACCTGCTGGATTACAT |
| | | R: TTGGGGCTGTACTGCTTAAC |
| 18S | Rat | F: TTCCTTACCTGGTTGATCCTGCCA |
| | | R: AGCGAGCGACCAAAGGAACCATAA |
| IL6 | Rat | F: CAGAGTCATTCAGAGCAATAC |
| | | R: CTTTCAAGATGAGTTGGATGG |
| IL-1β | Rat | F: TAAGCCAACAAGTGGTATTC |
| | | R: AGGTATAGATTCTTCCCCTTG |
| IL-10 | Rat | F: CCTGGTAGAAGTGATGCCCC |
| | | R: TGCTCCACTGCCTTGCTTTT |
| IL-12β | Rat | F: AGACCCTGCCCATTGAACTG |
| | | R: CAGGAGTCAGGGTACTCCCA |
| TNF-α | Rat | F: TCTTCTGTCTACTGAACTTCG |
| | | R: AAGATGATCTGAGTGTGAGG |
| GAPDH | Rat | F: CCAGCCCAGCAAGGATACTG |
| | | F: GGCCCCTCCTGTTGTTATGG |
| TNF-α | Mouse | F: CCCATTACTCTGACCCCTTT |
| | | R: TGAGCATCGTAGTTGTTGGA |
| MRC-1 | Mouse | F: GCA AAT GGA GCC GTCTGT GC |
| | | R: CTC GTG GAT CTC CGT GAC AC |

# REFERENCES


1. Go, A.S., et al., *Executive Summary: Heart Disease and Stroke Statistics--2013 Update: A Report From the American Heart Association.* Circulation, 2013. **127**(1): p. 143-152.
2. Go, A.S., et al., *Heart disease and stroke statistics--2014 update: a report from the American Heart Association.* Circulation, 2014. **129**(3): p. e28-e292.
3. Wang, Q.D., et al., *Pharmacological possibilities for protection against myocardial reperfusion injury.* Cardiovasc Res, 2002. **55**(1): p. 25-37.
4. Ertl, G. and S. Frantz, *Healing after myocardial infarction.* Cardiovasc Res, 2005. **66**(1): p. 22-32.
5. Xie, M., J.S. Burchfield, and J.A. Hill, *Pathological ventricular remodeling: therapies: part 2 of 2.* Circulation, 2013. **128**(9): p. 1021-30.
6. Kereiakes, D.J., *Adjunctive pharmacotherapy before percutaneous coronary intervention in non-ST-elevation acute coronary syndromes: the role of modulating inflammation.* Circulation, 2003. **108**(16 Suppl 1): p. III22-7.
7. Yellon, D.M. and D.J. Hausenloy, *Myocardial reperfusion injury.* N Engl J Med, 2007. **357**(11): p. 1121-35.
8. Eulalio, A., et al., *Functional screening identifies miRNAs inducing cardiac regeneration.* Nature, 2012. **492**(7429): p. 376-81.
9. Leri, A., J. Kajstura, and P. Anversa, *Cardiac stem cells and mechanisms of myocardial regeneration.* Physiol Rev, 2005. **85**(4): p. 1373-416.
10. Senyo, S.E., et al., *Mammalian heart renewal by pre-existing cardiomyocytes.* Nature, 2012.
11. Rosenzweig, A., *Medicine. Cardiac regeneration.* Science, 2012. **338**(6114): p. 1549-50.
12. Soh, B.S., H. Wu, and K.R. Chien, *Cardiac regenerative medicine 2.0.* Nat Biotechnol, 2013. **31**(3): p. 209-11.
13. Liu, N., et al., *microRNA-133a regulates cardiomyocyte proliferation and suppresses smooth muscle gene expression in the heart.* Genes Dev, 2008. **22**(23): p. 3242-54.
14. Padin-Iruegas, M.E., et al., *Cardiac progenitor cells and biotinylated insulin-like growth factor-1 nanofibers improve endogenous and exogenous myocardial regeneration after infarction.* Circulation, 2009. **120**(10): p. 876-87.
15. Qian, L., et al., *In vivo reprogramming of murine cardiac fibroblasts into induced cardiomyocytes.* Nature, 2012. **485**(7400): p. 593-8.
16. Leuschner, F., et al., *Rapid monocyte kinetics in acute myocardial infarction are sustained by extramedullary monocytopoiesis.* J Exp Med, 2012. **209**(1): p. 123-37.
17. Nahrendorf, M., M.J. Pittet, and F.K. Swirski, *Monocytes: protagonists of infarct inflammation and repair after myocardial infarction.* Circulation, 2010. **121**(22): p. 2437-45.
18. Troidl, C., et al., *Classically and alternatively activated macrophages contribute to tissue remodelling after myocardial infarction.* J Cell Mol Med, 2009. **13**(9B): p. 3485-96.

19. Heymes, C., et al., *Increased myocardial NADPH oxidase activity in human heart failure.* J Am Coll Cardiol, 2003. **41**(12): p. 2164-71.
20. Krijnen, P.A., et al., *Increased Nox2 expression in human cardiomyocytes after acute myocardial infarction.* J Clin Pathol, 2003. **56**(3): p. 194-9.
21. Cave, A.C., et al., *NADPH oxidases in cardiovascular health and disease.* Antioxid Redox Signal, 2006. **8**(5-6): p. 691-728.
22. Levine, B., et al., *Elevated circulating levels of tumor necrosis factor in severe chronic heart failure.* N Engl J Med, 1990. **323**(4): p. 236-41.
23. Torre-Amione, G., et al., *Tumor necrosis factor-alpha and tumor necrosis factor receptors in the failing human heart.* Circulation, 1996. **93**(4): p. 704-11.
24. Meldrum, D.R., *Tumor necrosis factor in the heart.* The American journal of physiology, 1998. **274**: p. R577-R595.
25. Mokarram, N., et al., *Effect of modulating macrophage phenotype on peripheral nerve repair*. Biomaterials, 2012. **33**(34): p. 8793-801.
26. Mosser, D.M. and J.P. Edwards, *Exploring the full spectrum of macrophage activation.* Nat Rev Immunol, 2008. **8**(12): p. 958-69.
27. Hastings, C.L., et al., *Drug and cell delivery for cardiac regeneration.* Adv Drug Deliv Rev, 2014.
28. Luo, X., et al., *C-jun DNAzymes inhibit myocardial inflammation, ROS generation, infarct size, and improve cardiac function after ischemia-reperfusion injury.* Arteriosclerosis, Thrombosis, and Vascular Biology, 2009. **29**: p. 1836-1842.
29. Giljohann, D.a., et al., *Gene regulation with polyvalent siRNA-nanoparticle conjugates.* Journal of the American Chemical Society, 2009. **131**: p. 2072-2073.
30. Seferos, D.S., et al., *Polyvalent DNA nanoparticle conjugates stabilize nucleic acids.* Nano Letters, 2009. **9**: p. 308-311.
31. Yehl, K., et al., *Catalytic deoxyribozyme-modified nanoparticles for RNAi-independent gene regulation.* ACS Nano, 2012. **6**: p. 9150-9157.
32. Phelps, E.A., et al., *Maleimide cross-linked bioactive PEG hydrogel exhibits improved reaction kinetics and cross-linking for cell encapsulation and in situ delivery.* Adv Mater, 2012. **24**(1): p. 64-70, 2.
33. Salimath, A.S., et al., *Dual Delivery of Hepatocyte and Vascular Endothelial Growth Factors via a Protease-Degradable Hydrogel Improves Cardiac Function in Rats.* PLoS One, 2012. **7**(11): p. e50980.
34. Gordon, S., *Alternative activation of macrophages.* Nat Rev Immunol, 2003. **3**(1): p. 23-35.
35. Frangogiannis, N.G., *Targeting the inflammatory response in healing myocardial infarcts.* Current medicinal chemistry, 2006. **13**: p. 1877-1893.
36. Zuidema, M.Y. and C. Zhang, *Ischemia/reperfusion injury: The role of immune cells.* World J Cardiol, 2010. **2**(10): p. 325-32.
37. Frangogiannis, N.G., C.W. Smith, and M.L. Entman, *The inflammatory response in myocardial infarction.* Cardiovasc Res, 2002. **53**(1): p. 31-47.
38. Wang, F., et al., *Late coronary stent thrombosis: early vs. late stent thrombosis in the stent era.* Catheter Cardiovasc Interv, 2002. **55**(2): p. 142-7.

39. Reffelmann, T. and R.A. Kloner, *The no-reflow phenomenon: A basic mechanism of myocardial ischemia and reperfusion.* Basic Res Cardiol, 2006. **101**(5): p. 359-72.
40. Ferrari, R., et al., *Occurrence of oxidative stress during reperfusion of the human heart.* Circulation, 1990. **81**(1): p. 201-11.
41. Bonvini, R.F., *Inflammatory response post-myocardial infarction and reperfusion: a new therapeutic target?* European Heart Journal Supplements, 2005. **7**(Suppl I): p. I27-I36.
42. Hausenloy, D.J. and D.M. Yellon, *Myocardial ischemia-reperfusion injury: a neglected therapeutic target.* J Clin Invest, 2013. **123**(1): p. 92-100.
43. Frangogiannis, N.G., *The mechanistic basis of infarct healing.* Antioxid Redox Signal, 2006. **8**(11-12): p. 1907-39.
44. Kempf, T., et al., *Anti-inflammatory mechanisms and therapeutic opportunities in myocardial infarct healing.* Journal of Molecular Medicine, 2012. **90**: p. 361-369.
45. Pfeffer, J.M., M.A. Pfeffer, and E. Braunwald, *Influence of chronic captopril therapy on the infarcted left ventricle of the rat.* Circ Res, 1985. **57**(1): p. 84-95.
46. Cohn, J.N., R. Ferrari, and N. Sharpe, *Cardiac remodeling--concepts and clinical implications: a consensus paper from an international forum on cardiac remodeling. Behalf of an International Forum on Cardiac Remodeling.* J Am Coll Cardiol, 2000. **35**(3): p. 569-82.
47. Seropian, I.M., et al., *Anti-inflammatory strategies for ventricular remodeling following ST-segment elevation acute myocardial infarction.* J Am Coll Cardiol, 2014. **63**(16): p. 1593-603.
48. Frangogiannis, N.G., *Targeting the inflammatory response in healing myocardial infarcts.* Curr Med Chem, 2006. **13**(16): p. 1877-93.
49. Hill, J.H. and P.A. Ward, *The phlogistic role of C3 leukotactic fragments in myocardial infarcts of rats.* J Exp Med, 1971. **133**(4): p. 885-900.
50. Sorescu, D. and K.K. Griendling, *Reactive oxygen species, mitochondria, and NAD(P)H oxidases in the development and progression of heart failure.* Congest Heart Fail, 2002. **8**(3): p. 132-40.
51. Looi, Y.H., et al., *Involvement of Nox2 NADPH oxidase in adverse cardiac remodeling after myocardial infarction.* Hypertension, 2008. **51**(2): p. 319-25.
52. Bolli, R., *Causative role of oxyradicals in myocardial stunning: a proven hypothesis. A brief review of the evidence demonstrating a major role of reactive oxygen species in several forms of postischemic dysfunction.* Basic Res Cardiol, 1998. **93**(3): p. 156-62.
53. Kinugawa, S., et al., *Treatment with dimethylthiourea prevents left ventricular remodeling and failure after experimental myocardial infarction in mice: role of oxidative stress.* Circ Res, 2000. **87**(5): p. 392-8.
54. Li, Q., et al., *Gene therapy with extracellular superoxide dismutase protects conscious rabbits against myocardial infarction.* Circulation, 2001. **103**(14): p. 1893-8.
55. Sia, Y.T., et al., *Beneficial effects of long-term use of the antioxidant probucol in heart failure in the rat.* Circulation, 2002. **105**(21): p. 2549-55.

56. Wang, P., et al., *Overexpression of human copper, zinc-superoxide dismutase (SOD1) prevents postischemic injury.* Proc Natl Acad Sci U S A, 1998. **95**(8): p. 4556-60.
57. Cave, A., *Selective targeting of NADPH oxidase for cardiovascular protection.* Curr Opin Pharmacol, 2009. **9**(2): p. 208-13.
58. Fukui, T., et al., *Expression of p22-phox and gp91-phox, essential components of NADPH oxidase, increases after myocardial infarction.* Biochem Biophys Res Commun, 2001. **281**(5): p. 1200-6.
59. Bendall, J.K., et al., *Pivotal role of a gp91(phox)-containing NADPH oxidase in angiotensin II-induced cardiac hypertrophy in mice.* Circulation, 2002. **105**(3): p. 293-6.
60. Grieve, D.J., et al., *Involvement of the nicotinamide adenosine dinucleotide phosphate oxidase isoform Nox2 in cardiac contractile dysfunction occurring in response to pressure overload.* J Am Coll Cardiol, 2006. **47**(4): p. 817-26.
61. Nian, M., et al., *Inflammatory cytokines and postmyocardial infarction remodeling.* Circ Res, 2004. **94**(12): p. 1543-53.
62. Ono, K., et al., *Cytokine gene expression after myocardial infarction in rat hearts: possible implication in left ventricular remodeling.* Circulation, 1998. **98**(2): p. 149-56.
63. Frangogiannis, N.G., et al., *Cytokines and the microcirculation in ischemia and reperfusion.* J Mol Cell Cardiol, 1998. **30**(12): p. 2567-76.
64. Bozkurt, B., et al., *Pathophysiologically relevant concentrations of tumor necrosis factor-alpha promote progressive left ventricular dysfunction and remodeling in rats.* Circulation, 1998. **97**: p. 1382-1391.
65. Frangogiannis, N.G., et al., *Resident cardiac mast cells degranulate and release preformed TNF-alpha, initiating the cytokine cascade in experimental canine myocardial ischemia/reperfusion.* Circulation, 1998. **98**(7): p. 699-710.
66. Halawa, B., et al., *[Levels of tumor necrosis factor (TNF-alpha) and interleukin 6 (IL-6) in serum of patients with acute myocardial infarction]*. Pol Arch Med Wewn, 1999. **101**(3): p. 197-203.
67. Heba, G., et al., *Relation between expression of TNF alpha, iNOS, VEGF mRNA and development of heart failure after experimental myocardial infarction in rats.* J Physiol Pharmacol, 2001. **52**(1): p. 39-52.
68. Jacobs, M., et al., *Tumor necrosis factor-alpha at acute myocardial infarction in rats and effects on cardiac fibroblasts.* Journal of molecular and cellular cardiology, 1999. **31**: p. 1949-1959.
69. Kaur, K., A.K. Sharma, and P.K. Singal, *Significance of changes in TNF-alpha and IL-10 levels in the progression of heart failure subsequent to myocardial infarction.* Am J Physiol Heart Circ Physiol, 2006. **291**(1): p. H106-13.
70. Kleinbongard, P., R. Schulz, and G. Heusch, *TNFα in myocardial ischemia/reperfusion, remodeling and heart failure.* Heart Failure Reviews, 2011. **16**: p. 49-69.
71. Meldrum, D.R., et al., *Increased myocardial tumor necrosis factor-alpha in a crystalloid-perfused model of cardiac ischemia-reperfusion injury.* Ann Thorac Surg, 1998. **65**(2): p. 439-43.

72. Pagani, F.D., et al., *Left ventricular systolic and diastolic dysfunction after infusion of tumor necrosis factor-alpha in conscious dogs.* The Journal of clinical investigation, 1992. **90**: p. 389-98.
73. Sack, M., *Tumor necrosis factor-alpha in cardiovascular biology and the potential role for anti-tumor necrosis factor-alpha therapy in heart disease.* Pharmacology & therapeutics, 2002. **94**: p. 123-35.
74. Sinagra, E., et al., *Heart failure and anti tumor necrosis factor-alpha in systemic chronic inflammatory diseases.* European Journal of Internal Medicine, 2013. **24**: p. 385-392.
75. Sivasubramanian, N., et al., *Left ventricular remodeling in transgenic mice with cardiac restricted overexpression of tumor necrosis factor.* Circulation, 2001. **104**: p. 826-831.
76. Gao, X., et al., *Role of TNF-alpha-induced reactive oxygen species in endothelial dysfunction during reperfusion injury.* Am J Physiol Heart Circ Physiol, 2008. **295**(6): p. H2242-9.
77. Maekawa, N., et al., *Improved myocardial ischemia/reperfusion injury in mice lacking tumor necrosis factor-alpha.* J Am Coll Cardiol, 2002. **39**(7): p. 1229-35.
78. Gulick, T., et al., *Interleukin 1 and tumor necrosis factor inhibit cardiac myocyte beta-adrenergic responsiveness.* Proc Natl Acad Sci U S A, 1989. **86**(17): p. 6753-7.
79. Kumar, A., et al., *Tumor necrosis factor alpha and interleukin 1beta are responsible for in vitro myocardial cell depression induced by human septic shock serum.* J Exp Med, 1996. **183**(3): p. 949-58.
80. Nian, M., et al., *Inflammatory cytokines and postmyocardial infarction remodeling.* Circulation Research, 2004. **94**: p. 1543-1553.
81. Ono, K., et al., *Cytokine gene expression after myocardial infarction in rat hearts: possible implication in left ventricular remodeling.* Circulation, 1998. **98**: p. 149-156.
82. Irwin, M.W., et al., *Tissue expression and immunolocalization of tumor necrosis factor-alpha in postinfarction dysfunctional myocardium.* Circulation, 1999. **99**: p. 1492-1498.
83. Kurrelmeyer, K.M., et al., *Endogenous tumor necrosis factor protects the adult cardiac myocyte against ischemic-induced apoptosis in a murine model of acute myocardial infarction.* Proceedings of the National Academy of Sciences of the United States of America, 2000. **97**: p. 5456-5461.
84. Swirski, F.K., et al., *Identification of splenic reservoir monocytes and their deployment to inflammatory sites.* Science, 2009. **325**(5940): p. 612-6.
85. Frangogiannis, N.G., C.W. Smith, and M.L. Entman, *The inflammatory response in myocardial infarction.* Cardiovascular Research, 2002. **53**(1): p. 31-47.
86. Edwards, J.P., et al., *Biochemical and functional characterization of three activated macrophage populations.* J Leukoc Biol, 2006. **80**(6): p. 1298-307.
87. Lambert, J.M., E.F. Lopez, and M.L. Lindsey, *Macrophage roles following myocardial infarction.* Int J Cardiol, 2008. **130**(2): p. 147-58.
88. Nahrendorf, M., et al., *The healing myocardium sequentially mobilizes two monocyte subsets with divergent and complementary functions.* J Exp Med, 2007. **204**(12): p. 3037-47.

89. Hilgendorf, I., et al., *Ly-6Chigh monocytes depend on Nr4a1 to balance both inflammatory and reparative phases in the infarcted myocardium.* Circ Res, 2014. **114**(10): p. 1611-22.
90. Prabhu, S.D., *It takes two to tango: Monocyte and macrophage duality in the infarcted heart.* Circulation Research, 2014. **114**: p. 1558-1560.
91. Abizaid, A. and J.R. Costa, Jr., *New drug-eluting stents: an overview on biodegradable and polymer-free next-generation stent systems.* Circ Cardiovasc Interv, 2010. **3**(4): p. 384-93.
92. Perin, E.C. and J. Lopez, *Methods of stem cell delivery in cardiac diseases.* Nat Clin Pract Cardiovasc Med, 2006. **3 Suppl 1**: p. S110-3.
93. Panyam, J. and V. Labhasetwar, *Biodegradable nanoparticles for drug and gene delivery to cells and tissue.* Adv Drug Deliv Rev, 2003. **55**(3): p. 329-47.
94. Cohen, S., et al., *Controlled delivery systems for proteins based on poly(lactic/glycolic acid) microspheres.* Pharm Res, 1991. **8**(6): p. 713-20.
95. Sinha, V.R. and A. Trehan, *Biodegradable microspheres for protein delivery.* J Control Release, 2003. **90**(3): p. 261-80.
96. Fujimoto, K.L., et al., *An elastic, biodegradable cardiac patch induces contractile smooth muscle and improves cardiac remodeling and function in subacute myocardial infarction.* J Am Coll Cardiol, 2007. **49**(23): p. 2292-300.
97. Censi, R., et al., *Hydrogels for protein delivery in tissue engineering.* J Control Release, 2012. **161**(2): p. 680-92.
98. Hoffman, A.S., *Hydrogels for biomedical applications.* Advanced Drug Delivery Reviews, 2012. **64**: p. 18-23.
99. Botchwey, E.a., et al., *Tissue engineered bone: measurement of nutrient transport in three-dimensional matrices.* Journal of biomedical materials research. Part A, 2003. **67**: p. 357-367.
100. Vermonden, T., R. Censi, and W.E. Hennink, *Hydrogels for protein delivery.* Chem Rev, 2012. **112**(5): p. 2853-88.
101. Grover, G.N., N. Rao, and K.L. Christman, *Myocardial matrix-polyethylene glycol hybrid hydrogels for tissue engineering.* Nanotechnology, 2014. **25**(1): p. 014011.
102. Davis, M.E., et al., *Injectable self-assembling peptide nanofibers create intramyocardial microenvironments for endothelial cells.* Circulation, 2005. **111**: p. 442-450.
103. Hsieh, P.C.H., et al., *Controlled delivery of PDGF-BB for myocardial protection using injectable self-assembling peptide nanofibers.* Journal of Clinical Investigation, 2006. **116**.
104. Holmes, T.C., et al., *Extensive neurite outgrowth and active synapse formation on self-assembling peptide scaffolds.* Proceedings of the National Academy of Sciences of the United States of America, 2000. **97**: p. 6728-6733.
105. Chaikof, E.L., et al., *Biomaterials and scaffolds in reparative medicine.* Annals of the New York Academy of Sciences, 2002. **961**: p. 96-105.
106. Rane, A.A., et al., *Increased infarct wall thickness by a bio-inert material is insufficient to prevent negative left ventricular remodeling after myocardial infarction.* PLoS One, 2011. **6**(6): p. e21571.

107. Kadner, K., et al., *The beneficial effects of deferred delivery on the efficiency of hydrogel therapy post myocardial infarction.* Biomaterials, 2012. **33**(7): p. 2060-6.
108. Jayawardena, T.M., et al., *MicroRNA-mediated in vitro and in vivo direct reprogramming of cardiac fibroblasts to cardiomyocytes.* Circulation Research, 2012. **110**: p. 1465-1473.
109. Liu, J., et al., *Functionalized dendrimer-based delivery of angiotensin type 1 receptor siRNA for preserving cardiac function following infarction.* Biomaterials, 2013. **34**: p. 3729-3736.
110. Ding, Q., et al., *Permanent alteration of PCSK9 with in vivo CRISPR-Cas9 genome editing.* Circ Res, 2014. **115**(5): p. 488-92.
111. Zangi, L., et al., *Modified mRNA directs the fate of heart progenitor cells and induces vascular regeneration after myocardial infarction.* Nat Biotechnol, 2013. **31**(10): p. 898-907.
112. Santoro, S.W. and G.F. Joyce, *A general purpose RNA-cleaving DNA enzyme.* Proceedings of the National Academy of Sciences of the United States of America, 1997. **94**: p. 4262-4266.
113. Iversen, P.O., G. Nicolaysen, and M. Sioud, *DNA enzyme targeting TNF-alpha mRNA improves hemodynamic performance in rats with postinfarction heart failure.* American journal of physiology. Heart and circulatory physiology, 2001. **281**: p. H2211-H2217.
114. de Fougerolles, A., et al., *Interfering with disease: a progress report on siRNA-based therapeutics.* Nat Rev Drug Discov, 2007. **6**(6): p. 443-53.
115. Dykxhoorn, D.M. and J. Lieberman, *The silent revolution: RNA interference as basic biology, research tool, and therapeutic.* Annu Rev Med, 2005. **56**: p. 401-23.
116. Li, C.X., et al., *Delivery of RNA interference.* Cell Cycle, 2006. **5**(18): p. 2103-9.
117. Zhang, X., J.P. Edwards, and D.M. Mosser, *The expression of exogenous genes in macrophages: obstacles and opportunities.* Methods Mol Biol, 2009. **531**: p. 123-43.
118. Jiang, G., et al., *Target specific intracellular delivery of siRNA/PEI-HA complex by receptor mediated endocytosis.* Mol Pharm, 2009. **6**(3): p. 727-37.
119. Lv, H., et al., *Toxicity of cationic lipids and cationic polymers in gene delivery.* J Control Release, 2006. **114**(1): p. 100-9.
120. Yang, Y.Y., T.S. Chung, and N.P. Ng, *Morphology, drug distribution, and in vitro release profiles of biodegradable polymeric microspheres containing protein fabricated by double-emulsion solvent extraction/evaporation method.* Biomaterials, 2001. **22**(3): p. 231-41.
121. Seshadri, G., et al., *The delivery of superoxide dismutase encapsulated in polyketal microparticles to rat myocardium and protection from myocardial ischemia-reperfusion injury.* Biomaterials, 2010. **31**(6): p. 1372-9.
122. Yang, S.C., et al., *Polyketal copolymers: a new acid-sensitive delivery vehicle for treating acute inflammatory diseases.* Bioconjug Chem, 2008. **19**(6): p. 1164-9.
123. Lee, S., et al., *Solid polymeric microparticles enhance the delivery of siRNA to macrophages in vivo.* Nucleic Acids Res, 2009. **37**(22): p. e145.

124. Sy, J.C., et al., *Sustained release of a p38 inhibitor from non-inflammatory microspheres inhibits cardiac dysfunction.* Nat Mater, 2008. **7**(11): p. 863-8.
125. Wilson, D.S., et al., *Orally delivered thioketal nanoparticles loaded with TNF-alpha-siRNA target inflammation and inhibit gene expression in the intestines.* Nat Mater, 2010. **9**(11): p. 923-8.
126. Giljohann, D.A., et al., *Oligonucleotide loading determines cellular uptake of DNA-modified gold nanoparticles.* Nano Letters, 2007. **7**: p. 3818-3821.
127. Hurst, S.J., A.K.R. Lytton-Jean, and C.a. Mirkin, *Maximizing DNA loading on a range of gold nanoparticle sizes.* Analytical Chemistry, 2006. **78**: p. 8313-8318.
128. Rosi, N.L., et al., *Oligonucleotide-modified gold nanoparticles for intracellular gene regulation.* Science (New York, N.Y.), 2006. **312**: p. 1027-1030.
129. Anversa, P., et al., *Ischaemic myocardial injury and ventricular remodelling.* Cardiovascular Research, 1993. **27**(2): p. 145-57.
130. Bolli, R., et al., *Direct evidence that oxygen-derived free radicals contribute to postischemic myocardial dysfunction in the intact dog.* Proc Natl Acad Sci U S A, 1989. **86**(12): p. 4695-9.
131. Ferdinandy, P. and R. Schulz, *Nitric oxide, superoxide, and peroxynitrite in myocardial ischaemia-reperfusion injury and preconditioning.* Br J Pharmacol, 2003. **138**(4): p. 532-43.
132. Byrne, J.A., et al., *Contrasting roles of NADPH oxidase isoforms in pressure-overload versus angiotensin II-induced cardiac hypertrophy.* Circ Res, 2003. **93**(9): p. 802-5.
133. Matsushima, S., et al., *Broad Suppression of NADPH Oxidase Activity Exacerbates Ischemia/Reperfusion Injury Through Inadvertent Downregulation of Hypoxia-inducible Factor-1alpha and Upregulation of Peroxisome Proliferator-activated Receptor-alpha.* Circ Res, 2013. **112**(8): p. 1135-49.
134. Fernandes, D.C., et al., *Analysis of DHE-derived oxidation products by HPLC in the assessment of superoxide production and NADPH oxidase activity in vascular systems.* Am J Physiol Cell Physiol, 2007. **292**(1): p. C413-22.
135. Peshavariya, H.M., G.J. Dusting, and S. Selemidis, *Analysis of dihydroethidium fluorescence for the detection of intracellular and extracellular superoxide produced by NADPH oxidase.* Free Radic Res, 2007. **41**(6): p. 699-712.
136. Zielonka, J., J. Vasquez-Vivar, and B. Kalyanaraman, *Detection of 2-hydroxyethidium in cellular systems: a unique marker product of superoxide and hydroethidine.* Nat Protoc, 2008. **3**(1): p. 8-21.
137. Fink, B., et al., *Detection of intracellular superoxide formation in endothelial cells and intact tissues using dihydroethidium and an HPLC-based assay.* Am J Physiol Cell Physiol, 2004. **287**(4): p. C895-902.
138. Zhao, H., et al., *Superoxide reacts with hydroethidine but forms a fluorescent product that is distinctly different from ethidium: potential implications in intracellular fluorescence detection of superoxide.* Free Radic Biol Med, 2003. **34**(11): p. 1359-68.
139. Maejima, Y., et al., *Regulation of myocardial growth and death by NADPH oxidase.* J Mol Cell Cardiol, 2011. **50**(3): p. 408-16.
140. Akhtar, S. and I.F. Benter, *Nonviral delivery of synthetic siRNAs in vivo.* J Clin Invest, 2007. **117**(12): p. 3623-32.

141. Leirdal, M. and M. Sioud, *Gene silencing in mammalian cells by preformed small RNA duplexes.* Biochem Biophys Res Commun, 2002. **295**(3): p. 744-8.
142. Zhang, S., et al., *Cationic lipids and polymers mediated vectors for delivery of siRNA.* J Control Release, 2007. **123**(1): p. 1-10.
143. Champion, J.A., Y.K. Katare, and S. Mitragotri, *Particle shape: a new design parameter for micro- and nanoscale drug delivery carriers.* J Control Release, 2007. **121**(1-2): p. 3-9.
144. Champion, J.A., A. Walker, and S. Mitragotri, *Role of particle size in phagocytosis of polymeric microspheres.* Pharm Res, 2008. **25**(8): p. 1815-21.
145. Yue, H., et al., *Particle size affects the cellular response in macrophages.* Eur J Pharm Sci, 2010. **41**(5): p. 650-7.
146. DeChatelet, L.R., P.S. Shirley, and R.B. Johnston, Jr., *Effect of phorbol myristate acetate on the oxidative metabolism of human polymorphonuclear leukocytes.* Blood, 1976. **47**(4): p. 545-54.
147. Dikalov, S.I., A.E. Dikalova, and R.P. Mason, *Noninvasive diagnostic tool for inflammation-induced oxidative stress using electron spin resonance spectroscopy and an extracellular cyclic hydroxylamine.* Arch Biochem Biophys, 2002. **402**(2): p. 218-26.
148. Dikalov, S.I., et al., *Production of extracellular superoxide by human lymphoblast cell lines: comparison of electron spin resonance techniques and cytochrome C reduction assay.* Biochem Pharmacol, 2007. **73**(7): p. 972-80.
149. Khalil, I.A., et al., *Uptake pathways and subsequent intracellular trafficking in nonviral gene delivery.* Pharmacol Rev, 2006. **58**(1): p. 32-45.
150. Kim, S.S., et al., *Targeted delivery of siRNA to macrophages for anti-inflammatory treatment.* Mol Ther, 2010. **18**(5): p. 993-1001.
151. MacCarthy, P.A., et al., *Impaired endothelial regulation of ventricular relaxation in cardiac hypertrophy: role of reactive oxygen species and NADPH oxidase.* Circulation, 2001. **104**(24): p. 2967-74.
152. Peng, T., X. Lu, and Q. Feng, *Pivotal role of gp91phox-containing NADH oxidase in lipopolysaccharide-induced tumor necrosis factor-alpha expression and myocardial depression.* Circulation, 2005. **111**(13): p. 1637-44.
153. Siwik, D.A., et al., *Inhibition of copper-zinc superoxide dismutase induces cell growth, hypertrophic phenotype, and apoptosis in neonatal rat cardiac myocytes in vitro.* Circ Res, 1999. **85**(2): p. 147-53.
154. Anversa, P., et al., *Ischaemic myocardial injury and ventricular remodelling.* Cardiovasc Res, 1993. **27**(2): p. 145-57.
155. Blankesteijn, W.M., et al., *Dynamics of cardiac wound healing following myocardial infarction: observations in genetically altered mice.* Acta Physiol Scand, 2001. **173**(1): p. 75-82.
156. Fernández-Velasco, M., S. González-Ramos, and L. Boscá, *Involvement of monocytes/macrophages as key factors in the development and progression of cardiovascular diseases.* The Biochemical journal, 2014. **458**: p. 187-93.
157. Nahrendorf, M., *Macrophages in the infarct: fiery friends or friendly fire?* J Mol Cell Cardiol, 2012. **53**(5): p. 591-2.
158. Chung, E.S., et al., *Randomized, double-blind, placebo-controlled, pilot trial of infliximab, a chimeric monoclonal antibody to tumor necrosis factor-alpha, in*

*patients with moderate-to-severe heart failure: results of the anti-TNF Therapy Against Congestive Heart Failure (ATTACH) trial.* Circulation, 2003. **107**(25): p. 3133-40.
159. Mann, D.L., et al., *Targeted Anticytokine Therapy in Patients with Chronic Heart Failure: Results of the Randomized Etanercept Worldwide Evaluation (RENEWAL).* Circulation, 2004. **109**: p. 1594-1602.
160. Anker, S.D. and A.J. Coats, *How to RECOVER from RENAISSANCE? The significance of the results of RECOVER, RENAISSANCE, RENEWAL and ATTACH.* Int J Cardiol, 2002. **86**(2-3): p. 123-30.
161. Czech, B. and G.J. Hannon, *Small RNA sorting: matchmaking for Argonautes.* Nat Rev Genet, 2011. **12**(1): p. 19-31.
162. Karpala, A.J., T.J. Doran, and A.G.D. Bean, *Immune responses to dsRNA: Implications for gene silencing technologies.* Immunology and Cell Biology, 2005. **83**(3): p. 211-216.
163. Sledz, C.A., et al., *Activation of the interferon system by short-interfering RNAs.* Nature Cell Biology, 2003. **5**(9): p. 834-839.
164. Gilleron, J., et al., *Image-based analysis of lipid nanoparticle-mediated siRNA delivery, intracellular trafficking and endosomal escape.* Nature biotechnology, 2013. **31**: p. 638-46.
165. Semple, S.C., et al., *Rational design of cationic lipids for siRNA delivery.* Nat Biotechnol, 2010. **28**(2): p. 172-6.
166. Cutler, J.I., E. Auyeung, and C.A. Mirkin, *Spherical Nucleic Acids.* Journal of the American Chemical Society, 2012. **134**(3): p. 1376-1391.
167. Choi, C.H.J., et al., *Mechanism for the endocytosis of spherical nucleic acid nanoparticle conjugates.* Proceedings of the National Academy of Sciences of the United States of America, 2013. **110**(19): p. 7625-7630.
168. Zheng, D., et al., *Topical delivery of siRNA-based spherical nucleic acid nanoparticle conjugates for gene regulation.* Proceedings of the National Academy of Sciences of the United States of America, 2012. **109**(30): p. 11975-11980.
169. Jensen, S.A., et al., *Spherical Nucleic Acid Nanoparticle Conjugates as an RNAi-Based Therapy for Glioblastoma.* Science Translational Medicine, 2013. **5**(209).
170. Yehl, K., et al., *Catalytic Deoxyribozyme-Modified Nanoparticles for RNAi-Independent Gene Regulation.* Acs Nano, 2012. **6**(10): p. 9150-9157.
171. Hill, H.D. and C.a. Mirkin, *The bio-barcode assay for the detection of protein and nucleic acid targets using DTT-induced ligand exchange.* Nature protocols, 2006. **1**: p. 324-336.
172. Hurst, S.J., A.K.R. Lytton-Jean, and C.A. Mirkin, *Maximizing DNA loading on a range of gold nanoparticle sizes.* Analytical Chemistry, 2006. **78**(24): p. 8313-8318.
173. Wang, G.W., et al., *Acrolein consumption exacerbates myocardial ischemic injury and blocks nitric oxide-induced PKCepsilon signaling and cardioprotection.* J Mol Cell Cardiol, 2008. **44**(6): p. 1016-22.
174. Mann, D.L., *Inflammatory mediators and the failing heart: past, present, and the foreseeable future.* Circ Res, 2002. **91**(11): p. 988-98.

175. Bozkurt, B., et al., *Results of targeted anti-tumor necrosis factor therapy with etanercept (ENBREL) in patients with advanced heart failure.* Circulation, 2001. **103**(8): p. 1044-7.
176. Bhindi, R., L.M. Khachigian, and H.C. Lowe, *DNAzymes targeting the transcription factor Egr-1 reduce myocardial infarct size following ischemia-reperfusion in rats.* Journal of Thrombosis and Haemostasis, 2006. **4**: p. 1479-1483.
177. Xiang, G., et al., *Downregulated expression of plasminogen activator inhibitor-1 augments myocardial neovascularization and reduces cardiomyocyte apoptosis after acute myocardial infarction.* Journal of the American College of Cardiology, 2005. **46**: p. 536-541.
178. Zhang, L., et al., *Angiogenic Inhibition Mediated by a DNAzyme That Targets Vascular Endothelial Growth Factor Receptor 2.* Cancer Research, 2002. **62**: p. 5463-5469.
179. Yang, L.F., et al., *Targeting EBV-LMP1 DNAzyme enhances radiosensitivity of nasopharyngeal carcinoma cells by inhibiting telomerase activity.* Cancer Biology & Therapy, 2014. **15**(1): p. 61-68.
180. Habib, F.M., et al., *Tumour necrosis factor and inducible nitric oxide synthase in dilated cardiomyopathy.* Lancet, 1996. **347**(9009): p. 1151-5.
181. Yokoyama, T., et al., *Cellular basis for the negative inotropic effects of tumor necrosis factor-alpha in the adult mammalian heart.* J Clin Invest, 1993. **92**(5): p. 2303-12.
182. Moe, G.W., *In vivo TNF- inhibition ameliorates cardiac mitochondrial dysfunction, oxidative stress, and apoptosis in experimental heart failure.* AJP: Heart and Circulatory Physiology, 2004. **287**: p. H1813-H1820.
183. Finkel, M.S., et al., *Negative inotropic effects of cytokines on the heart mediated by nitric oxide.* Science, 1992. **257**(5068): p. 387-9.
184. Mazurek, S.R., E. Bovo, and A.V. Zima, *Regulation of sarcoplasmic reticulum Ca(2+) release by cytosolic glutathione in rabbit ventricular myocytes.* Free Radic Biol Med, 2014. **68**: p. 159-67.
185. Zima, A.V. and L.A. Blatter, *Redox regulation of cardiac calcium channels and transporters.* Cardiovasc Res, 2006. **71**(2): p. 310-21.
186. Song, W., X. Lu, and Q. Feng, *Tumor necrosis factor-alpha induces apoptosis via inducible nitric oxide synthase in neonatal mouse cardiomyocytes.* Cardiovascular research, 2000. **45**: p. 595-602.
187. Watson, D.C., M. Sargianou, and G. Panos, *Interleukin-12 (IL-12)/IL-10 ratio as a marker of disease severity in Crimean-Congo hemorrhagic fever.* Clin Vaccine Immunol, 2012. **19**(5): p. 823-4.
188. Nahrendorf, M. and F.K. Swirski, *Monocyte and macrophage heterogeneity in the heart.* Circulation Research, 2013. **112**: p. 1624-1633.
189. Lavine, K.J., et al., *Distinct macrophage lineages contribute to disparate patterns of cardiac recovery and remodeling in the neonatal and adult heart.* Proceedings of the National Academy of Sciences, 2014. **111**: p. 16029-16034.
190. Keul, P., et al., *Sphingosine-1-phosphate receptor 3 promotes recruitment of monocyte/macrophages in inflammation and atherosclerosis.* Circ Res, 2011. **108**(3): p. 314-23.

191. Leuschner, F., et al., *Therapeutic siRNA silencing in inflammatory monocytes in mice*, in *Nature Biotechnology*. 2011. p. 1005-1010.
192. Gordon, S., A. Plüddemann, and F. Martinez Estrada, *Macrophage heterogeneity in tissues: phenotypic diversity and functions.* Immunological Reviews, 2014. **262**: p. 36-55.
193. Martinez, F.O. and S. Gordon, *The M1 and M2 paradigm of macrophage activation: time for reassessment.* F1000prime reports, 2014. **6**: p. 13.
194. Mosser, D.M. and J.P. Edwards, *At a glance : Exploring the full spectrum of macrophage activation : Nature Reviews Imm... Page 1 of 2.* Nature Reviews Immunology, 2008. **969**: p. 2008-2009.
195. Murray, P.J., et al., *Macrophage Activation and Polarization: Nomenclature and Experimental Guidelines.* Immunity, 2014. **41**: p. 14-20.
196. Heredia, J.E., et al., *Type 2 innate signals stimulate fibro/adipogenic progenitors to facilitate muscle regeneration.* Cell, 2013. **153**(2): p. 376-88.
197. Goh, Y.P.S., et al., *Eosinophils secrete IL-4 to facilitate liver regeneration.* Proceedings of the National Academy of Sciences of the United States of America, 2013. **110**: p. 9914-9.
198. Zhang, X., R. Goncalves, and D.M. Mosser, *The isolation and characterization of murine macrophages.* Curr Protoc Immunol, 2008. **Chapter 14**: p. Unit 14 1.
199. Seshadri, G., et al., *Characterization of superoxide dismutases in cardiac progenitor cells demonstrates a critical role for manganese superoxide dismutase.* Stem Cells Dev, 2012. **21**(17): p. 3136-46.
200. Corraliza, I.M., et al., *Determination of arginase activity in macrophages: a micromethod.* J Immunol Methods, 1994. **174**(1-2): p. 231-5.
201. von Overbeck, J., P. Saraga, and D. Gardiol, *An autofluorescence method for the diagnosis of early ischaemic myocardial lesions. A systematic study on 732 autopsies, including 182 cases of sudden death.* Virchows Arch A Pathol Anat Histopathol, 1986. **409**(4): p. 535-42.
202. Zhou, X., et al., *Modulation of Mononuclear Phagocyte Inflammatory Response by Liposome-Encapsulated Voltage Gated Sodium Channel Inhibitor Ameliorates Myocardial Ischemia/Reperfusion Injury in Rats.* PLoS ONE, 2013. **8**: p. 1-13.
203. Harel-Adar, T., et al., *Modulation of cardiac macrophages by phosphatidylserine-presenting liposomes improves infarct repair.* Proc Natl Acad Sci U S A, 2011. **108**(5): p. 1827-32.
204. Aurora, A.B., et al., *Macrophages are required for neonatal heart regeneration.* Journal of Clinical Investigation, 2014. **124**: p. 1382-1392.
205. Moldovan, N.I., et al., *Contribution of monocytes/macrophages to compensatory neovascularization: the drilling of metalloelastase-positive tunnels in ischemic myocardium.* Circ Res, 2000. **87**(5): p. 378-84.
206. Godwin, J.W., A.R. Pinto, and N.a. Rosenthal, *Macrophages are required for adult salamander limb regeneration.* Proceedings of the National Academy of Sciences of the United States of America, 2013. **110**: p. 9415-20.
207. Ben-Mordechai, T., et al., *Macrophage subpopulations are essential for infarct repair with and without stem cell therapy.* Journal of the American College of Cardiology, 2013. **62**: p. 1890-1901.

208. Swirski, F.K. and M. Nahrendorf, *Macrophage-stem cell crosstalk after myocardial infarction.* Journal of the American College of Cardiology, 2013. **62**: p. 1902-1904.
209. Wong, M.M., et al., *Macrophages control vascular stem/progenitor cell plasticity through tumor necrosis factor-α-mediated nuclear factor-κB activation.* Arteriosclerosis, Thrombosis, and Vascular Biology, 2014. **34**: p. 635-643.
210. Eggenhofer, E. and M.J. Hoogduijn, *Mesenchymal stem cell-educated Macrophages.* Transplantation Research, 2012. **1**: p. 12.
211. Cho, D.-I., et al., *Mesenchymal stem cells reciprocally regulate the M1/M2 balance in mouse bone marrow-derived macrophages.* Experimental & molecular medicine, 2014. **46**: p. e70.
212. Freytes, D.O., et al., *Macrophages modulate the viability and growth of human mesenchymal stem cells.* Journal of Cellular Biochemistry, 2013. **114**: p. 220-229.
213. Chen, J.J.W., et al., *Tumor-associated macrophages: the double-edged sword in cancer progression.* Journal of clinical oncology : official journal of the American Society of Clinical Oncology, 2005. **23**: p. 953-964.
214. David, S. and A. Kroner, *Repertoire of microglial and macrophage responses after spinal cord injury.* Nature Reviews Neuroscience, 2011. **12**: p. 388-399.
215. Wynn, T.A., A. Chawla, and J.W. Pollard, *Macrophage biology in development, homeostasis and disease.* Nature, 2013. **496**(7446): p. 445-55.
216. Tabas, I., *Macrophage apoptosis in atherosclerosis: consequences on plaque progression and the role of endoplasmic reticulum stress.* Antioxidants & redox signaling, 2009. **11**: p. 2333-9.
217. Sica, A. and A. Mantovani, *Macrophage plasticity and polarization: In vivo veritas.* Journal of Clinical Investigation, 2012. **122**: p. 787-795.
218. Lawrence, T. and G. Natoli, *Transcriptional regulation of macrophage polarization: enabling diversity with identity.* Nature Reviews Immunology, 2011. **11**: p. 750-761.
219. Stout, R.D., et al., *Macrophages sequentially change their functional phenotype in response to changes in microenvironmental influences.* J Immunol, 2005. **175**(1): p. 342-9.
220. Davis, M.J., et al., *Macrophage M1/M2 polarization dynamically adapts to changes in cytokine microenvironments in Cryptococcus neoformans infection.* mBio, 2013. **4**: p. 1-10.
221. Erwig, L.P., et al., *Initial cytokine exposure determines function of macrophages and renders them unresponsive to other cytokines.* Journal of immunology (Baltimore, Md. : 1950), 1998. **161**: p. 1983-1988.
222. Mantovani, A., A. Sica, and M. Locati, *Macrophage polarization comes of age.* Immunity, 2005. **23**: p. 344-346.
223. Zhu, J., *Bioactive Modification of Poly(ethylenglykol) Hydrogels for Tissue Engineering.* Biomaterials, 2010. **31**: p. 4639-4656.
224. Zustiak, S.P. and J.B. Leach, *Hydrolytically degradable poly(ethylene glycol) hydrogel scaffolds with tunable degradation and mechanical properties.* Biomacromolecules, 2010. **11**: p. 1348-1357.

225. Woodrow, K.A., et al., *Intravaginal gene silencing using biodegradable polymer nanoparticles densely loaded with small-interfering RNA.* Nat Mater, 2009. **8**(6): p. 526-33.
226. Heffernan, M.J. and N. Murthy, *Polyketal nanoparticles: a new pH-sensitive biodegradable drug delivery vehicle.* Bioconjugate chemistry, 2005. **16**: p. 1340-2.
227. Gray, W.D., et al., *N-acetylglucosamine conjugated to nanoparticles enhances myocyte uptake and improves delivery of a small molecule p38 inhibitor for post-infarct healing.* J Cardiovasc Transl Res, 2011. **4**(5): p. 631-43.
228. Sohn, Y.D., et al., *Induction of pluripotency in bone marrow mononuclear cells via polyketal nanoparticle-mediated delivery of mature microRNAs.* Biomaterials, 2013. **34**(17): p. 4235-41.
229. Schulz, R., et al., *TNFalpha in ischemia/reperfusion injury and heart failure.* Basic Res Cardiol, 2004. **99**(1): p. 8-11.
230. Headen, D.M., et al., *Microfluidic-based generation of size-controlled, biofunctionalized synthetic polymer microgels for cell encapsulation.* Adv Mater, 2014. **26**(19): p. 3003-8.
231. Vasconcelos, D.P., et al., *Macrophage polarization following chitosan implantation.* Biomaterials, 2013. **34**(38): p. 9952-9.
232. Chenite, A., et al., *Novel injectable neutral solutions of chitosan form biodegradable gels in situ.* Biomaterials, 2000. **21**(21): p. 2155-61.
233. Kumar, M.N.V.R., *A review of chitin and chitosan applications.* Reactive & Functional Polymers, 2000. **46**: p. 1-27.
234. Tamura, H., *Biomedical applications of chitin hydrogel membranes and scaffolds.* Carbohydrate Polymers, 2011. **84**: p. 820-824.
235. Segers, V.F.M., et al., *Local delivery of protease-resistant stromal cell derived factor-1 for stem cell recruitment after myocardial infarction.* Circulation, 2007. **116**: p. 1683-92.
236. Caplan, M.R., et al., *Control of self-assembling oligopeptide matrix formation through systematic variation of amino acid sequence.* Biomaterials, 2002. **23**: p. 219-227.
237. Galler, K.M., et al., *Self-assembling multidomain peptide hydrogels: Designed susceptibility to enzymatic cleavage allows enhanced cell migration and spreading*, in *Journal of the American Chemical Society*. 2010. p. 3217-3223.
238. Boehler, R.M., et al., *Lentivirus delivery of IL-10 to promote and sustain macrophage polarization towards an anti-inflammatory phenotype.* Biotechnology and Bioengineering, 2014. **111**: p. 1210-1221.
239. Frangogiannis, N.G., et al., *IL-10 is induced in the reperfused myocardium and may modulate the reaction to injury.* Journal of immunology (Baltimore, Md. : 1950), 2000. **165**: p. 2798-2808.
240. Gesser, B., et al., *Identification of functional domains on human interleukin 10.* Proceedings of the National Academy of Sciences of the United States of America, 1997. **94**: p. 14620-14625.
241. Swirski, F.K. and M. Nahrendorf, *Leukocyte behavior in atherosclerosis, myocardial infarction, and heart failure.* Science, 2013. **339**(6116): p. 161-6.

242. Bartneck, M., et al., *Inducing healing-like human primary macrophage phenotypes by 3D hydrogel coated nanofibres.* Biomaterials, 2012. **33**(16): p. 4136-46.